A NEW INSIGHT INTO THE GEOCHEMISTRY OF SULFUR IN LOW SULFATE
ENVIRONMENTS

A THESIS
SUBMITTED TO THE FACULTY OF
UNIVERSITY OF MINNESOTA
BY

MOJTABA FAKHRAEE

IN PARTIAL FULFILLMENT OF THE REQUIREMENTS
FOR THE DEGREE OF
DOCTOR OF PHILOSPHY

SERGEI KATSEV

AUGUST 2018

Last but not the least, special thanks to my family, friends, and LLO colleagues who have always been there for me, supporting and encouraging me, especially in the past four years.

Abstract

As an essential element for life, sulfur plays an important role in the biosphere, hydrosphere, atmosphere and lithosphere. Studies of sulfur cycling have been traditionally concentrated on modern marine environments with 28mM of sulfate, yet its importance in low sulfate environments such as large freshwater systems as well as the oceans of the geologic past (>0.5 billion years ago) cannot be neglected. This thesis, through modeling and theoretical approach, aims to provide a new insight into several aspects of sulfur cycling in low sulfate environments. For example, it is widely assumed that water-column sulfate is the main sulfur source to fuel microbial sulfate reaction in sediments. While this assumption may be justified in high-sulfate environments such as modern seawater, I show that in low-sulfate environments mineralization of organic sulfur compounds can be an important source of sulfate and sedimentary sulfide. The results in this thesis indicate that in low sulfate environments (<500 µM) the in-sediment production of sulfate can support a substantial portion (>50%) of sulfate reduction. Extrapolating the results to Archean oceans with tens of µM of sulfate, modeling results reveal that sulfite generated by mineralization of organic sulfur could fuel microbial S reduction in the absence of ambient sulfate, and hydrogen sulfide generated by mineralization of reduced organic S compounds could provide a pathway to pyrite that bypassed the microbial reduction of sulfate or sulfite. Reproducing isotopic records in the sedimentary sulfides from the rock record, modeling results show that in the low sulfate (<10 µM) environment of the Archean oceans (2.5-4 billion years ago), oxygen could have accumulated to up to 25 µM, while being consistent with the sulfur isotopic

composition in Neoarchean rocks. A mass balance model coupled to a sediment diagenesis model suggests that seawater sulfate concentrations during the Proterozoic Eon (0.5-2.4 billion years ago) remained below 1.5% of modern values (<500 µM), and possibly as low as 100 µM. Using exploratory modeling of sulfur cycling, I also constrain the geochemical factors that control the fluxes of methylmercury from modern freshwater sediments. Modeling results identify oxygen, sulfate, and organic matter as leading geochemical parameters. They also suggest a critical level of oxygen at the sediment water interface, below which methylation rate dominates demethylation rate, resulting in an efflux of methylmercury into overlying water.

Table of Contents

List of Tables

List of Figures

Introduction

Sulfur plays an important role in the biosphere, hydrosphere, atmosphere and lithosphere. This is mainly due to its high abundance and a broad range of oxidation states (+VI to –II), and ability to be present in ionic (e.g. as sulfate), elemental and gaseous forms (e.g. as SO_2 and H_2S). Sulfur cycling in aquatic sediments involves both reductive and oxidative processes (Jørgensen, 1990). Biologically mediated reduction of sulfate in low oxygen environments is the most dominant process in sulfur cycling. It regulates production of hydrogen sulfide, mobilization of phosphorus, mercury and other pollutants, and biogeochemical cycling of several elements through "cryptic" cycles (Canfield et al. 2010; Holmkvist et al. 2011; Johnston et al. 2014). These processes have strong impacts in the environment, from small temporal scales (e.g. degradation of organic matter in a contaminated aquifer) to large scales (e.g. influence on atmospheric oxygen concentrations on geologic time scales). Sulfur cycling in freshwater sediments has received less attention than in marine systems, as sulfate concentrations are typically low (0.01-0.5 mmol L^{-1}) compared to those in marine waters (28 mmol L^{-1}). The importance of sulfur cycle in freshwater sediments, however, cannot be neglected as its spatial and temporal dynamics strongly interact with the cycles of other elements such as iron and phosphorus (e.g. Katsev 2016). Understanding the sulfur cycle in low sulfate environments, therefore, is key to understanding environmental changes. Moreover, modern low-sulfate environments may serve as analogues of ancient Archean and Proterozoic oceans, which contained low levels of sulfate (Habicht et al. 2002; Crowe et al. 2014; Fakhraee et al. 2018). Studying them helps us understand the elemental cycles

of Early Earth, including processes that regulated climate and the conditions under which early life evolved.

This thesis addresses four themes, outlined below.

1. New insight into the contributions of organic sulfur to microbial sulfur reduction and pyrite formation

Sulfur is an essential element for life. However, at any given time, only a small fraction of it is bound in biomass. Sulfur makes up about 1% of the dry weight of organisms (Ho et al. 2003). It occurs mainly as constituents of proteins (primarily the amino acids cysteine and methionine), but also in coenzymes (e.g., coenzyme A, biotin, thiamine), in the form of iron-sulfur clusters in metalloproteins, and in bridging ligands (molecules that bind to proteins, for example, in cytochrome c oxidase). Higher oxidation state compounds, such as sulfonates $R-SO_3-H$, sulfones $R-SO_2-R$, and organo-sulfates, can be found in lipids (e.g., Sulfoquinovosyl diacylglycerols) and are components of cell walls and photosynthetic membranes. At 28 mM of sulfate in modern seawater, microorganisms uptake inorganic sulfur, mainly as sulfate, to form these organic compounds in an energy-dependent process referred to as assimilation (Ksionzek et al. 2016). Molar S:C ratios in modern plankton (Ho et al. 2003) typically range between 0.003 and 0.01, with freshwater values (Fagerbakke et al. 1996) being more varied than in marine environments because of a wider range of geochemical conditions. In addition to assimilation, many bacteria and archaea can use inorganic sulfur in energy-yielding reactions, sustaining dissimilatory sulfur metabolisms. These latter processes, namely,

microbial sulfur reduction, are essential for the cycling of sulfur on our planet (Friend 1973).

While the process of sulfate reduction is well understood, the source of oxidized sulfur, especially in environments with low concentrations of sulfur, may be overlooked. Previous studies focused on inorganic sulfur as the main source of sulfate for sulfate reduction (SR). In marine environments, sulfate is delivered into sediments overwhelmingly from the abundant pool of bottom water sulfate. In contrast, in freshwater environments where sulfate concentrations are considerably lower, the contribution to sediment biogeochemistry of organic sulfur delivered with the particulate organic matter (POM) may be potentially significant. The contribution of organic sulfur in supporting sediment sulfate reduction (King and Klug 1982), however, has been mostly neglected.

Early work implicated S-esters, a major component of S_{org}, as potential sources of sulfate (King and Klug 1980; 1982; Lovley and Klug 1986), while little information was provided on the fate of other organic sulfur compounds, such as amino acid S and other thiols. Surprisingly, little research has been done on the fate of S_{org} since the 1980s, and extrapolations to low-sulfate or carbon-poor systems have not been done. Past studies of sedimentary organic sulfur mostly focused on post-depositional sulfidization of organic matter and preservation of the resultant compounds over long time scales (oil maturation) (Amrani 2014; Goldhaber 2003). The role of organic sulfur delivered to sediment in sustaining SR has not been well quantified. Sulfide incorporation in organic matter has frequently been reported in marine sediments (Werne et al., 2008) but less so in lakes

despite evidence of high thiol concentrations in freshwater sediments (Urban et al., 1999).

In the first two chapters of this thesis, I discuss the critical, and yet overlooked, role that organic sulfur plays in low sulfate environments. The study is performed first in Lake Superior, and the results are then extrapolated to other low sulfate environments of the present, as well as of the past, including primordial oceans. Based on the significant role of organic sulfur in Lake Superior (SO_4^{2-} = 40 µM) reported in Chapter 1, in the second chapter I discuss the role of organic sulfur in the sulfur cycle on Early Earth, at low levels of seawater sulfate (<200 µM; Fakhraee et al. 2018), with implications for the chemistry and biology of the early earth oceans.

2. Low sulfate and oxygenation of Early Earth

Sulfur has four stable isotopes, ^{32}S, ^{33}S, ^{34}S, and ^{36}S, with approximate abundances of 95.04%, 0.75%, 4.20%, and 0.015%, respectively. The isotope values are reported relative to international standards according to a conventional δ-notation (‰; per mil):

$$\delta^x S = (\frac{\frac{^xS_{Sample}}{^{32}S_{Sample}}}{\frac{^xS_{CDT}}{^{32}S_{CDT}}} - 1) \times 1000 \qquad (1)$$

where x = 33, 34, or 36, and CDT refers to the $^xS/^{32}S$ ratio of the standard troilite, an iron monosulfide from the Canyon Diablo Meteroite.

Isotopic fractionation is defined as the relative partitioning of the heavier and lighter isotopes between two coexisting phases in a natural system. Fractionation of

sulfur isotopes is widely used in reconstructions of sulfur cycling with wide ranging applications to modern and ancient environments. The strongest fractionation is imparted by microbial sulfate reduction (~30 ‰; Habicht et al. 1998), with minor contributions from sulfide oxidation and elemental sulfur disproportionation (~5 ‰; Habicht et al. 1998).

There are two major types of sulfur isotope fractionations: mass dependent sulfur isotope fractionation, and mass independent fractionation. Mass-dependent fractionation effects arise when variations in chemical and physical properties of isotopologous species depend on the relative differences in the masses of atoms in a molecule, or the mass of the molecular species itself. Mass-dependent fractionations include, but are not limited to, equilibrium isotope exchange, diffusion, gravitational separation and biological effects. Non-mass-dependent fractionations arise when variations in chemical and physical properties of molecular species depend on factors other than or in addition to the mass of the constituent isotopes. In the modern Earth, variations in sulfur isotope ratios are essentially always mass dependent and δ^{33}S and ^{36}S are related to variations in δ^{34}S as: δ^{33}S = 0.515 x δ^{34}S, and δ^{36}S = 1.90 x δ^{34}S, where the coefficients 0.515 and 1.90 reflect the approximate relative mass differences between the numerator and denominator of $^{33}S/^{32}S$ and $^{36}S/^{32}S$ compared to those of $^{34}S/^{32}S$. Deviation the from mass dependent line can be defined as:

$$\Delta^{33}S \ (‰) = \delta^{33}S \ (‰) - 0.515 * \delta^{34}S \ (‰) \tag{2}$$

Mass independent fractionation of sulfur (MIF-S), then, can be described as non-zero Δ^{33}S.

It is well established that the Earth's ocean and atmosphere were essentially anoxic prior to the evolution of oxygenic photosynthesis but deciphering the subsequent redox evolution of the earth system has been challenging. Geochemical proxies indicate a complex oxygenation history in which the transition to the modern, well-oxygenated world occurred in several stages (e.g., Lyons et al. 2014). Oxygenation of the atmosphere and surface ocean preceded the eventual oxygenation of the deep ocean by nearly two billion years (Canfield et al., 2007; Scott et al. 2008) (Fig. 1), and atmospheric oxygenation was apparently separated from the onset of biological oxygen production by perhaps 300 million years (Crowe et al. 2013).

The narrow range of $\delta^{34}S$ and presence of MIF-S ($\Delta^{33}S \neq 0$) in Archean (2.4-4 billion years ago) sedimentary pyrites (Farquhar et al. 2000; Habicht et al. 2002) has been viewed as consistent with a globally predominant anoxia, while local evidence for seawater oxygen was interpreted as restricted to oxygenated "oases" (Olson et al. 2013). Mass independent fractionations are produced in an ozone-free atmosphere, and atmospheric photochemical models suggest delivery of MIF-S to the Earth's surface only when atmospheric O_2 concentrations are less than 10^{-5} present atmospheric levels (PAL) (Farquhar et al. 2000). The relatively restricted ranges of $\delta^{34}S$ in Archean pyrites, particularly before 2.7 Ga, point to low sulfate concentrations in the oceans reflecting both restricted oxidative weathering of pyrites on land and little oxidative recycling of sulfur in the oceans. Evidence from redox-sensitive elements (Planavsky et al. 2010; Liu et al. 2016), however, points to the possibility of oxygen being present in the ocean before the Great Oxygenation Event (GOE; 2.3-2.5 billion years ago). An important

remaining question is therefore the degree of oxygenation that is consistent with the observed isotopic signatures of sedimentary Archean pyrites. Given the emerging evidence (Czaja et al. 2012; Planavsky et al. 2014) for the early rise of oxygen in the atmosphere, the possibility of oceanic accumulation of oxygen prior to this oxidation event becomes particularly important.

In the third chapter, through modeling of sulfur diagenesis, I demonstrate that the small sulfate-sulfide isotopic differences in $\delta^{34}S$ observed in Archean sedimentary sulfides (Johnston 2011) require deposition from seawater with less than 25 μM of oxygen. At these oxygen levels, the preservation of mass independent fractionation of sulfur (MIF-S), which is considered a strong indicator of anoxic atmosphere, is not necessarily suppressed, but is instead controlled by the details of S biogeochemical cycling in the ocean, and depends on the availability of reactive organic matter, sulfate, and electron acceptors for sulfide re-oxidation. This finding suggests a Neoarchean world with nearly anoxic atmosphere but where marine oxygen concentrations were limited to low μM levels.
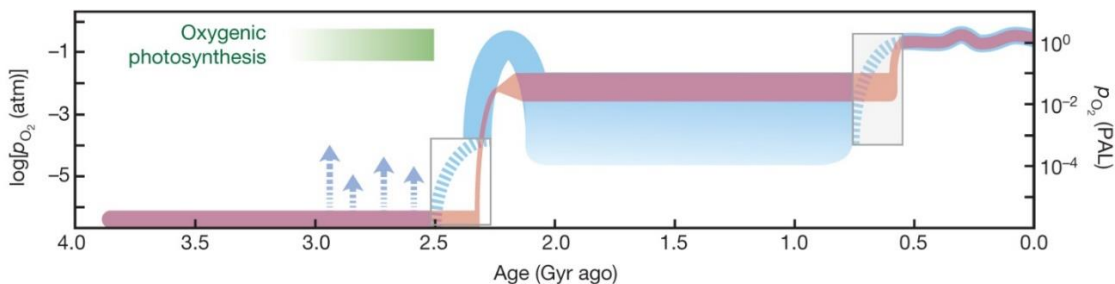
Figure 1. *Evolution of Earth's atmospheric oxygen content through time (Lyons et al. 2014).*

3. Sulfate scarcity in the first 3.5 billion years

The Great Oxygenation Event (GOE; 2.3-2.5 billion years ago), the first accumulation of oxygen in atmosphere, is thought to trigger the weathering of sulfide minerals on land. This weathering would provide another source of sulfate to the oceans and result in increased sulfate concentration in the oceans. Before 2.4 billion years ago, due to limited oxygen and suppressed weathering, sulfate concentrations in the oceans were suggested to be 100 times lower (<200 µM; Fakhraee et al. 2018) than those in the modern oceans. After the GOE and until a second stage of oxygenation around 0.7 billion years ago, during the Proterozoic eon, marine sulfate concentrations were suggested to have increased by an order of magnitude, reaching approximately one tenth of the modern value (2-4 mM; Kah et al. 2004). While accumulation of oxygen would have enhanced the weathering flux of sulfate, increasing sulfate concentration in the oceans, the degree of this increase has not been accurately quantified.

In Chapter 4, modeling approach is used to constrain the seawater sulfate level during the Proterozoic Eon, a critical geological time in the history of the Earth and the evolution of life. A mass balance model is coupled with a sediment diagenesis model, and the results are compared against the sulfur isotope records. The modeling results reveal that sulfate concentrations during the Proterozoic may not have increased as strongly as previously believed, remaining below 1.5% modern values (<0.5 mM), and possibly as low as 100 µM.

4. Predicting methylmercury flux from sediments

Sulfate reducing bacteria mediate the transformation of inorganic mercury to a highly toxic form of organic mercury, methylmercury. While a number of different factors were suggested to control the methylmercury flux from sediments, their effects have not been quantified to a level that might allow a quantitative prediction, and contributions from individual factors have been rarely separated. In Chapter 5, using a reaction-transport modeling approach, I investigate the factors that control the methylmercury flux from sediments, under a range of sediment conditions. The model was calibrated to data from the St. Louis River estuary (SLRE), a freshwater estuary upstream of Lake Superior, and cross-validated to marine sediments. Sensitivity analysis identified oxygen, sulfate, and organic matter as leading geochemical parameters controlling methylmercury fluxes. The results suggest a critical threshold for oxygen level, below which methylation rate dominates demethylation rate, and the flux of methylmercury is directed from sediment into the overlying water.

Chapter 1 Significant role of organic sulfur in supporting sedimentary sulfate reduction in low-sulfate environments

Title: Significant role of organic sulfur in supporting sedimentary sulfate reduction in low-sulfate environments

Authors: [1]Mojtaba Fakhraee, [1]Jiying Li, [1,2]Sergei Katsev

[1] Large Lakes Observatory, University of Minnesota Duluth

[2] Department of Physics, and Astronomy, University of Minnesota Duluth

1.1. Synopsis

Dissimilatory sulfate reduction (DSR) is a major carbon mineralization pathway in aquatic sediments, soils, and groundwater, which regulates the production of hydrogen sulfide and the mobilization rates of biologically important elements such as phosphorus and mercury. It has been widely assumed that water-column sulfate is the main sulfur source to fuel this reaction in sediments. While this assumption may be justified in high-sulfate environments such as modern seawater, we argue that in low-sulfate environments mineralization of organic sulfur compounds can be an important source of sulfate. Using a reaction-transport model, we investigate the production of sulfate from sulfur-containing organic matter for a range of environments. The results show that in low sulfate environments (<500 μM) the in-sediment production of sulfate can support a substantial portion (>50%) of sulfate reduction. In well-oxygenated systems, porewater sulfate profiles often exhibit sub-interface peaks so that sulfate fluxes are directed out of the sediment. Our measurements in Lake Superior, the world's largest lake, corroborate this conclusion: offshore sediments act as sources rather than sinks of sulfate for the water column, and sediment DSR is supported entirely by the in-sediment production of sulfate. Sulfate reduction rates are correlated to the depth of oxygen penetration and strongly regulated by the supply of reactive organic matter; rate co-regulation by sulfate availability becomes appreciable below 500 μM level. The results indicate the need to consider the mineralization of organic sulfur in the biogeochemical cycling in low-sulfate environments, including several of the world's largest freshwater bodies, deep subsurface, and possibly the sulfate-poor oceans of the Early Earth.

11

1.2. Introduction

Biologically mediated reduction of sulfate is the dominant process in the sedimentary cycling of sulfur (Jørgensen 1982; Holmer and Storkholm 2001). It serves as an important mineralization pathway of organic carbon, regulates the production of hydrogen sulfide, mobilizes bioavailable phosphorus (Caraco et al. 1989; Katsev et al. 2006), mediates methylation of mercury (Gilmour et al. 1992), and affects the cycles of nitrogen and iron (Canfield et al. 1993; Hansel et al. 2015). On geological time scales, it affects the rates of organic matter preservation (Gaines et al. 2012) and shapes the isotopic signatures preserved in sedimentary sulfide rocks (Crowe et al. 2014). Whereas the process of sulfate reduction (SR) is relatively well understood, the source of sulfate, especially in environments with low concentrations of sulfur, may be overlooked. In marine environments, sulfate is delivered into sediments overwhelmingly from the abundant pool of bottom water sulfate. Sulfate, however, may also be generated from the pool of organic sulfur (S_{org}) that is delivered into the sediment with particulate organic matter (POM), during its diagenetic mineralization (King and Klug 1982). Despite the ubiquitousness of this bioavailable S pool, bottom water sulfate has been assumed to be the main source of sulfate even in environments where sulfate concentrations are low, such as freshwater lakes (Gorham et al. 1974; Nriagu 1984; Dornblaser et al. 1994). The contribution of the organic sulfur source in supporting sediment sulfate reduction has been characterized only under a limited range of conditions (King and Klug 1982) and has been mostly neglected.

Sedimentary organic matter contains predominantly oxygen-bound S (R-O-SO$_3$H groups, such as ester-sulfates) characterized by high oxidation states of S$_{org}$ (+4 to +6), and carbon-bound S (R-SH groups, such as amino acids and thiols), typically at low oxidation states (-2 to 0) (Sievert et al. 2007; Fitzgerald 1976). Carbon-bonded S is present in peptides and proteins, coenzymes, amino acids (methionine and cysteine), and heterocyclics. Some C-bound compounds, such as sulfonates (R-SO$_3$) and sulfones (R-SO$_2$-R), are characterized by higher oxidation states of S. Examples in soils and sediments include the sulfated polysaccharides produced by algae and bacteria, sulfated phenols and lipids, and choline sulfate (Nriagu and Soon 1985). The sulfur-bearing organic matter, originating from either allochthonous terrestrial sources or autochthonous primary production (Zhao et al. 2006), enters the seston and becomes deposited at the sediment surface, where it often dominates the total S pool (Nriagu and Soon 1985; Kokkonen and Tolonen 1987; Couture et al. 2016). Oxidized fractions (S-esters) make up between 35% and 60% of the organic sulfur (S$_{org}$) pool, with more common values at the lower end of this range (David and Mitchell 1985), e.g. in eutrophic Lake Wintergreen (35%; King and Klug 1982). Carbon-bound S, mostly in the form of proteins, is estimated to make up another 20-40% (King and Klug 1982). Other minor fractions include sulfolipids, coenzymes, and other compounds, with minimal contribution from elemental sulfur (King and Klug 1982). In the dissolved fraction, soluble S$_{org}$ (esters and C-bound) likely contributes less than 20% of total S (David and Mitchell 1985).

Early work suggested that S$_{org}$ could become a source of sulfate as the settled organic matter undergoes diagenetic mineralization (King and Klug 1980; 1982; Lovley

and Klug 1986). Bacteria can access S_{org} using enzymes that cleave off the bonds in the respective chemical groups: $R-O-SO_3H$ (e.g., aryl sulfatase) and $R-SH$ (e.g., cysteine liase). The produced SO_4^{2-} and HS^- then can be released into sediment porewater. In presence of oxygen, the reduced inorganic sulfur can be oxidized to sulfate, whereas in the anoxic sediment SO_4^{2-} can be used for dissimilatory reduction (Canfield et al. 2005). Based on the work in eutrophic lakes with sulfate concentrations in excess of 120 μM (King and Klug 1980; 1982), the in-sediment production of sulfate was suggested to be minor (<10%) relative to the fluxes of sulfate from overlying water. Surprisingly, little research was done on the fate of sedimentary S_{org} since the 1980s, and extrapolations to low-sulfate or carbon-poor systems have not been done. Studies of sedimentary organic sulfur mostly focused on the post-depositional sulfidization of organic matter (Couture et al. 2016; Werne et al. 2008; Goldhaber 2003), which is the enrichment of organic matter with S as a result of hydrogen sulfide generation in anoxic sediment. Preservation of the resultant compounds is an important component of oil maturation process (Amrani 2014). The geochemical transformations of the organic sulfur that was delivered into sediment by sedimentation, in contrast, have been poorly quantified. Figure 1.1 illustrates the sediment S cycling that includes the degradation of S-bearing organic matter in both oxic and anoxic sediment zones, anaerobic microbial sulfate reduction, assimilatory reduction, oxidation of hydrogen sulfide by iron oxides, disproportionation of elemental sulfur, organic matter sulfurization, and precipitation of mineral sulfides. The sulfate generated from S_{org} within the sediment oxic layer can support sulfate reduction when it diffuses into the sediment anoxic zone. When S-bearing organic matter is buried below the

14

penetration depth of water column sulfate, its mineralization may drive a cryptic cycle (Canfield et al. 2010; Holmkvist et al. 2011; Johnston et al. 2014) of sulfur reduction-oxidation. Cryptic cycling refers to a situation where a compound is produced and consumed quickly enough so that its concentration remains low despite high turnover rates. Cryptic production and oxidation of hydrogen sulfide, for example, was shown to mediate anammox and other N-cycling processes in marine oxygen minimum zones (Canfield et al. 2010), and crypric formation of sulfate was shown to mediate the cycling of Fe in the sediment methane zone (Holmkvist et al. 2011). Such cycling could also affect the redox transformations of S and other elements in a zone where porewater sulfate concentrations are below detection and therefore where sulfate reduction could be otherwise thought of as negligible.

To quantify the contributions of organic S to sediment sulfate reduction and the resultant effects on S biogeochemical cycling, we set up a diagenetic diffusion-reaction model. The model is first applied to oligotrophic Lake Superior where sulfate levels are <40 µM, and then used to extrapolate the results to a broader range of aquatic environments. We show that the contributions from S_{org} may dominate sediment SR, in which case sediments may act as sources rather than sinks of sulfate to the overlying water columns. We then discuss the implications of our findings for the rates of sulfate reduction, total sulfur budgets, and sedimentary records of S cycling in low-sulfate ecosystems.
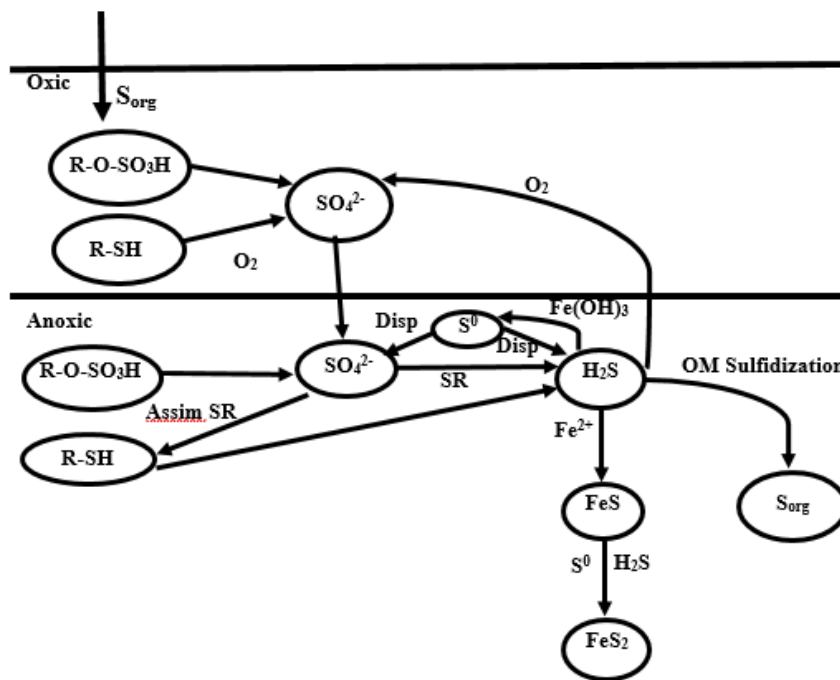
Figure 1.1 *Sediment sulfur cycle with contributions from organic sulfur sedimentation*

1.3. Methods
1.3.1. Sampling and analyses

Sediment and water column samples were taken previously in Lake Superior on multiple cruises aboard the *R/V Blue Heron* (Table 1.1; Fig. 1.2) (Li 2014 – PhD thesis). Geochemical analysis was conducted by Li (2014). Briefly, temperature and dissolved oxygen distributions in the water column were measured using a Seabird 911plus

conductivity, temperature, depth (CTD) probe with an Oxyguard flow-through oxygen sensor. Sediment cores of 94 mm inner diameter were recovered using an Ocean Instruments multi-corer. The landing sites were monitored using a Knudsen 320/R echo sounder with a 28kHz transducer to select flat areas with laterally homogeneous sediment accumulation. The cores were subsequ ently stored at 4° C, which corresponds to the temperature $(3 - 5^o$ C) of Lake Superior bottom waters. Vertical distributions of dissolved oxygen in sediment porewaters were determined on-board using a Unisense (Clark-type) microelectrode (Revsbech 1989). Separate sediment cores were sectioned on-board under a N_2 atmosphere at vertical intervals varying from 0.5 cm at the sediment surface to 5 cm below 20 cm. Pore waters were extracted immediately after sectioning under anaerobic conditions using Rhizon porous polymer micro samplers (0.1 µm membrane pore size) (Dickens et al. 2007). Porewater samples for sulfate analyses were frozen at -18°C until measurements. Sulfate concentrations were measured by ion chromatography (DIONEX ICS 1100) with the detection limit of 0.5 µmol L^{-1}. The organic carbon content was determined in freeze-dried sediment samples by coulometry on a CM150 total carbon (TC), total organic carbon (TOC), total inorganic carbon (TIC) analyzer. Sediment dating using ^{210}Pb was performed on cores from Sta. EM, CM, IR and FWM (Li et al. 2012). Sediment porosity was calculated from water content (Li et al. 2012; Li and Katsev 2014).

Table 1.1 *Sampling dates and locations.*

Date	Station	Depth (m)	Latitude (N)	Longitude (W)
07 Jun 2010	FWM.1	166	47° 09.13´	91° 16.44´
20 Jul 2010	FWM.2	168	47° 02.14´	91° 16.38´
21 Sep 2010	FWM.3	166	47° 01.98´	91° 16.50´
21 Apr 2011	FWM.4	166	47° 02.15´	91° 16.31´
22 Aug 2011	FWM.5	166	47° 02.21´	91° 16.32´
10 Jun 2010	EM.1	229	47° 33.38´	86° 35.76´
22 Jul 2010	EM.2	228	47° 33.36´	86° 35.65´
22 Sep 2010	EM.3	226	47° 33.37´	86° 35.68´
26 Jul 2012	EM.4	232	47° 32.26´	86° 35.79´
11 Jun 2010	WM.1	169	47° 19.01´	89° 50.73´
22 Jul 2010	WM.2	174	47° 18.26´	89° 49.33´
25 Sep 2010	WM.3	169	47° 19.05´	89° 50.76´
23 Apr 2011	WM.4	171	47° 19.01´	89° 50.80´
08 Jun 2010	IR.1	234	47° 58.41´	88° 28.01´
21 Jul 2010	IR.2	237	47° 58.42´	88° 28.07´
22 Sep 2010	IR.3	235	47° 58.41´	88° 28.08´
21 Apr 2011	IR.4	235	47° 58.40´	88° 27.97´
25 Aug 2011	IR.5	235	47° 58.38´	88° 28.09´
27 Jul 2012	IR.6	235	47° 58.44´	88° 28.05´
08 Jun 2010	CM.1	252	48° 01.06´	87° 46.44´
21 Jul 2010	CM.2	236	48° 02.84´	87° 47.32´
22 Sep 2010	CM.3	235	48° 02.66´	87° 47.17´
22 Apr 2011	CM.4	239	48° 03.04´	87° 47.74´
21 Jul 2010	ED.1	316	47° 31.81´	87° 07.81´
22 Sep 2010	ED.2	318	47° 31.53´	87° 07.49´
22 Apr 2011	ED.3	312	47° 31.76´	87° 07.65´
22 Aug 2011	SW.1	117	46° 50.28´	90° 16.00´
24 Jul 2012	SW.2	120	46° 50.49´	90° 16.33´
25 Jul 2012	BB.1	26	48° 30.06´	88° 36.48´
25 Jul 2012	NB.1	29	48° 52.46´	88° 11.77´
26 Jul 2012	NIP.1	124	48° 36.62´	87° 20.52´
25 Jul 2012	TB.1	237	48° 11.29´	88° 53.04´
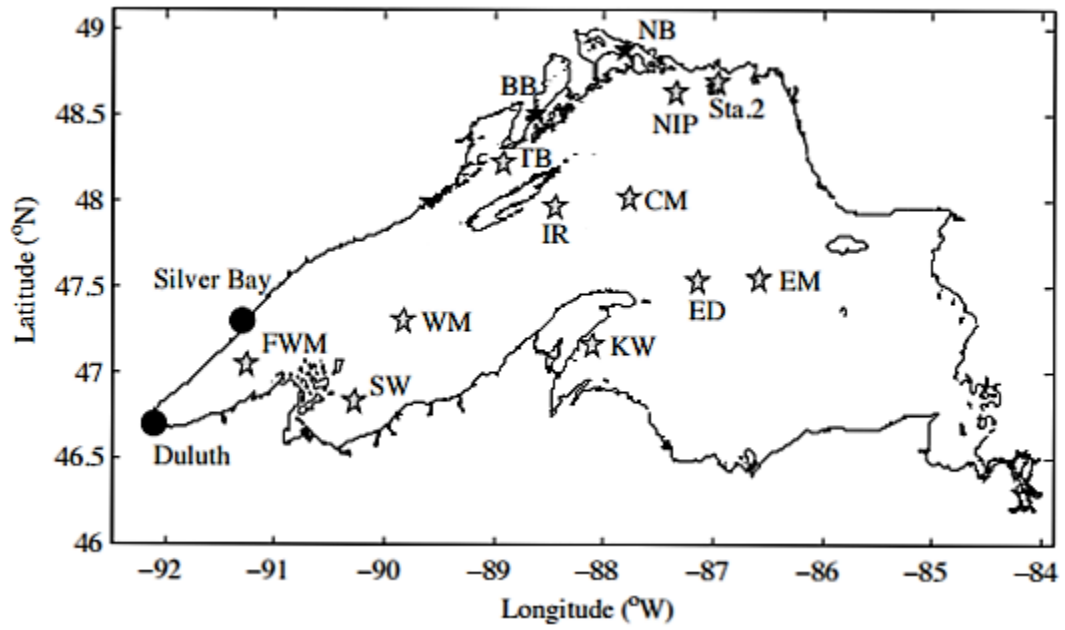
Figure 1.2 *Sampling locations in Lake Superior.*

1.3.2. Geochemical Model

The biogeochemical cycling of sulfur was simulated with a diagenetic reaction-transport model (e.g., Katsev et al. 2006; Katsev et al. 2007; Katsev and Dittrich 2013). As bottom conditions in Lake Superior experience little seasonal variation (Li et al. 2012), vertical distributions of chemical species within the sediment were simulated with a diagenetic equation (Berner 1980) at steady state:

$$0 = \frac{\partial}{\partial x}(\varphi D_i \frac{\partial C_i}{\partial x}) - \frac{\partial}{\partial x}(\varphi v C_i) + \varphi \sum_j R_{ij} \qquad (1.1)$$

Here, x is depth below the sediment surface, C_i is the concentration of species i, D_i is the corresponding molecular diffusion coefficient corrected for sediment porosity φ using the Archie's law factor of $\varphi^{1.14}$ (Boudreau 1997), and v is the burial velocity (neglected for solutes). R_{ij} are the rates of reactions that consume or produce species i. The diffusive fluxes within the sediment were calculated using the Fick's law of diffusion:

$$F_{C_i} = -\varphi D_i \frac{\partial C_i}{\partial x} \qquad (1.2)$$

The intensities of bioturbation and bioirrigation in the sediments of Lake Superior were characterized previously (Li et al. 2012) and shown to be negligible below 2 cm depth. Based on the difference between the diffusive and total fluxes of oxygen, the contribution of bioirrigation to the total sediment-water exchanges of oxygen across the interface was estimated at 30-50%. While the bioirrigation contribution to the fluxes of sulfate is expected to be on the same order of magnitude, flux calculations in the present

model include only the molecular diffusion fluxes, as they are better constrained from the vertical concentration profiles and the absolute values of sulfate fluxes are of secondary importance (in contrast to their direction). Importantly, the direction of bioirrigation fluxes is set by the concentration gradient (e.g. Katsev et al. 2007) and thus coincides with the direction of the diffusive flux.

The geochemical reactions included in the model and their rate formulations are listed in Tables 2 and 3. Model parameter values are listed in Table 4. In particular, the rate of sulfate reduction was simulated using the Michaelis-Menten kinetics:

$$R_{SR} = 0.5 \; \frac{V_m [SO_4^{2-}]}{K_m + [SO_4^{2-}]} \frac{K_i}{K_i + [O_2]} \tag{1.3}$$

Here, the Monod constant K_m describes the affinity of enzymes for substrate, K_i describes the inhibition effect of oxygen on sulfate reduction, and the stoichiometric factor 0.5 corresponds to two carbon atoms being oxidized for each sulfur atom reduced (Table 2). The organic carbon (OC) mineralization rate V_m was approximated as $V_m = k$ [OC] where the reactivity k was described by the Middelburg power law (Middelburg 1989) as a function of carbon age t: $\log_{10} k = -(0.95) \log_{10} t - (0.81)$. This power law was recently shown to hold over a range of conditions including low-sulfate environments including Lake Superior (Katsev and Crowe 2015; O'Beirne et al. 2017). Organic carbon concentrations at the sediment water interface were taken from measurements. Porosity profiles in the model were interpolated using the measured profiles for each station (Li 2014). Sediment age (from Li et al. 2012) was linked to depth below the sediment surface using porosity φ and assumed solid sediment density $\rho = 2.65$ g cm^{-3}, as described in Li et

al. (2012); the initial carbon age at the sediment surface was chosen from best fit (O'Beirne et al. 2017; Katsev and Crowe 2015).

Table 1.2 *Reactions included in the model*

Reactions	Rate
$CH_2O + O_2 \Rightarrow CO_2 + H_2O$	R_{OX}
$CH_2O + 4\ FeOOH_{(s)} + 7CO_2 + H_2O \Rightarrow 4Fe^{2+} + 8\ HCO_3^-$	R_{FeOOH}
$SO_4^{2-} + 2CH_2O \Rightarrow H_2S + 2HCO_3$	R_{SR}
$H_2S + 2O_2 + 2HCO_3^- \Rightarrow SO_4^{2-} + 2CO_2 + 2H_2O$	R_{SOX}
$R\text{-}O\text{-}SO_3H + H_2O \Rightarrow HSO_4^{2-} + R\text{-}OH_2$	R_{PSO4}
$R\text{-}SH + H_2O \Rightarrow H_2S + R\text{-}OH$	R_{PH2S}
$Fe^{2+} + HS^- \Rightarrow FeS(s) + H^+$	R_{FeS}
$2FeOOH_{(s)} + 3H_2S_{(aq)} => S^0_{(s)} + 2FeS_{(s)} + 4H_2O$	R_{S0}
$SO_4^{2-} \Rightarrow R\text{-}SH$	R_{Assim}
$4\ S^0_{(s)} + 4H_2O => SO_4^{2-} + 3HS^- + 5H^+$	R_{Disp}
$FeS + S^0 => FeS_2$	R_{FeS+S}
$FeS + H_2S => FeS_2 + H_2$	R_{FeS+HS}

Table 1.3 *Kinetics of the reactions included in the model. Kinetics of the reactions included in the model. K_{FeS}, K_{H2S}, and k_{Disp} are the equilibrium constants for FeS precipitation, acidity constant for H₂S, and rate constant of S^0 disproportionation, respectively.*

Reaction	Rate expression
Sulfide Oxidation	$R_{SOX} = k_{SOX}[O_2][H_2S]$
Sulfate production from R-O-SO₃H	$R_{PSO4} = 0.6 * \frac{S}{C} V_m$; Where S/C is the sulfur to carbon molar ratio
Sulfide production from R-SH	$R_{PH2S} = 0.4 * \frac{S}{C} V_m$; Where S/C is the sulfur to carbon molar ratio
Aerobic Respiration	$R_{OX} = \dfrac{V_m[O_2]}{K_i + [O_2]}$
Iron Reduction	$R_{FeOOH} = \dfrac{V_m[FeOOH]}{K_{FeOOH} + [FeOOH]} \dfrac{K_i}{K_i + [O_2]}$
Sulfide Precipitation	$R_{FeS} = k_{FeS}(\dfrac{\Omega}{K_{FeS}} - 1)$ $\Omega = \dfrac{[Fe^{2+}][HS^-]}{[H^+]}$ $[HS^-] = \dfrac{[H_2S]}{1 + [H^+]K_{H_2S}}$
FeS₂ precipitation with S⁰	$R_{FeS+S} = k_{FeS+S}[FeS][S^0]$
FeS₂ precipitation with H₂S	$R_{FeS+HS}k_{FeS+HS} = [FeS][H_2S]$
Sulfate Reduction	$R_{SR} = \dfrac{V_m[SO_4^{2-}]}{K_m + [SO_4^{2-}]} \dfrac{K_i}{K_i + [O_2]}$
Assimilatory Sulfate Reduction	$R_{Assim} = k_{Assim}(R_{FeOOH} + R_{OX} + R_{SR})$
Elemental Sulfur Formation	$R_{S0} = k_{S0}[FeOOH][H_2S]$
Elemental Sulfur Disproportionation	$R_{Disp} = k_{Disp}[S^0](1 - \dfrac{[H_2S]}{[H_2S]_{stop}})$ For [H₂S] < [H₂S] $_{stop}$ 0 For [H₂S] ≥ [H₂S] $_{stop}$

In contrast to previous models (e.g. Katsev et al. 2006), the present model considered sulfur compounds of intermediate oxidation state, as they potentially can play a role in the sulfur cycle and the production of sulfate (Schulz and Zabel 2006). In marine and lake sediments, these compounds are typically produced through the oxidation of hydrogen sulfide via several pathways (Table 1.5). We considered the oxidation of sulfide by iron oxides, which results in the formation of elemental sulfur. Production of S^0 through other pathways (Table 1.5) is thermodynamically unfavorable at the low sulfide levels considered in our model (Table 1.5), though some become favorable under higher levels of sulfide (>100 µM) (Canfield et al. 2005; Couture et al. 2016). The model did not consider thiosulfate and sulfite (Canfield and Andreas 1996), as their contributions to sulfate production are expected to be minor: at low sulfide availability sulfide-oxidizing bacteria are expected to oxidize sulfide directly to sulfate without intermediate reactions (Pfennig 1975; Canfield and Andreas 1996). Although in marine sediments concentrations of thiosulfate may be of the same order of magnitude or even higher than sulfide concentrations (Zopfi et al. 2004), in oligotrophic lakes with deep oxygen penetration, reoxidation of sulfide is suggested to be more complete, with fewer intermediate products (Urban et al. 1994).

The rate of organic sulfur mineralization, a multi-step process, was simulated as proportional to the rate of organic C mineralization with a fixed S:C ratio. In the absence of empirical information linking the rates of organic carbon mineralization and rates of organic sulfur mineralization, the release of oxidized and reduced S compounds from organic matter was assumed to occur stoichiometrically. While in soil literature

24

enzymatic hydrolysis was hypothesized to be affected by SO_4^{2-} concentrations (Scherer 2009), such inhibition was not demonstrated in sediments and was not considered in the model for lack of any quantitative information on sulfate levels at which inhibition might occur. The R-O-SO_3H groups were assumed to constitute ~60% of the organic sulfur pool, based on results in oligotrophic lakes (Prietzel et al. 2011). Their hydrolysis and mineralization was assumed to generate SO_4^{2-}. The rest of organic sulfur (R-SH groups, ~40%) such as in thiols and amino acids was expected to generate sulfide. The numerical significance of this partitioning between the oxidized vs reduced forms of organic sulfur is insignificant in well oxygenated systems like Lake Superior, as most of the reduced organic sulfur becomes aerobically oxidized and converted to sulfate within the sediment oxic zone. As the S:C ratios in lake sediments are not well established, the S:C ratio was varied in the model within a range of literature values for seston (Urban et al. 1999), which was assumed to be the major source of organic S to sediments (Urban 1994). In contrast to marine ecosystems where S:C ratios are relatively consistent (0.008-0.014 wt/wt; Burdige 2007), the S:C ratios in freshwater sediments vary within a wide range (0.03-0.40 wt/wt; King and Klug 1982; Nriagu and Soon 1985; Urban 1994; Fagerbakke et al. 1996). This variability in organic S is likely driven by a combination of organism physiology (specific sulfur requirements for biomass) and environmental conditions such as nutrient limitation. For example, in environments such as Lake Superior, P limitation in plankton results in a substitution of sulfolipids (and N-based lipids) for phospholipids (Bellinger et al. 2014), amplifying the sulfur deposition into sediments.

25

As the FeOOH profiles were not explicitly modeled, the distributions of FeOOH were specified in the model explicitly (see Fig. 4), to mimick the measured profiles of 0.5 M HCl-extractable ferric iron (Roden and Wetzel 2002) in Lake Superior sediments (Li 2014). The boundary conditions for hydrogen sulfide, oxygen, sulfate, and dissolved iron were chosen as fixed-concentration at the sediment-water interface (SWI) (Table 1.4) and zero-gradient in the bottom of the integration domain. Equations (1.1) were iteratively solved in Matlab as a boundary-value problem using the ″bvp4c″ function.

__Table 1.4__ Parameters for reactive transport modeling

Parameter	Symbol	Value	Unit	Typical Range	Ref.
Diffusion coefficient of sulfate	D_{SO4}	300	$cm^2/year$	200-400	Canfield 2006
Diffusion coefficient of sulfide	D_{H2S}	500	$cm^2/year$	400-600	Burdige 2006
Diffusion coefficient of oxygen	D_{O2}	500	$cm^2/year$	300-500	Burdige 2006
Sulfide oxidation rate constant	k_{OXD}	160	$uM^{-1}year^{-1}$	16-1600	Katsev et al. 2004
FeS precipitation rate constant	k_{FeS}	10^{-5}	$mol\ g^{-1}\ yr^{-1}$	10^{-7}-10^{-5}	Katsev et al. 2004
FeS equilibrium constant	K_{FeS}	10^{-4}	M	-	Dyrssen & Kremling 1990
Rate constant for FeS_2 precipitation with S^0	k_{FeS+S}	10^4	$mol^{-1}g\ yr^{-1}$	-	Dyrssen & Kremling 1990
Rate constant for FeS_2 precipitation with H_2S	k_{FeS+HS}	0.003	$uM^{-1}year^{-1}$	-	Dyrssen & Kremling 1990
Sulfur-to-carbon ratio in organic matter	S:C	0.007	mol/mol	0.002-0.015	Urban et al. 1999

Acid-base equilibrium constant for H_2S	K_{H2S}	2.48×10^{-7}	-	-	Dyrssen & Kremling 1990
S^0 formation rate constant	k_{S0}	8×10^{-3}	$uM^{-1}year^{-1}$	$10^{-5}-10^{-1}$	Van Cappellen & Wang 1996
Assimilatory reduction of sulfate rate constant	k_{Assim}	10^{-4}	-	-	-
S^0 disproportionation rate constant	k_{Disp}	0.01	$year^{-1}$	0.001-0.1	Jourabchi 2007
Threshold H_2S concentration for disproportionation	$[H_2S]_{stop}$	10	mM	-	Jourabchi 2007
Monod constant for SO_4^{2-} reduction	K_m	20	uM	5-25	Katsev et al. 2004
Monod constant for O_2 (inhibition constant)	K_i	1	uM	0.5 – 2	Katsev et al. 2004
Monod constant for FeOOH reduction	K_{FeOOH}	20	umol/g	15-30	Katsev et al. 2004
Sulfate at SWI (sediment water interface)	$[SO_4^{2-}]$	40	uM	-	-
Sulfide at SWI	$[H_2S]$	0	uM	-	-
Oxygen at SWI	$[O_2]$	350	uM	-	-
Iron at SWI	$[Fe^{2+}]$	0	uM	-	-
$Fe(OH)_3$ concentration scale	$[Fe(OH)_3]_1$	10	mg/g	-	-
Density of dry sediment	ρ_s	2.65	g/cm^3	-	-
Grid size	dz	6.67×10^{-3}	cm	-	-
pH	pH	6	-	-	Li 2014
Organic Matter content	OM	3.5	wt%	3-5	Li 2014
Burial Velocity at the bottom	V_{burial}	0.05	$cm.yr^{-1}$	0.04-0.08	Li 2014
Initial Carbon age	C_{age}	15	year	-	O'Beirne et al. (2017); Katsev & Crowe 2015

Table 1.5 *Thermodynamic favorability of reactions for elemental sulfur formation. Gibbs free energy at in situ conditions, ΔGr, was calculated as $\Delta Gr = \Delta G0 \neg + RTlnQ$, where $\Delta G0$ is the standard-state free energy, Q is the reaction quotient, T is temperature (277.15 K), and R is the ideal gas constant (8.314 J/mol-K)*

Reaction	ΔG^0 (kJ/ mol)	ΔGr(k J/mol)	Concentration Ranges					
			[H₂S] or [HS⁻] (µM)	[H⁺] (µM)	[Fe²⁺] (µM)	[Mn²⁺] (µM)	[CO₂] (µM)	[HCO₃⁻] (µM)
$2FeOOH_{(s)} + 3H_2S_{(aq)} => S^0_{(s)} + 2FeS_{(s)} + 4H_2O$	-79	-57	10	-	-	-	-	-
$MnO_{2(s)} + HS^-_{(aq)} + 3H^+_{(aq)} => Mn^{2+}_{(aq)} + S^0_{(s)} + 2H_2O$	-52	34	10	1	-	40	-	-
$H_2S_{(aq)} + 4CO_2 + 2Fe(OH)_{3(s)} => 2Fe^{2+}_{(aq)} + S^0_{(s)} + 2H_2O + 4HCO_3^-$	98	104	10	-	40	-	10	1000
$Fe_3O_{4(s)} + HS^-_{(aq)} + 7H^+_{(aq)} => 3Fe^{2+}_{(aq)} + S^0_{(s)} + 4H_2O$	171	182	10	1	40	-	-	-
$HS^-_{(aq)} + 2Fe(OH)_{3(s)} + 5H^+_{(aq)} => 2Fe^{2+}_{(aq)} + S^0_{(aq)} + 6H_2O$	78	31	10	1	40	-	-	-

1.3.3. Lake Superior sulfur budget

The geochemical budget of sulfur for the water column of Lake Superior was calculated using values from literature and sediment fluxes calculated from this work (Table 1.6). Sulfate inputs from watershed included discharges through St. Louis River, Pigeon River, White River, Kaministiquia River, Nipigon River, and Michipicoten River (Neff and Nicholas 2005). Atmospheric deposition was calculated by extrapolating inputs (Minnesota Pollution Control Agency 2002) to the area of Lake Superior. Outflow with St. Mary's River was calculated by multiplying the sulfate concentration in Lake Superior (38 μM) by the average outflow rate of 68 km^3/year. Lakewide fluxes in/out of sediment were estimated from fluxes calculated in this work by assuming 30 and 70% contribution from, respectively, high and low sedimentation areas. Sedimentation of organic sulfur was calculated by multiplying the S:C ratio (0.007) by the average organic carbon sedimentation flux (Li et al. 2012). As the terrestrial contribution to the bulk POM in Lake Superior was estimated at 5% (Zigah et al. 2012), the input of particulate organic sulfur to the lake from watershed was calculated as 5% of S_{org} sedimentation. The rate of sulfate buildup in the lake was calculated from the rate of historical increase in the water column sulfate concentration (Chapra et al. 2012).

Table 1.6 *Estimated sulfur budget in Lake Superior water column (mol s^{-1}).*
Positive=inputs, negative=outputs.

Sulfate input from watershed	375
S input from atmosphere	5
Organic S input from watershed	3
Outflow	-100
Sediment exchange fluxes	
Organic S sedimentation	-54
Sulfate flux in	-30
Sulfate flux out	4
Total	**203**
Buildup	192

1.4. Results

The distributions of porewater sulfate in the sediments of Lake Superior (Fig. 1.3)

exhibit strong spatial heterogeneity, similarly to the previously described distributions of

organic carbon, oxygen, and nitrogen species (Li and Katsev 2014; Li et al. 2012). As in

Lake Superior sediment composition and appearance often vary even within the same

oceanographic station (~100 meters radius) (Li et al. 2012), differences among the

profiles obtained from different cruises (Table 1.1) are more likely to reflect spatial rather

than temporal variability, as sulfate concentrations in the overlying water remain largely

unchanged (Fig. 1.3). In a striking departure from commonly observed diagenetic profiles

where sulfate concentrations decrease monotonically downward from the sediment-water

interface (e.g. Katsev and Dittrich 2013), porewater sulfate distributions (Fig. 1.3) in

Lake Superior often exhibit peaks at or several mm below the interface. The sulfate

concentrations below the peaks typically decrease into the anoxic sediments. A notable exception is Sta. NIP where sulfate concentrations continue to increase with depth. At this station, the sediment below about 5 cm depth consisted of dense cm-scale varves characteristic of organic-poor post-glacial sedimentation in Lake Superior (Johnson et al. 2012). Whereas in the offshore areas of Lake Superior oxygen typically penetrates into sediment by 3-12 cm (Fig. 1.4; Li et al. 2012), at this location the penetration depth was measured at 42 cm, creating an exceptionally deep oxidized zone. At locations where sulfate concentrations were higher in porewater than in overlying water (Fig. 1.3), the resultant diffusive effluxes of sulfate were calculated in a range from 0.007 mmol m^{-2} d^{-1} at Sta. EM to 0.047 mmol m^{-2} d^{-1} at Sta. TB. At several high-sedimentation sites (e.g., Sta. NB and several cores at Sta. IR), sulfate concentrations were higher in the overlying waters than in the sediments (Fig. 1.3). The corresponding sulfate fluxes into the sediment were 0.026 mmol m^{-2} d^{-1} at Sta. IR and 0.010 mmol m^{-2} d^{-1} at Sta. NB. Sulfate typically penetrated several cm below the penetration depths of O_2 and NO_3 (described in Li and Katsev 2014). In sediments with deep oxygen penetration, sulfate penetrations were also deep (e.g., Sta. WM, CM, and several cores at Sta. FWM, ED, SW) (Fig. 1.3).

The model reproduced the measured distributions of sulfate, oxygen and organic carbon (OC) (Fig. 1.4). By considering the in-sediment generation of sulfate from organic S source, it also replicated the peaks in dissolved sulfate observed within the oxic zone (e.g., Sta. ED, and EM). In fitting the data, parameters were selected as to provide a satisfactory fit against the whole dataset, rather than fit specific features of a single depth profile. The obtained profiles were used to calculate the rates of individual reactions:

31

sulfate reduction, hydrogen sulfide reoxidation, iron sulfide precipitation, and elemental sulfur formation and disproportionation (Tables 1.2 and 1.3). Values of the depth integrated rates at each station are presented in Table 7. The depth integrated SR rates (Eq. 1.1) range from 0.004 mmol m^{-2} d^{-1} (Sta. NIP) to 0.2 mmol m^{-2} d^{-1} (Sta. IR), with the average of 0.084 mmol m^{-2} d^{-1}. Based on the previously determined rates of total sediment respiration (Li et al. 2012), sulfate reduction in Lake Superior sediments accounts for 0.6 – 5% of organic carbon mineralization. Sulfate reduction rates were higher at locations with high sedimentation rates (e.g. Sta. IR; average 0.18 mmol m^{-2} d^{-1}) than at locations with low sedimentation rates (average 0.05 mmol m^{-2} d^{-1}). The depth-integrated rates of sulfate production from organic source ranged between 0.07 and 0.008 mmol m^{-2} d^{-1} (average 0.034 mmol m^{-2} d^{-1}). The depth distributions of these rates (Fig. 1.4) indicate that the production of inorganic sulfur from S$_{org}$ is most significant in the upper layers of sediment where the rate of OC mineralization is high. In Lake Superior, this sediment zone (0-5 cm) is typically well oxygenated (Fig. 1.4). The depth integrated rates of sulfide oxidation ranged from 0.005 mmol m^{-2} d^{-1} (at Sta. NIP) to 0.09 mmol m^{-2} d^{-1} (at Sta. IR). The rates of elemental sulfur formation were significantly lower, ranging from 0.0001 mmol m^{-2} d^{-1} (Sta. NIP) to 0.0009 mmol m^{-2} d^{-1} (Sta. IR); the rates of FeS precipitation ranged from 0.009 (Sta. FWM) to 0.014 mmol m^{-2} d^{-1} (Sta. IR). The rates of elemental S disproportionation were low (0.00006 - 0.0006 mmol m^{-2} d^{-1}).
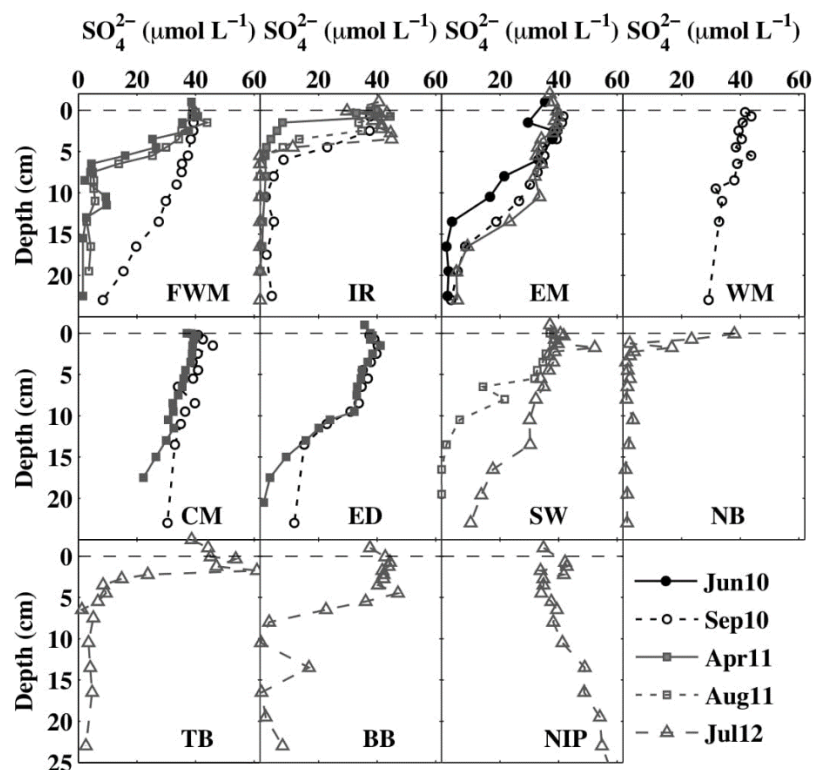
Figure 1.3 *Vertical distributions of porewater sulfate in Lake Superior sediments. Vertical distributions of porewater sulfate in Lake Superior sediments. Horizontal and vertical dashed lines correspond to sediment water interface (SWI), and sulfate level at SWI.*

1.5. Discussion
1.5.1. The in-sediment production of sulfate

The presence of sub-interface peaks in the porewater sulfate profiles at many locations in Lake Superior indicates that the flux of sulfate there is directed from sediment into the overlying water column. As in that situation the water column cannot be a source of sulfate for the sediment, this suggests that the sulfate for sediment sulfate

reduction must be generated entirely from an internal sedimentary source of sulfur. The clearest case of sulfate production within the sediment is at Sta. NIP. The sediment at this location consists of glacial lacustrine varved clays underlying a thin layer of modern sediment (0-5cm). This old (>8000 yr; Johnson et al. 2012) sediment contains little organic matter (~0.2 wt%; Johnson et al. 2012) and has low O_2 uptake, which results in an exceptionally deep oxygen penetration (42 cm). The sulfate concentrations there increase into the sediment (Fig. 1.4), indicating that sulfate continues to be produced within the sediment during diagenesis. We hypothesize that in Lake Superior the internal sedimentary source of dissolved sulfate is predominantly the organic sulfur deposited to the sediment surface with settling organic matter.

Contribution of groundwater and dissolution of detrital sulfate minerals such as gypsum (the most abundant sulfate mineral) or other trace mineral sulfates, in principle, may also serve as internal sources of sulfate in some environments. In Lake Superior, however, the deep sediments are underlain by bedrock and the groundwater sources can be excluded (Grannemann et al. 2000). Regarding the dissolution of sulfate minerals, freshwater systems with low levels of sulfate and calcium are undersaturated with respect to gypsum: based on the available water column concentrations (Chapra et al. 2012), the corresponding ratios of the ion activity products (IAP) to solubility products (K_{sp}) in Lakes Michigan, Baikal, and Superior are respectively 0.007, 0.003, and 0.0006; so potentially gypsum could become a source of sulfate if its particles survive dissolution in the water
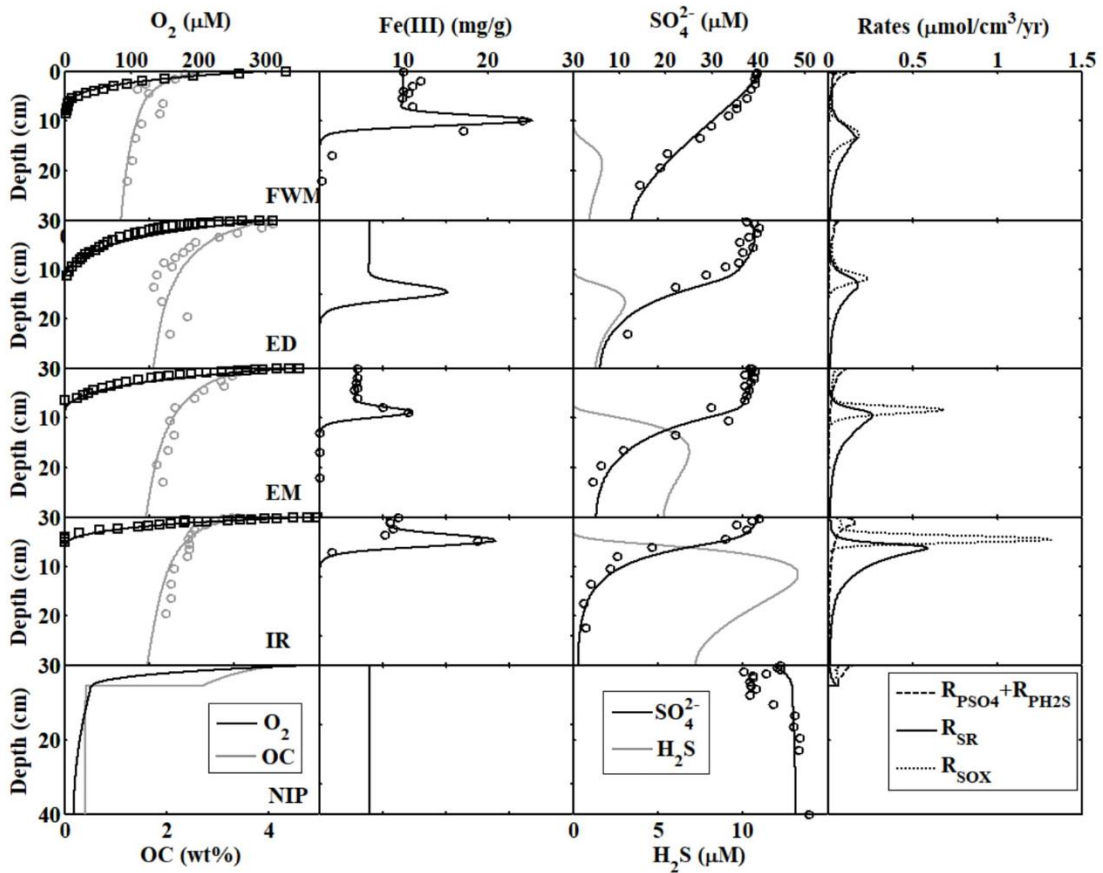
Figure 1.4 *Sediment profiles of oxygen, organic carbon (OC), HCl (0.5 N)- extractable iron, sulfate, sulfide and rates of organic sulfur hydrolysis (RPSO4+RPH2S), sulfate reduction (RSR), and sulfide re-oxidation(RSOX) for five stations in Lake Superior. Symbols correspond to measured values and lines are results from the model.*

column. Sulfate also can be incorporated into authigenic minerals such as calcium carbonates and be subsequently released upon their dissolution in sediments. The available data on the dissolution kinetics of typical sulfur minerals (Katsev et al. 2004) suggest that these processes may supply sulfate to porewaters for up to several thousand years. In lakes with high abundances of sulfur-bearing minerals in the catchment, such as Lake Michigan (Black 1997), their dissolution is thus likely to amplify the sub-interface

peaks in porewater sulfate (e.g. Thomsen et al. 2004). However, as Lake Superior is surrounded by non-carbonate terrain with low gypsum and calcium levels (Dell 1971), the contributions of mineral sulfur sources to sulfur sedimentation are expected to be insignificant. While data on trace mineral sulfur levels in Lake Superior sediments are absent, the fact that our model reproduces the observed sulfate peaks using realistic organic S:C ratios strongly argues for organic sulfur being the dominant source.

Peaks in the porewater sulfate profiles are not unique to Lake Superior and have been reported in other systems (Och et al. 2012, 2016; Thomsen et al. 2004; Sass et al. 1997; Jørgensen 1990). In particular, in Lakes Baikal (Och et al., 2012, 2016), and Michigan (Thomsen et al. 2004), where sulfate and oxygen levels are similar to those in Lake Superior, sediment porewaters exhibited similar peaks below the interface, indicating sulfate fluxes out of the sediment and suggesting an in-sediment source of sulfate. In Lake Baikal, sulfate peaks were also found within the deeper reduced sediment (25cm; Och et al. 2012; 2016), coincident with iron rich layers, and were hypothesized to have resulted from re-oxidation of sulfide by Fe(III) in a multi-step reaction. Given that the sediment at that location was a source of dissolved S to the water column, the ultimate source of S at that depth within the sediment must have been particulate sedimentation. In principle, peaks in dissolved sulfate may also reflect non-steady state conditions, for example in a situation where bottom water sulfate levels fluctuate seasonally. However, as sulfate levels in the bottom waters of large lakes, such as Lake Superior or Lake Baikal, are very stable over interannual time scales, and with little

evidence for seasonal variability in porewater sulfate (Fig. 1.3), non-steady state effects are unlikely to explain these observations.

In Lake Superior, in addition to strongly affecting the sediment sulfur cycle, organic S also plays an important role in balancing the sulfur budget (Table 1.6). Mass balance budget calculation indicates that, contrary to the paradigm that sulfate behaves as a conservative hydrological tracer (Michel et al. 2002), sulfate incorporation into organic S and its subsequent sedimentation account for 32% of the total S outputs from the water column (Table 1.6).

Table 1.7 *Depth integrated rates of sulfate reduction, hydrogen sulfide reoxidation, production of sulfate and sulfide via Sorg hydrolysis, elemental sulfur disproportionation and formation, and iron sulfide precipitation, and the contribution of S_{org} to sulfate reduction (η), for individual stations in Lake Superior.*

Stations	Rates (mmol m^{-2} d^{-1})							η
	R_{SR}	R_{SOX}	R_{PSO4}	R_{PH2S}	R_{Disp}	R_{S0}	R_{FeS}	
IR	0.2	0.09	0.07	0.04	0.0006	0.0009	0.014	0.73406
FWM	0.05	0.035	0.012	0.008	0.0002	0.0005	0.009	0.87146
EM	0.095	0.05	0.05	0.03	0.0005	0.0008	0.012	1.06844
ED	0.07	0.045	0.03	0.02	0.0003	0.0007	0.01	1.11296
NIP	0.004	0.005	0.008	0.005	0.00006	0.0001	-	3.26223
Average	0.0838	0.045	0.034	0.0206	0.000332	0.0006	0.01125	-

1.5.2 Contribution of S_{org} to sulfate reduction

To quantify the contribution of the internal sediment organic sulfur source to the production of sulfate, we define a parameter η as the ratio of the depth-integrated rates of sulfate generation and sulfate reduction. To account for the in-sediment recycling of sulfur, the latter is corrected (using the stoichiometry in Table 1.2) for the disproportionation of elemental sulfur and re-oxidation of hydrogen sulfide that is produced by sulfate reduction in the sediment anoxic zone. Sulfide produced from the mineralization of reduced organic sulfur is oxidized predominantly within the sediment oxic zone and contributes to sulfate generation there. Using R^* as the notation for depth-integrated rates of the respective reactions (Table 1.2), the fraction of the sediment sulfate reduction that is supported by S_{org} is thus defined as

$$\eta = \frac{R^*_{PSO4} + R^*_{PH2S}}{(R^*_{SR} - (R^*_{SOX} - R^*_{PH2S}) - 0.25 * R^*_{Disp})} \tag{1.4}$$

Values of η greater than one corresponds to a situation where sediment acts as a source of sulfate to the water column, as all sulfate for SR is ultimately sourced from organic S. For η < 1, the flux of sulfate is directed into the sediment and sediment SR is supported by both water-column and sediment-produced sulfate. The fraction of sulfate originated from the external inorganic source is given by 1-η. The values of η for individual locations in Lake Superior were calculated from the model-fitted profiles in Fig. 1.4. The contribution of organic source to sulfate reduction is highest at Sta. NIP: η = 3.26 (Table 7). At Sta. FWM and IR, the η values are respectively 0.87 and 0.73 (Table 7), i.e. 87% and 73% of SR are supported by organic-sourced S. At Sta. ED and EM, they are,

respectively, 1.11 and 1.07 (Table 1.7), indicating that the in-sediment sulfate reduction is supported there entirely by organic-sourced S.

To estimate the potential contribution of organic S to sulfate reduction rates (SRR) in other environments, we extrapolated our results by varying in the model the water column concentrations of oxygen (20-350 µM) and sulfate (10-1000 µM), as well as the organic sulfur-to-carbon ratio (0.002-0.02). The sediment organic matter content and sedimentation rate were kept constant at values typical for Lake Superior (Table 1.4). Fig. 1.5 illustrates how the contribution of organic sulfur to SRR, η, varies with sulfate and oxygen concentrations, for a reasonable range of organic S:C ratios. Simulations reveal that the conditions in Lake Superior are near a threshold for the formation of porewater sulfate peaks, in agreement with the observed sulfate profiles (Fig. 1.4) and the η values around 1. In oligotrophic lakes characterized by low sulfate levels (<100 µM) and high levels of benthic oxygen (O_2>300 µM), production of sulfate from organic source is predicted to support more than 80% of sulfate reduction (Fig. 1.5). This finding is in strong contrast to the previously suggested (King and Klug 1980, 1982; Marnette et al. 1992) minor role (<10%) of S_{org} in supporting lacustrine microbial sulfate reduction. At higher sulfate levels, the contribution of external inorganic sulfur to SR increases, and the relative importance of the organic S source decreases. At >500 µM of sulfate, for oxygen levels <200 µM, S_{org} contributes <15% to sulfate reduction, though in well oxygenated systems ($O_2 > 300uM$) its contribution could be still significant, up to 60% (Fig. 1.5).
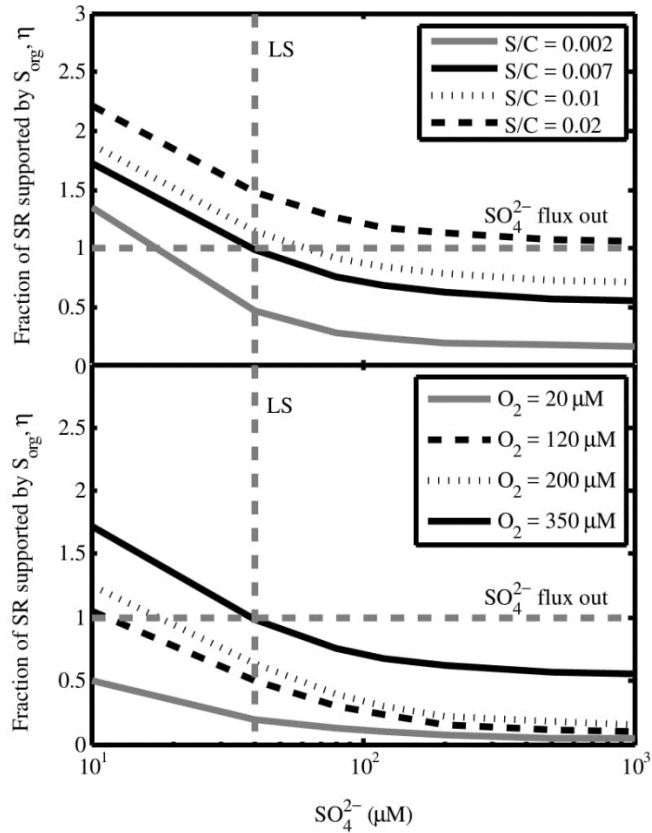
Figure 1.5 *Simulated contribution of Sorg to sulfate reduction in Lake Superior-type sediments. Vertical axis is the ratio of the depth-integrated rates of sulfate production from S$_{org}$ and sulfate reduction (corrected for sulfide re-oxidation and S^0 disproportionation). Ratios above 1 correspond to a situation where the excess sulfate effluxes into the water column. (a) Lines correspond to S:C molar ratios in settled material, for oxygen level of 350 μM. (b) Lines correspond to different oxygen concentrations at sediment water interface, for the S:C ratio of 0.007. Vertical line (LS) marks the sulfate level in Lake Superior.*

40

1.5.3 Sulfate reduction rates

While S_{org} can be a dominant source of sulfate, the provenance of sulfate from within sediment rather than from overlying water does not automatically mean a strong effect on sulfate reduction rates. Sulfate is generated from S_{org} predominantly in the sediment's upper 1-2 cm (Fig. 1.4) where the abundance of labile OC assures high mineralization rates. The in-sediment source of sulfate is thus spatially proximate to the water column, whereas the reduction takes place deeper in the sediment. In Lake Superior, for example, the sulfate reduction zone begins 4-8 cm below the interface, a few mm below the depth of oxygen penetration. Near that redox boundary, oxidation of sulfide by ferric iron constitutes an additional source of sulfate (Fig. 1.4). At several stations, this is manifested in kinks in the sulfate profiles (e.g. at 10 cm at Sta. ED (Fig. 1.3, 1.4): the increased slope indicates that the downward fluxes of sulfate into the anoxic zone exceed the downward fluxes in the oxic layer. Sulfate is typically depleted to μM levels within several centimeters below the oxic zone.

The effect of the in-sediment production of sulfate on total (depth integrated) SR rates can be evaluated by comparing the model results that are obtained with vs. without the S_{org} contribution (Fig. 1.6). While sulfate production from S_{org} alleviates the limitation imposed by low sulfate availability, the effect is only significant at sulfate levels below about 500 μM. At 40 μM level characteristic of Lake Superior, the S_{org} increases SRR by about 20%. The effect on depth integrated SRR is thus relatively minor for most environmentally relevant sulfate levels. Simulations also reveal that, irrespective

41

of the role of S_{org}, sulfate becomes a limiting factor for sulfate reduction only at concentrations below about 500 µM. At higher levels, the SR rates are limited by the amount and reactivity of organic carbon. This is reflected in the similarity of the sulfate reduction rates in Lake Superior and other freshwater lakes to those in marine sediments (Fig. 1.7a): despite the three orders of magnitude difference in sulfate concentrations (5-500 µM in freshwater vs. 28,000 µM in marine environments), the SRR are similar among sediments of similar sedimentation rates. The higher concentrations of OC in freshwater sediments make up for the SRR limitation imposed by lower sulfate. Correspondingly, in Lake Superior sulfate reduction accounts for a much smaller fraction (0.6–5%) of the sedimentary organic carbon mineralization (Li 2014; Li et al. 2012) than in marine environments (e.g. Katsev et al. 2007). The availability of OC affects the SR rates even at low sulfate levels (<500 µM), especially for low carbon concentrations (Fig. 1.6). The low-sedimentation areas (typically offshore) in Lake Superior have lower rates of sulfate reduction (average 0.012 mmol m^{-2} d^{-1}) than high-sedimentation nearshore areas (average 0.085 mmol m^{-2} d^{-1}).

As the organic carbon amount within the sulfate reduction zone, its reactivity, and the concentration gradients of sulfate are all affected by the position of the sulfate reduction zone below the interface, the SRR becomes correlated with the penetration depth of oxygen. As oxygen penetration deepens, both the amount and reactivity of organic matter that reaches the sulfate reduction zone decrease, while sulfate diffusion is slowed by a decreasing gradient. As a single parameter that reflects these changes, oxygen penetration depth (OPD) is expected to be a better predictor of SRR than organic

sedimentation alone. Model simulations (Fig. 1.7b) illustrate that the relationship between the SRR and OPD holds for a number of systems that range from well oxygenated low-sulfate sediments in Lake Superior and other freshwater lakes, to marine sediments in a range of water depths. To obtain the model datapoints in Fig. 1.7b, model parameters that affect the SRR were varied within their corresponding wide ranges: sedimentation rate 0.01-0.2 g cm^{-2} yr^{-1}, organic carbon content 1-10 wt%, SWI oxygen concentration 0-350 μM, and SWI sulfate concentration 40-10000 μM. The produced correlations suggest that, irrespective of the contribution of S$_{org}$, the OPD can be used as a good predictor for sulfate reduction rates where oxygen penetration exceeds several mm (Fig. 1.7b).
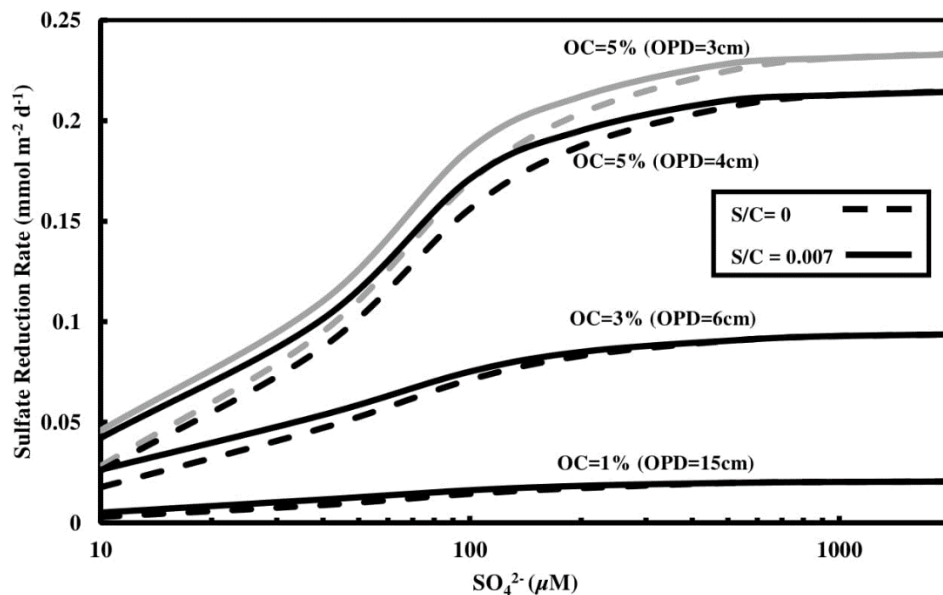
Figure 1.6 Simulated effect of sulfate concentration, organic matter content (OC), and Sorg mineralization on the depth-integrated rates of sulfate reduction. Oxygen level at the sediment water interface is 350 μM (black; typical in Lake Superior), and 200 μM (gray; near saturation value in seawater).

1.5.4 Implications for other environments

In addition to low-sulfate sediments of freshwater lakes, the organic sulfur may be an important source of substrates for the sulfate reducing microbial communities in deep subsurface, below the depth of sulfate penetration. In recent studies it was repeatedly shown that sulfate reducers survive over long times of burial (D'Hondt et al. 2002; D'Hondt et al. 2004; Schippers et al. 2005). A conclusive explanation, however, is missing for how these organisms survive. An order-of-magnitude calculation suggests that the energy derived from the S_{org}-supported sulfate reduction may be sufficient to support communities of sulfate reducers in the deep subsurface even in the absence of external sources of sulfate. For example, a 100,000 years old sediment might contain 0.1 wt% of organic carbon, with mineralization rate characterized by the first-order reactivity constant on the order of 10^{-5} y^{-1} (Middelburg 1989; Katsev and Crowe 2015). For sediment porosity of 0.6, solid sediment density of 2.65 g cm^{-3}, and the orgS:orgC molar ratio of 0.005, such sediment is expected to support SRR on the order of 10 pmol cm^{-3} y^{-1}. At the cell density of 10^3 cells cm^{-3} (near detection limit for common methods), this translates into a cell-specific rate of 1 fmol y^{-1} $cell^{-1}$, which is an order of magnitude greater than the minimum rates required for cell maintenance (D'Hondt et al. 2004). Under standard conditions, these rates of sulfate reduction would provide cells with 80 picojoules y^{-1} $cell^{-1}$ of energy.

The significant role of S_{org} in shaping the S cycling in low sulfate environments may also have important implications for the interpretations of the geological records

from ancient oceans. Before the Great Oxygenation Event (GOE) about 2.35 Ga ago, oceanic sulfate levels were low, possibly below 10 μM (Crowe et al. 2014). Bottom waters were largely anoxic, with a possible exception of oxygenated "oases" in shallow environments (Olson et al. 2013). After the GOE and before 0.5 Ma, Proterozoic oceans were characterized by sulfate levels that were similar to those in modern lakes, below 1 mM (Canfield and Farquhar 2009); oxygen levels could reach tens of μM (Lyons et al. 2014). Our knowledge about the sulfate levels in those early oceans comes from the analyses of the isotopic S signals preserved in sedimentary sulfides and their inferred isotopic differences from seawater sulfate (Crowe et al. 2014). The reconstructions of the sulfate levels under which those signatures have formed, however, assumed that the sedimentary sulfate reduction was fueled by the sulfate from seawater (Cameron 1982; Habicht et al. 2002; Canfield and Farquhar 2009). The results above suggest that, for oxygen levels <20 μM and sulfate <100 μM, production of sulfate from organic source (including reoxidation of organic-sourced sulfide) could have supported up to 40% of sediment sulfate reduction. This may necessitate a reinterpretation of the isotopic S records. Importantly, in addition to altering the diagenetic cycle of S by serving as an in-sediment source for biogeochemical cycling, organic sulfur may affect the isotopic composition of S directly, as the hydrolysis of organic S compounds is likely to generate isotopic fractionation (Kharasch 2013). The magnitude of such fractionation is currently not constrained but thermodynamic estimates suggest that it may be significant, on the order of 15‰ (Kharasch 2013). For comparison, isotopic fractionations occurring during

45

microbial sulfate reduction at sulfate concentrations below 100 μM are thought to be on the order of 5-30‰ (Bradley et al. 2016).
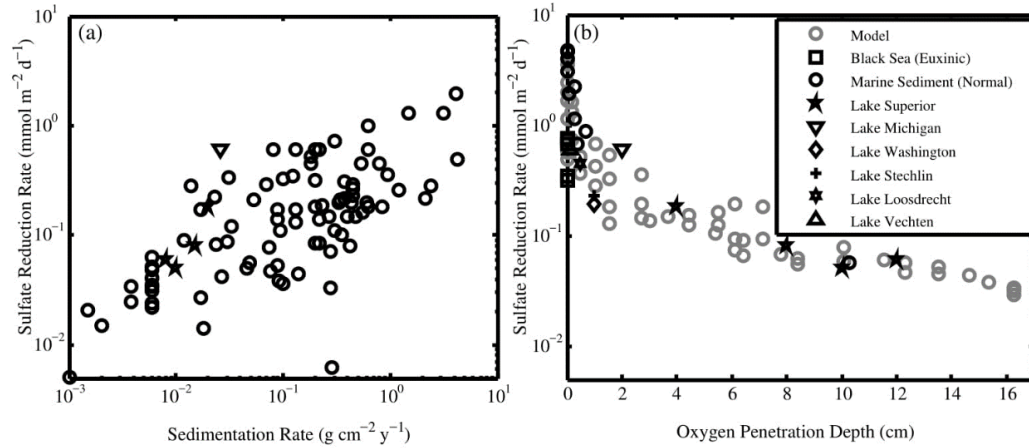
Figure 1.7 *The depth-integrated rates of sediment sulfate reduction vs. sedimentation rate (a) and oxygen penetration depth (b). Data are from Lake Superior (this study), marine sediments (Jørgensen1982; Vaynshteyn et al. 1984; Christensen et al. 1984; Canfield 1989; Sagemann et al. 1998; Ferdelman et al. 1997 & 1999), Lake Michigan (Thomsen et al. 2004), Lake Washington (Kuivilal et al. 1988 &1989), Lake Stechlin (Sass et al. 1997), Lake Loosdrecht (Sinke et al. 1992), and Lake Vetchten (Steenbergen et al. 1993). Model datapoints are obtained by varying the sedimentation rate, organic carbon content, and sulfate and oxygen levels within ranges specified in the text.*

1.6. Conclusions

Organic sulfur supplied into the sediment with organic sedimentation, upon its mineralization, supplies sediment porewaters with oxidized and reduced forms of inorganic sulfur. Modeling results demonstrate that in environments such as oligotrophic lakes the sulfate produced from this internal source may dominate sediment sulfate reduction, with excess sulfate fluxing into the water column. When the sediment serves as a sink for the water column sulfate, organic sulfur may support up to 60% of sediment

sulfate reduction for the water column sulfate levels of <500 μM. Its contribution may also be potentially important in supporting microbial communities in the deep subsurface below the depth of sulfate penetration. In sulfate-poor environments, the sedimentation, mineralization, and burial of organic S compounds may strongly contribute to the geochemical cycling and overall geochemical budgets of sulfur. As the rate of the sedimentary sulfate reduction is strongly affected by the supply of reactive organic matter, organic sedimentation should be considered as an important factor for processes (e.g., methylation of mercury) that are controlled by the rates of sulfate reduction.

1.7. Acknowledgements

1.8. Organic sulfur content and composition in Lake Superior sediments

This section presents and discusses additional results from the total sulfur analyses and X-ray absorption near-edge structure (XANES) spectroscopy that were obtained after the manuscript publication.

Total sulfur in two off-shore (CM and EM) and one near-shore (IR) sediments in Lake Superior were measured by elemental analyzer (EA) at the stable isotope laboratory at Northwestern University. Depth profiles of sediment total sulfur are presented in Fig. 1.8. In the deep oxygenated zone of sediments in Lake Superior formation of pyritic sulfur and elemental sulfur are expected to be strongly inhibited, hence total sulfur is expected to predominantly represent organic sulfur. As shown in Fig. 1.8, in oxic sediment zones, total sulfur decreases with depth, concurrently with the decrease in organic carbon due to mineralization. This supports the idea that mineralization of organic sulfur releases sulfur into the porewater, potentially supporting sulfate reduction. The molar sulfur to carbon ratio does not experience much variation, suggesting that mineralization of organic matter is the main process that controls the depth profiles of total sulfur. The measured sulfur to carbon ratios are slightly higher than the value used in the model (0.007; Table 1.4), but consistent with the suggested range in freshwater sediments (Urban et al. 1999). The higher measured sulfur to carbon ratio increases the significance of organic sulfur in Lake Superior relative to the one predicted by the model.
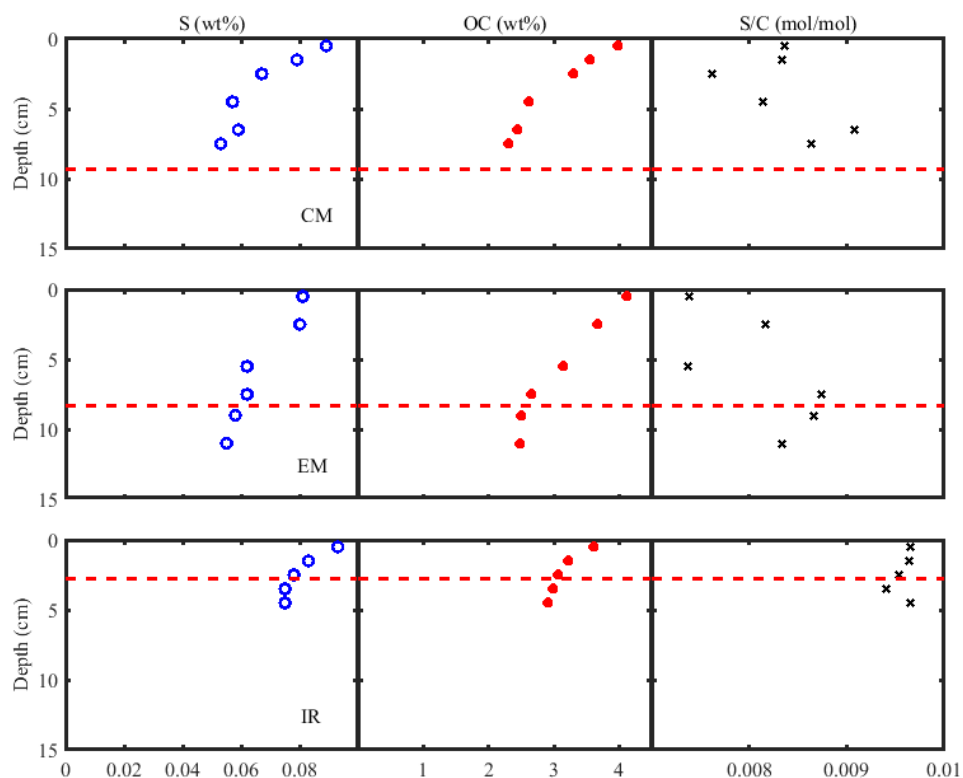
Figure 1.8 *Sediment profiles of measured total sulfur, organic carbon (OC), and molar sulfur to carbon ratio in two off-shore sediments (CM and EM) and one near-shore sediment (IR) across the Lake Superior. Vertical red dashed lines correspond to the oxygen penetration depths.*

Preliminary results from (XANES) spectroscopy suggest the predominance of oxidized organic sulfur pool in offshore sediments. The data were obtained with the help of the B. Toner's lab (Department of Soil, Water, and Climate, University of Minnesota Twin Cities). Raw data (Fig. 1.9) are similar in shape and intensity, and suggest a decrease in the sulfur amount with depth, consistent with the total sulfur analyses above (Fig. 1.8). The left part of the graph, at lower energy, corresponds to more reduced organic sulfur compounds (e.g. sulfone, thiols, cysteine), whereas the right part of the

49

graph represents more oxidized organic sulfur compounds (e.g. ester sulfate). As shown in Fig. 1.9 and Fig. 1.10, most of the organic sulfur at the CM station is in oxidized form, consistent with the assumption made in the model above (Table 1.3). Table 1.8 presents the results from fitting of XANES spectra. Fitting was performed with linear combinations of reference spectra over the energy range of 2460−2560 eV using custom beamline software. The results reveal that most of the organic sulfur at the CM station consists of ester sulfate, a highly oxidized group of compounds with the oxidation state of +6. This supports the significant role of oxidized organic sulfur in replenishing the pore water sulfate pool, which could diffuse into the anoxic zone, fueling microbial sulfate reduction. The origin and abundance of this highly oxidized organic pool are, however, poorly constrained.
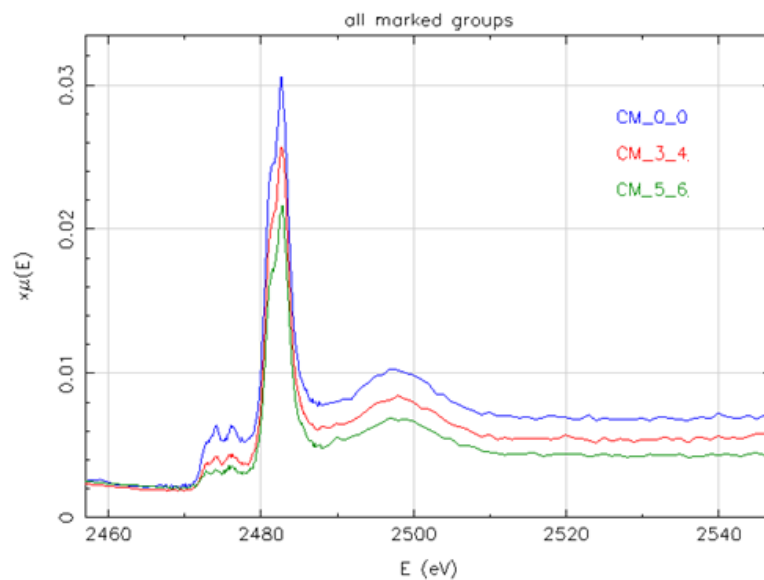
Figure 1.9 *XANES spectra for three different depth intervals (0, 3-4, and 5-6 cm) at CM station.*

50
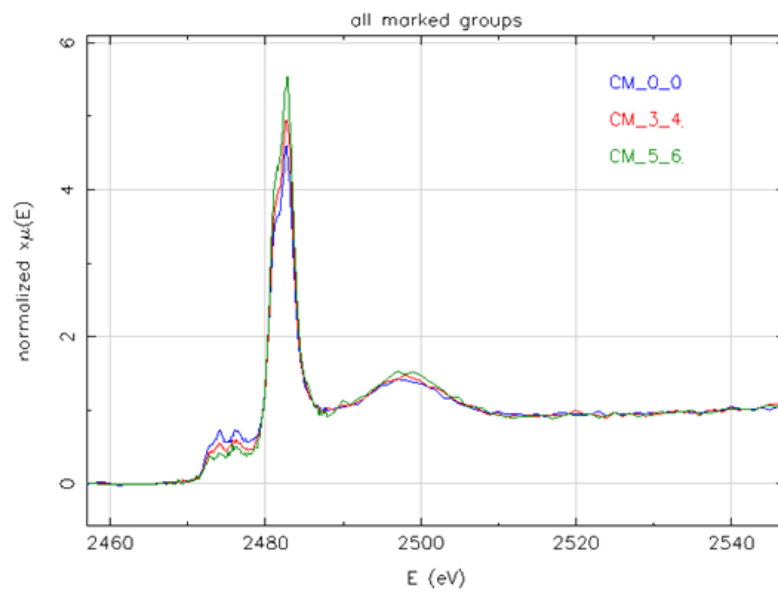
Figure 1.10 *Normalized XANES spectra at CM station.*

Table 1.8 *Fraction of different organic sulfur pools in the CM sediment, resulted from fitting of XANES spectra.*

Fraction	Reference	Moiety	
0.76	SDS	ester-sulfate	
0.28	benzo-thio	R-S-R' (cyclic)	
0.11	sulfamide	sulfone	
0.09	sulfoxide	sulfoxide	
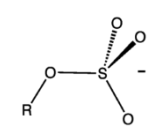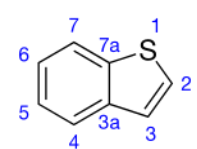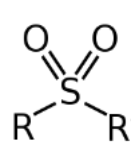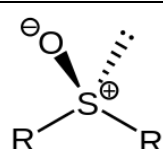
1.9. Potential role of organic sulfur for abundant large sulfide-oxidizing bacteria in Lake Superior

In addition to fueling sedimentary sulfate reduction, mineralization of reduced organic sulfur can provide substrate for large sulfur oxidizing bacteria in the low sulfate environment of Lake Superior, playing a potentially important role in the benthic ecology in parts of the lake. Hydrogen sulfide and other reduced sulfur compounds serve as electron donors for sulfur-oxidizing microorganisms (SOM) or are abiotically oxidized. SOMs are generally present in the upper sediment layers where electron acceptors with high redox potentials, such as oxygen or nitrate, are available. While microorganisms are central to sulfide oxidation in freshwater sediments (Lavik et al. 2009), their contribution to total sulfide oxidation in freshwater sediments is not well constrained. A major limiting factor for sulfur oxidation in sediments like in Lake Superior is the gradients of electron acceptors like oxygen and nitrate and sulfide as electron donor, so that results in spatially distinguished maximal concentrations of these electron donors and acceptors (Canfiled and Thamdrup 2009). Therefore, many SOMs cannot reach their most energetic electron acceptors at the depths where sulfide is available. This challenges SOMs to overcome this problem by employing additional strategies for electron transfer. Distinct examples of these strategies are Large Sulfur Bacteria (Teske and Salman 2014) and Cable Bacteria (Nielsen et al. 2010; Marzocchi et al. 2014). A representative of LSBs is *Thioploca*, a genus of filamentous, motile sulfur bacteria which are mostly found in marine sediments, e.g. along the 3,000 kilometres of coast off the west of South America (Ferdelman et al. 1997) (Fig. 1.11). They bridge the spatial gap between the electron

acceptors and electron donors by internally storing large amounts of electron acceptor such as nitrate and electron donors such as sulfide or elemental sulfur. They move between the oxic/suboxic and sulfidic sediment layers to replenish their electron acceptor and donor supplies. It has been shown that *Thioploca* cells are able to store nitrate to up to 500 mM in a liquid vacuole that occupies >80% of the cell volume (Fossing et al. 1995). They uniquely can fuel the anaerobic oxidation of ammonia to N_2 by associated anammox bacteria and thereby drive a significant nitrogen loss (Prokopenko et al., 2013). They also have been suggested to couple sulfate reduction and elemental sulfur disproportionation to the oxidation of reduced sulfur. While a number of studies suggest an important role of these bacteria in marine sediments with high sulfate and sulfide levels, their contribution to the sulfur and nitrogen cycles in low sulfate environments has not been reported. *Thioploca* have been reported in the Great Lakes in Lake Ontario (Dermott and Legner 2002), and recently were identified in several nearshore areas in Lake Superior (T. Ozersky, pers. comm.). Here we report results from a small pilot study that may serve as a basis for future investigations. To elucidate the role of organic sulfur compounds in providing sulfur substrate for *Thioploca*, two sediment cores were taken in 24 and 40 m of water near the Apostle Islands. Oxygen profiles within the sediment were obtained onboard using a Pyroscience optical microsensor. Sediment cores were sectioned into 1 cm segments and the interstitial waters were extracted under anoxic N_2 atmosphere for further analyses. Nitrate and nitrite were analyzed spectrophotometrically using a SEAL AQ400 Discrete Analyzer at the Large Lakes Observatory (LLO).

Thioploca biomass was measured at Horn Point Laboratory by Sairah Malkin, University of Maryland Center for Environmental Science.
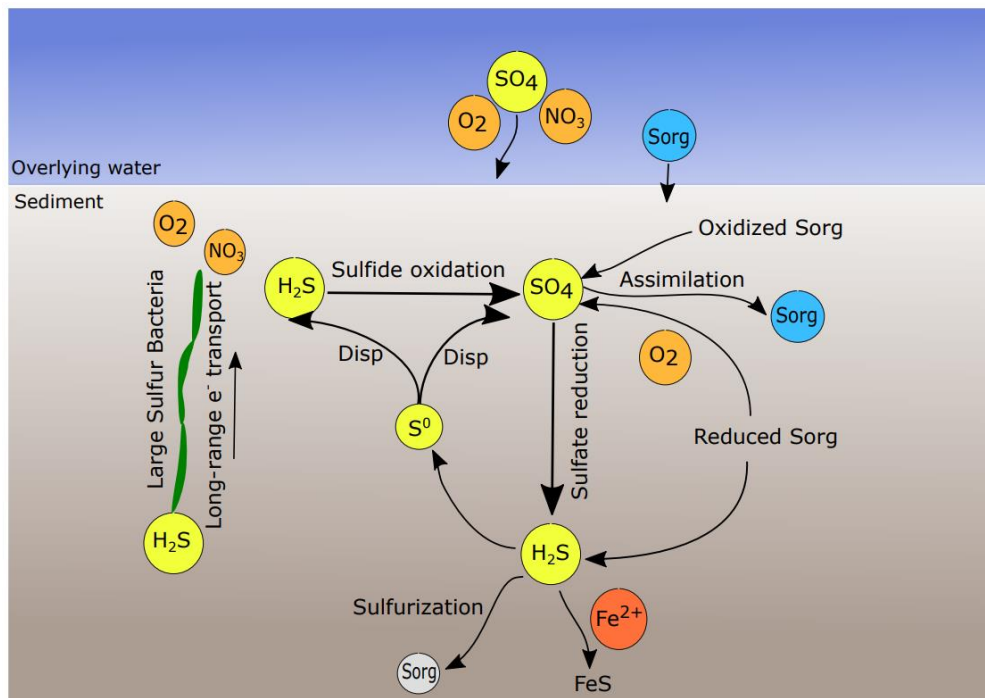
Figure 1.11 *Conceptual depiction of the sulfur cycle in the Lake Superior sediments, including main reactions of inorganic and organic sulfur compounds, and sulfur oxidation via long-range electron transport by large sulfur bacteria.*

The preliminary results in the Lake Superior sediment suggest an active role of *Thioploca* in oxidizing sulfur in such a low sulfate system. Specifically, in well oxygenated (O_2 = 300 µM) low-sulfate (SO_4^{2-} = 40 µM) freshwater sediment, a substantial biomass (8.6 g m^{-2}) of filamentous *Thioploca* species was found, comparable to the average biomass found in high sulfate and high sulfide sediment off the coast of Chile (10 g m^{-2}) (Gallardo, 1977; Schulz et al., 1996; Ferdelman et al, 1997). While

oxygen penetration depths in Lake Superior reach about 2 cm (Fig. 1.11), the maxima in the *Thioploca* biomass at both stations were observed near the denitrification zone (Fig. 1.12 & Fig. 1.13). There is, however, a caveat that the high concentrations of nitrate below 3 cm could be artifacts, as the core was sliced in the air for logistical reasons.

While sulfate level in Lake Superior is three orders of magnitude lower than in marine systems, the comparable biomass of *Thioploca* raises an important question: what sustains the *Thioploca* biomass? Is sulfate reduction rate rather than sulfate concentration more important, as the rate of sulfate reduction may be comparable to the rate in the marine systems (see *Section 1.5.3*). Given the significant role of organic sulfur in supporting sedimentary sulfur cycling in Lake Superior (Chapter 1), organic sulfur may be the main source of sulfur for *Thioploca*. Our results here propose a new link between organic sulfur and large sulfur bacteria. They raise several other important questions on the role of *Thioploca* in low sulfate environments: 1) Do they modulate the nitrogen and sulfur cycles? 2) How much nitrate can be reduced through nitrate reduction coupled to sulfur oxidation, mediated by these microorganisms? 3) How the sulfate and nitrate levels affect the biomass of *Thioploca*? Answers to these questions would help gain a broader understanding of the role of these less-known bacteria across different types of environments.
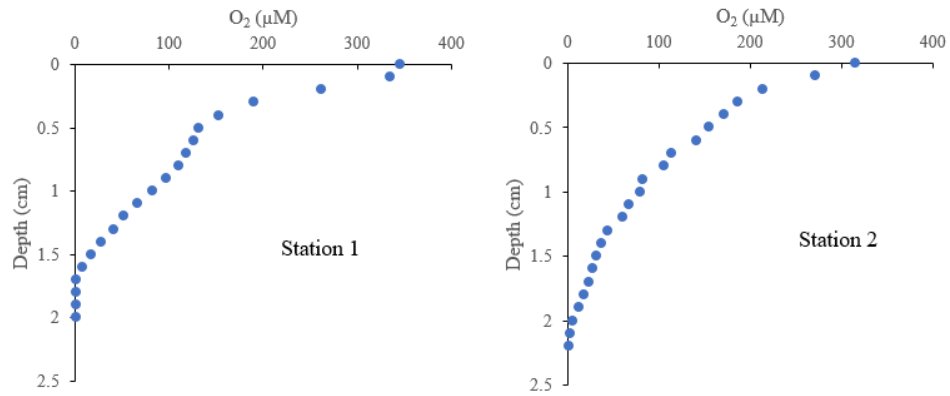
Figure 1.12 *Sediment oxygen profiles in two near shore stations, apostle islands, Lake Superior*
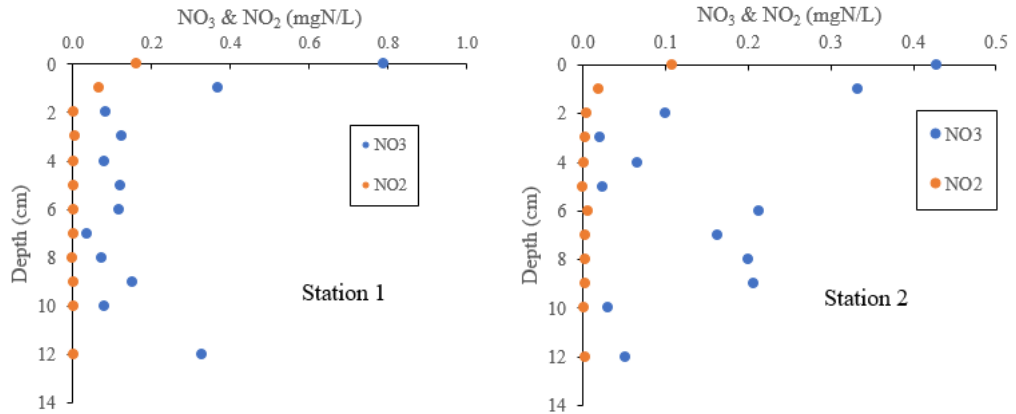
Figure 1.13 *Sediment nitrate, and nitrite profiles in two near shore stations, apostle islands, Lake Superior*
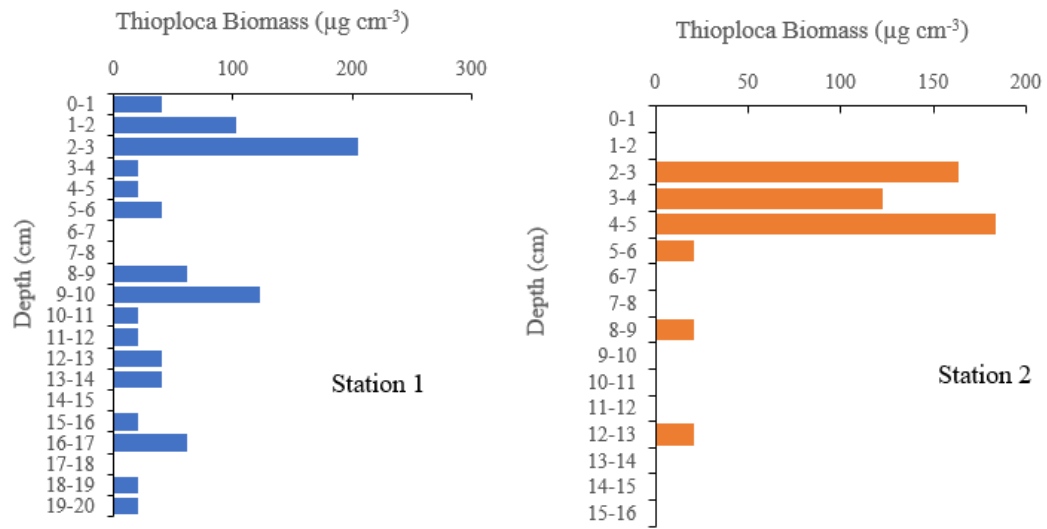
Figure 1.14 *Depth profiles of large sulfur bacteria, Thioploca, biomass in two near shore stations, apostle islands, Lake Superior*

Chapter 2 The organic component of the earliest sulfur cycling

Results in this Chapter have been submitted to Nature Communications

Title: The organic component of the earliest sulfur cycling

Authors: [1]Mojtaba Fakhraee, [1, 2]Sergei Katsev

[1] Large Lakes Observatory, University of Minnesota Duluth

[2] Department of Physics and Astronomy, University of Minnesota Duluth

2.1. Synopsis

The chemistry of the Early Earth is widely inferred from the elemental and isotopic compositions of sulfidic sedimentary rocks, which are presumed to have formed globally through the reduction of seawater sulfate or locally from hydrothermally supplied sulfide. Here we argue that, in the sulfate-poor ferruginous oceans of the Archean eon, organic sulfur must have played an important and previously unrecognized role in the formation of sulfides. In the anoxic ocean, mineralization of organic sulfur generated sulfite, which in the absence of ambient sulfate fueled microbial S reduction, and hydrogen sulfide, which provided a pathway to pyrite that bypassed the microbial reduction of sulfate or sulfite. Reaction transport modeling suggests that in coastal and deep sediments organic sulfur supported 20 to 100% of pyrite precipitation and up to 75% of microbial S reduction. By offering alternative explanations for the $\delta^{34}S$ and MIF isotopic records in Archean sulfides, these effects alter the presently accepted picture of the Early Earth sulfur cycle, with a significant proportion of oceanic sulfur throttled through living cells. They also raise a possibility that sulfate scarcity in the anoxic mid-Archean oceans delayed the evolution of dissimilatory reduction of sulfate until the initial ocean oxygenation around 2.7 Ga.

Since the beginning of Life, sulfur has cycled between the geosphere and biosphere as an essential component of all living matter. Organic S-bearing molecules have been ubiquitous throughout the planet's history(Martin et al. 2008)·(Sievert et al. 2007) and even have been detected on Mars (Eigenbrode et al. 2018). In modern oceans, however, their petagram inventory (Ksionzek et al. 2016) is dwarfed by the 10^9 Pg of inorganic sulfate, which at 28 mM is the second most abundant anion in seawater. At these concentrations, the geologically important cycling of sulfur through sulfate reduction, precipitation of pyrite, and reoxidation of sulfides is carried out overwhelmingly by inorganic sulfur. Abundant sulfate, however, was rare through most of the Earth's history. Proterozoic oceans were likely characterized by sub-mM to low mM levels (Canfield and Farquhar, 2009), and low-sulfate conditions returned episodically throughout the Phanerozoic (Newton et al. 2011). In the Archean, before the beginning of ocean oxygenation 2.7-2.5 billion years ago (Fakhraee et al. 2018; Eickmann et al. 2018), marine sulfate was scarce in coastal and surface pelagic ocean, at no more than tens of μM (Crowe et al. 2014; Fakhraee et al. 2018), and likely absent in ferruginous deep waters. The cycling of sulfur under these conditions was very different from the one in modern ocean, and freshwater systems, particularly stratified lakes, are commonly used as better analogues (Crowe et al. 2014). Recent work (Fakhraee et al. 2017) demonstrated that in low-sulfate lakes (<100 μM), organic sulfur supplies a significant portion of substrates for microbial sulfate reduction (King and Klug 1982), and a significant fraction of sulfide is traceable to organic source (Nriagu 1968; Cook and

61

Schindler 1983). Mineralization of organic sulfur (OS), for example, supported over 80% of sulfate reduction in the well-oxygenated sediments of oligotrophic Lake Superior (Fakhraee et al. 2017). Paradoxically, this organic component has not been considered in reconstructions of the Early Earth sulfur cycling. The histories of atmospheric oxygen and oceanic sulfate are widely inferred from the records of sulfur isotopes preserved in pyrites (Johnston 2011; Fakhraee et al. 2018), but non-hydrothermal pyrite formation was considered only from seawater sulfate (Habicht et al. 2002; Crowe et al. 2014) or elemental sulfur (Galić et al. 2017). Here we argue that organic sulfur must have been a significant component of the early biogeochemical cycling, and that its effects alter the presently accepted interpretations of the geochemical and isotopic proxies.

Sulfur makes up about 1% of dry weight of aquatic organisms (Ho et al. 2003). It occurs at lower oxidation states in proteins such as amino acids cysteine and methionine, in coenzymes (e.g., coenzyme A, biotin, thiamine), as iron-sulfur clusters in metalloproteins, and in bridging ligands (e.g., in cytochrome c oxidase)(Sievert et al., 2007). Higher oxidation state compounds, such as sulfonates $R-SO_3-H$, sulfones $R-SO_2-R$, and organo-sulfates, can be found in lipids (e.g., Sulfoquinovosyl diacylglycerols) and are components of cell walls and photosynthetic membranes. Molar S:C ratios in modern plankton (Ho et al. 2003) typically range between 0.003 and 0.01, with freshwater values (Fagerbakke et al. 1996) being more varied than in marine environments because of a wider range of geochemical conditions. Archean S:C ratios likely spanned a similar range, or perhaps were slightly higher at the times when sulfolipids could be used in place of phospholipids (Van Mooy et al. 2006; Bellinger et al. 2014) to alleviate strong P

62

limitation (Reinhard et al. 2017). The Archean organic sulfur pool was likely dominated by reduced compounds (Havig et al. 2017), which are thermodynamically easier to assimilate under anoxic conditions (Schulz H.D. Zabel M. 2006). Assimilation of sulfate requires energy even at the stage of cellular uptake by sulfate-binding proteins (Canfield et al. 2005), and sulfate (+6) is rare in prokaryotic cells (Canfield et al. 2005), while key molecules contain sulfites (+4) or sulfonates (+4) (Vairavamurthy et al. 1994; Levine 2016). Reduced sulfur appears in evolutionary key molecules such as methionine, cysteine, cystine, coenzymes M and acetyl CoA, aromatic sulfur and disulfides, and in primitive metabolic processes such as S oxidation in anoxygenic phototrophs. Hydrothermally supplied hydrogen sulfide (+2) in the presence of CO_2 could form thiols, critical coenzymes, CS_2 and dimethyldisulfide (Heinen and Lauwers 1996; Cody et al. 2000; Martin et al. 2008).

Mineralization of organic S compounds would recycle a significant portion of this organic pool as inorganic sulfur, making it available for processes that in the modern oceans are supported by seawater sulfate. Hydrolysis and mineralization of oxidized organic sulfur (R-SO_3-H) would generate sulfite (SO_3^{2-}), which in Archean oceans would add to the pool generated by the dissolution of volcanic SO_2 (Fig. 2.1). In contrast to the volcanic input deposited primarily at the ocean surface, however, mineralization would supply sulfite throughout the entire water column as well as sediments. Sulfite is readily utilized by sulfur reducing bacteria for dissimilatory reduction, and thermodynamically provides more energy for cell metabolism than sulfate(Schulz H.D. Zabel M. 2006). Its liberation in the sulfate-depleted deep ocean would make it available as a substrate for S

reducing metabolisms. In a world that lacked a strong oxidant like molecular oxygen, the redox cycling of S could in fact rely on sulfite as the dominant oxidized species. This possibility is supported by genetic evidence that points to the evolution of sulfite reducing metabolisms as early as 3.7 Ga, while genes for sulfate reduction appear later(David and Alm 2011; Havig et al. 2017). Some Archaea are known to reduce sulfite while not being able to reduce sulfate, and some auxotroph bacteria are known to utilize sulfonate OS directly(Rabus et al. 2013; Ksionzek et al. 2016). Mineralization of the reduced organic S pool (R-SH) would provide an even more important input of inorganic sulfur. It generates hydrogen sulfide, which under ferruginous Archean conditions would react with dissolved iron (Fe^{2+}) to form iron sulfides, bypassing the traditionally assumed pathways of S reduction.

Even if the total inventory of OS in the Archean water column were small compared to dissolved inorganic S, the fluxes of organic sulfur were quantitatively significant. Assuming low (5% modern(del Giorgio and Duarte 2002)) respiration in the anoxic Archean water column, Archean mineralization rates below the photic zone were at least 100 Tmol C yr^{-1}, regenerating 0.3-1 Tmol S yr^{-1} of inorganic sulfur. This is higher than the estimated flux of sulfur from hydrothermal settings(Poulton and Canfield 2011) (0.2 - 0.5 Tmol S yr^{-1}). For a concentration of total S in the ocean water on the order of 10 uM(Crowe et al. 2014), the entire oceanic pool of sulfur would cycle through the organic pool on the order of 10,000 years, or even faster if one accounts for faster respiration rates in the photic zone. Through direct precipitation and S reduction in the ferruginous water column and sediments, the regenerated inorganic S would support a

significant portion of the pyrite burial in the ocean. For example, for the sulfate reduction rate of 1.4 x 10^{-2} mol S m^{-2} yr^{-1} estimated (Crowe et al. 2014) for the seawater sulfate concentration of 10 uM, the corresponding pyrite flux is 5 Tmol S yr^{-1}, and the potential contribution of OS is 20%; for sulfate levels below 2 uM, the contribution of organic sulfur increases to 75%. In surface sediments (e.g., at ~0.1% organic carbon content and the S:C ratio of 0.003), the abundance of organic sulfur (~100 umol S per liter of sediment) would compete with the low uM availability (Crowe et al. 2014) of inorganic S from the overlying water column, and could be the only source of reactive S in deeper sediment.
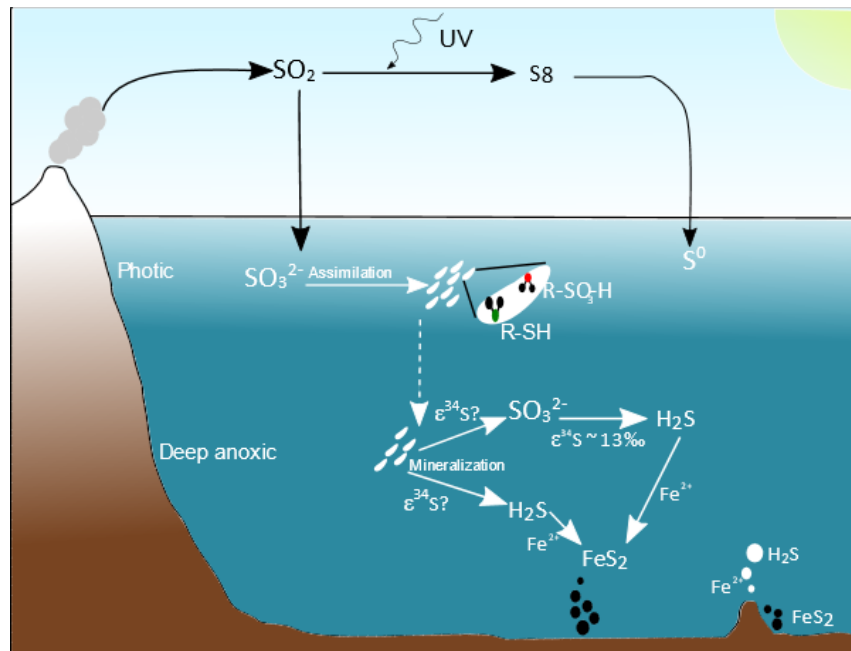
Figure 2.1 *Mediation of sulfur cycling by organic sulfur (OS) in anoxic ferruginous Archean oceans. Mineralization of OS serves as a source of both oxidized and reduced sulfur in the ferruginous deep-water column and sediments. In Neoarchean, the availability of free oxygen would replace sulfite with sulfate as the dominant oxidized specie.*

Generation of sulfite and sulfide from organic S within the sediments and deep water column radically changes the picture of the Archean S cycling. Traditional view and previous numerical models (Habicht et al. 2002; Crowe et al. 2014; Fakhraee et al. 2018) assumed that sulfate from surface ocean was transported into the deep waters or sediments where it underwent microbial reduction to sulfide, which in the presence of ferrous iron precipitated to eventually form pyrite. In contrast, the oxidized S (whether sulfite or sulfate) produced from OS may support S reduction even when sulfate is absent from ambient water, similarly to the way it happens in modern low-sulfate lakes (Fakhraee et al. 2017). Likewise, the hydrogen sulfide produced from reduced OS may generate pyrite even in the absence of sulfate reducing microbes. To illustrate the potential role of organic sulfur, we used a vertically resolved diffusion-reaction model, which we adapted from Ref. Fakhraee et al. (2017) and applied to Archean conditions (Fakhraee et al., 2018) (*see Model description*). For the sake of concreteness, we performed simulations in sediments, but similar arguments would also apply to a stratified water column. For a more straightforward comparison with previous models that did not consider sulfite, and to extend the results to potentially oxygenated conditions of the Neoarchean, the model uses sulfate as the oxidized form of inorganic sulfur; this does not change the generality of the argument. Mineralization of reduced OS was assumed in the model to generate hydrogen sulfide. The ratio of oxidized to reduced OS within organic matter was set to 40%:60% as a reference value and varied in a sensitivity analysis (*see Model description*). Similarly to previous work in freshwater environments (Fakhraee et al. 2017), the model calculated the fraction of the sedimentary sulfate

reduction that was supported by OS mineralization, and the fraction of pyrite that was formed through the mineralization of reduced S (Fig. 2.2). These fractions were calculated from the respective ratios of the depth-integrated rates for OS mineralization, sulfate reduction, and pyrite precipitation (*see Model description*).

Simulations reveal that, for <50 µM of sulfate in Archean seawater (Crowe et al. 2014; Fakhraee et al. 2018), between 20 and 100% of all precipitated pyrite would originate from organic sulfur (Fig. 2.2). For <10 µM, a significant fraction of pyrite may form from OS even at low organic S:C ratios. Mineralization of oxidized OS supports between 5 and 75% of total sedimentary S reduction. The OS contributions remain significant for sulfate concentrations up to >100 uM (Figs. 2.2, 2.3), at which point the seawater sulfate becomes the dominant source. These sulfate concentrations were not achieved in the oceans until the later stages of the Great Oxidation Event, suggesting that OS remained an important component throughout the Archean eon. At low sulfate concentrations, the presence of oxygen, in fact, enhances the organic sulfur contribution to S reduction (Fig. 2.2). Though oceans throughout the Archean Eon are thought to have been predominantly anoxic, Neoarchean sediments in shallow coastal regions could have been exposed to concentrations of up to tens of µM (Fakhraee et al. 2018; Eickmann et al. 2018). Being a more potent electron acceptor, oxygen decreases the sediment demand for seawater sulfate, decreasing its vertical flux and making the in-sediment generation of oxidized S proportionately more important. The (percentage) contribution of OS to S reduction increases also with the sediment organic matter content, as it supports higher OS mineralization rates, even though it also stimulates sulfate reduction, which increases

the drawdown of sulfate from overlying water (Fig. 2.5). In Neoarchean, environments with higher oxygen concentrations and higher organic carbon fluxes could be readily found in oxygenated oases in shallow coastal regions (Olson et al. 2013; Eickmann et al. 2018) where oxygenic photosynthesis fueled higher primary productivity, sedimentation rates were high, and most pyrite is thought to have originated.

The contribution of organic component to pyrite formation profoundly changes the accepted interpretations of the Archean isotopic signals. Microbial sulfate reduction depletes the sulfide in ^{34}S, generating isotopic differences between the seawater sulfate and sediment pyrite $\Delta^{34}S_{FeS} = \delta^{34}S_{SO4} - \delta^{34}S_{FeS}$. The limited range of $\Delta^{34}S$ <10‰ throughout the Archean is viewed as a consequence of low sulfate, which restricted sulfate reduction (Habicht et al. 2002; Crowe et al. 2014). The Rayleigh distillation, induced by the need for sulfate to diffuse downward to sulfate reduction zone, also limits the $\Delta^{34}S_{FeS}$ range: the sulfate diffusing into sediment from overlying water becomes isotopically heavier with depth and the $\delta^{34}S$ of the produced sulfide trends towards the $\delta^{34}S$ of the bulk seawater sulfate. Formation of pyrite from the OS-derived sulfur means that sulfidic rocks do not necessarily record the evidence of these processes but instead reflect a more complex mixture of isotopic influences. Sulfite produced at some depth within the sediment column may be reduced at the same depth, without undergoing Rayleigh distillation (Habicht et al. 1998). As fractionations associated with the reduction of sulfite are small (Habicht et al. 1998) (13±7‰) compared with those for sulfate (>30‰), they are consistent with observations of small $\Delta^{34}S$. The hydrogen sulfide produced from more abundant reduced OS compounds would generate solid sulfides,

bypassing microbial reduction. Rather than carrying an isotopic signature of redox processes, these sulfides could instead carry the isotopic signal of hydrolysis. The magnitudes of the fractionations during hydrolysis of organic sulfur are unknown, but thermodynamic considerations (Saunders 1967) limit them to less than 15‰, consistent with small observed $\Delta^{34}S$. Small fractionations are similarly consistent with the evidence in modern sediments where care was taken to analyze the hydrolyzable fraction of organic sulfur (Canfield et al. 1998; Raven et al. 2016). In particular, depth variations in the isotopic composition of hydrolyzable organic sulfur pool seem to indicate a preferential loss of isotopically light organic sulfur during the early stages of diagenesis (Canfield et al. 1998). The effects of OS hydrolysis and mineralization would also enhance the preservation of large mass-independent fractionations of sulfur (MIF-S), which are another key feature of Archean pyrites(Pavlov and Kasting 2002; Ohmoto et al. 2006). The MIF signal ($\Delta^{33}S \neq 0$) carried by atmospherically-derived elemental sulfur would be better preserved when pyrite is formed through a reaction with the OS-sourced sulfide rather than with the sulfide produced through microbial sulfate reduction, as the latter carries a strong mass-dependent signal.

The ambiguity of isotopic interpretations calls for a re-evaluation of the ancient sulfur cycling. The organic matter exported into the deep anoxic waters provided sulfur reducers not only with organic carbon as electron donor, but also with sulfite as electron acceptor. As $\Delta^{34}S_{FeS}$ records are equally consistent with sulfite reduction and formation of pyrite from reduced organic sulfur, neither of which requires sulfate, the isotopic evidence for an early (3.47 Ga) onset of sulfate reduction (Shen and Buick 2004; Aoyama

and Ueno 2018), suggested based on ~10‰ fractionations (Bottrell and Newton 2006), may need to be re-evaluated. Sulfur isotopes are the only reliable tracer for the sulfate reduction metabolism, as preserved cellular structures are not readily identifiable for sulfate-reducers, while molecular fossils (biomarkers) do not seem to survive over geological times (Shen and Buick 2004). In a low-oxygen world where sulfate was produced in limited quantities by atmospheric photochemical reactions or sulfite disproportionation, dissimilatory sulfate reduction may have become globally competitive for the first time when sulfate concentrations increased in the Neoarchean, following the initial marine oxygenation around 2.7 Ga (Fakhraee et al. 2018). The observed expansion in $\Delta^{34}S_{FeS}$ beginning around 2.7 Ga (Canfield and Farquhar 2009; Fakhraee et al. 2018) thus may reflect, in part, the corresponding increase in isotope fractionations (Marin-Carbonne et al. 2018). Similarly, while anoxygenic phototrophs nearly universally can oxidize sulfide to elemental sulfur (Canfield et al. 2005), evidence for the evolution of groups capable of completing the oxidation to sulfate seems to appear first around 2.7 Ga (Hohmann-Marriott and Blankenship 2011). As pyrite could be formed in non-hydrothermal settings from relatively abundant reduced organic sulfur (Fig. 2.2), its presence does not necessarily indicate active sulfate reduction, allowing a possibility of only trace amounts of sulfate (sulfite) in oceanic seawater. The OS pathway under such conditions could generate more pyrite than the reduction of seawater sulfate, and the geographic distribution of such pyrite could be broader than for the pyrite that formed from hydrothermal H_2S. The concentrations of dissolved inorganic sulfur in

ferruginous oceans thus could have been low enough to make sulfur a co-limiting

nutrient, consistent with the approximately similar S and P contents in living cells.
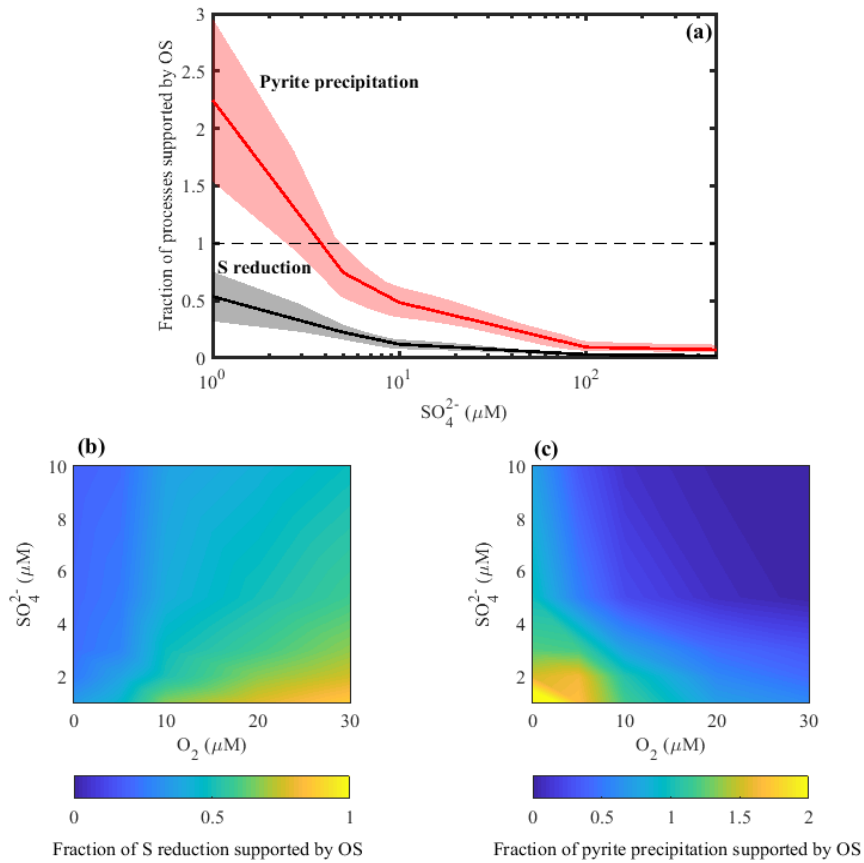
***Figure 2.2** Support of sulfate (or sulfite) reduction and iron sulfide formation by organic matter-sourced sulfur (OS), simulated with a sediment reaction-transport model. (a) As a function of sulfate (sulfite) concentration under anoxic conditions. Shaded bands reflect the corresponding $\pm 1\sigma$ ranges obtained in the sensitivity analysis (see Model description). (b,c) The same, in presence of oxygen. The fraction of supported S reduction was calculated as the ratio of the depth integrated rates of oxidized OS mineralization and sediment S reduction. The latter was corrected for the fraction of sulfate reduction supported by elemental S disproportionation and sulfide re-oxidation. The fraction of supported pyrite precipitation was calculated as the ratio of the depth integrated rates of reduced OS mineralization and Fe sulfide precipitation. The ratio was corrected for*

elemental S disproportionation and the fraction of produced hydrogen sulfide that becomes unavailable for precipitation because of aerobic oxidation (see Supplement). Values greater than 1 correspond to a situation where excess hydrogen sulfide diffuses out of the sediment. Sediment was assumed to contain 0.3% of organic carbon by dry weight, with the molar S:C ratio of 0.005.

We thus argue that, in the deep anoxic Ocean and sediments, organic sulfur mineralization could support activities of sulfur reducers and formation of sedimentary sulfides -- a role traditionally attributed to microbial reduction of ambient sulfate. Identifying these effects in the Archean rock record requires the currently missing information about the isotopic and geochemical transformations of organic sulfur during organic matter mineralization. We therefore suggest that further experimental efforts by the community should be directed at elucidating these contributions of organic sulfur, both in the lab and in modern low sulfate environments.

2.2 Model Description
2.2.1. Geochemical Model

The geochemical model for the transformations of organic sulfur and sediment sulfur cycling was adapted from Fakhraee et al. (2017), with the aspects pertaining to Archean conditions adjusted based on Fakhraee et al. (2018). Briefly, vertical distributions of chemical species within the sediment are simulated at steady state with a diagenetic equation:

$$0 = D_i \varphi \frac{d^2 C_i}{dx^2} - v \frac{dC_i}{dx} + \sum_j R_{ij} \tag{2.1}$$

Here, x is depth below the sediment surface. C_i is the concentration of species i, D_i is the corresponding molecular diffusion coefficient corrected for sediment porosity φ using the Archie's law factor of $\varphi^{1.14}$, and v is burial velocity which is neglected for solutes. R_{ij} are the rates of reactions that consume or produce species i. The included reactions and their rate formulations are listed in Tables S1 & S2. Model parameter values are listed in Table S3. For simplicity, we assume no sediment compaction, so porosity is constant with depth. Bioturbation and bioirigation are neglected, as macrofauna was absent during the simulated geological period. Boundary conditions are imposed at the sediment-water interface as fixed concentrations for solutes and fixed sedimentation flux for solids (elemental sulfur); no-gradient conditions are imposed at the bottom of the model domain.

Mineralization of organic carbon and the distributions of iron within the sediment were modeled as described in Fakhraee et al. (2018), and their control parameters were varied in the sensitivity analysis (see below). Diagenetic formation of elemental sulfur was considered through oxidation of sulfide by iron oxides, which is the pathway that is thermodynamically favorable at low sulfide concentrations (Fakhraee et al. 2018). Thiosulfate was not considered because at low sulfide availability aerobic oxidation of sulfide proceeds largely without intermediate redox compounds (Canfield et al. 2005; Pfennig 1975).

Organic sulfur was assumed to be delivered into the sediment with particulate organic matter. Similarly to treatment in Fakhraee et al. (2017), the rate of organic sulfur mineralization, a multi-step process, was simulated as proportional to the rate of organic

C mineralization. In the absence of empirical information linking the rates of organic carbon mineralization and organic sulfur mineralization, the release of oxidized and reduced S compounds from organic matter was assumed to occur stoichiometrically with a fixed S:C ratio. While enzymatic hydrolysis was hypothesized to be affected by SO_4^{2-} concentrations (Scherer 2009) in soil literature, such inhibition was not demonstrated in sediments and was not considered in the model for lack of any quantitative information on sulfate levels at which inhibition might occur. Hydrolysis and mineralization of R-SH compounds was assumed to generate HS^-/H_2S. Mineralization of oxidized organic sulfur (R-O-SO_3H groups) such as in sulfonates and esters was assumed to generate sulfite or sulfate. As the S:C ratios in the Archean ecosystem are not established, the S:C ratio was varied in the model within a range of literature values for modern marine ecosystems (Burdige 2007). The S:C ratios may reflect, for example, factors such as organism physiology (specific sulfur requirements for biomass) and environmental conditions such as nutrient limitation. For example, in modern systems, P limitation in plankton is known to stimulate substitution of sulfolipids (and N-based lipids) for phospholipids (Van Mooy et al. 2006; Bellinger et al. 2014), amplifying the sulfur deposition into sediments.

To quantify the fraction (α) of sediment S reduction supported by mineralization of organic sulfur, we used the ratio of the depth-integrated rates of sulfate generation and sulfate reduction, corrected for the in-sediment recycling of sulfur by the disproportionation of elemental sulfur and re-oxidation of hydrogen sulfide. To quantify the fraction (β) of pyrite precipitation supported by organic sulfur, we used the ratio of the depth-integrated rates of sulfide generation to iron sulfide formation, corrected for the

74

production of sulfide through elemental sulfur disproportionation and reduction of the mineralized oxidized OS. Using $R*$ as the notation for depth-integrated rates of the respective reactions (Table 2.2), the corresponding parameters α and β are thus defined as:

$$\alpha = \frac{R^*_{PSO4}}{(R^*_{SR} - R^*_{SOX} - 0.25 * R^*_{Disp})} \tag{2.2}$$

$$\beta = \frac{R^*_{PH2S} - R^*_{SOX}}{(R^*_{FeS} - 0.75 * R^*_{Disp})} \tag{2.3}$$

Values of α or β greater than 1 would correspond to a situation where mineralization of OS fully supports, respectively, sulfate reduction or pyrite precipitation, with the excess inorganic S fluxing out of the sediment. The fraction of sulfur originated from external inorganic sources, such as seawater sulfate or hydrogen sulfide produced from the reduction of seawater sulfate, are given by 1- α, and 1- β. At higher oxygen levels, the calculated value of α is expected to be a conservative estimate of the OS contribution, as oxidation of organic-sourced reduced sulfur would also replenish the sulfate pool.

Diagenetic equations (2.1) were iteratively solved in Matlab as a boundary-value problem using the "bvp4c" function.

2.2.2. Sensitivity Analysis

The dependence of model's results on its parameter values was investigated using a sensitivity analysis. The predicted ranges of α and β (Figs. 2.2 and 2.3) were calculated for multiple parameter sets (at least 10 for each sulfate concentration), by randomly and

independently selecting model parameter values within their uncertainty ranges (Table 2.3), assuming uniform probability distributions. For parameters whose uncertainty ranges span several orders of magnitude, such as reaction rate constants, the values were selected assuming uniform probability distributions of their logarithms. The analysis revealed that the conclusions presented in the main manuscript are not sensitive to most parameters including pH, initial age of organic matter deposited into sediment, diffusion coefficients, porosity, burial velocity, rate constants for oxidation of sulfide and FeS precipitation, Monod constants for sulfate reduction (K_m), and elemental sulfur disproportionation rate constant. The parameters that affected the values of α and β most strongly included the sediment organic matter content, sulfur to carbon ratio (S/C), and the proportion of organic sulfur present in oxidized (f_{SO4}) vs. reduced form (f_{H2S}). The sensitivity of α and β to the S/C ratio and organic matter content are illustrated in Figures 2.4 and 2.5. As expected, higher S:C ratios elevate the production of inorganic sulfur from organic compounds, which in turn, increases the contributions of organic sulfur in supporting S reduction and pyrite precipitation. Increasing organic matter content also enhances the contribution of OS, as it supports higher OS mineralization rates, even though it also stimulates sulfate reduction, which increases the drawdown of sulfate from overlying water (Fig. 2.5).

Table 2.1 *Reactions included in the model*

Reactions	Rate
$CH_2O + O_2 \Rightarrow CO_2 + H_2O$	R_{OX}
$CH_2O + 4\ FeOOH_{(s)} + 7CO_2 + H_2O \Rightarrow 4Fe^{2+} + 8\ HCO_3^-$	R_{FeOOH}
$SO_4^{2-} + 2CH_2O \Rightarrow H_2S + 2HCO_3$	R_{SR}
$H_2S + 2O_2 + 2HCO_3^- \Rightarrow SO_4^{2-} + 2CO_2 + 2H_2O$	R_{SOX}
$R\text{-}O\text{-}SO_3H + H_2O \Rightarrow HSO_4^{2-} + R\text{-}OH_2$	R_{PSO4}
$R\text{-}SH + H_2O \Rightarrow H_2S + R\text{-}OH$	R_{PH2S}
$Fe^{2+} + HS^- \Rightarrow FeS(s) + H^+$	R_{FeS}
$2FeOOH_{(s)} + 3H2S_{(aq)} \Rightarrow S^0_{(s)} + 2FeS_{(s)} + 4H_2O$	R_{S0}
$4\ S^0_{(s)} + 4H_2O \Rightarrow SO_4^{2-} + 3HS^- + 5H^+$	R_{Disp}

Table 2.2 *Kinetics of the reactions included in the model. K_{FeS}, K_{H2S}, and k_{Disp} are the equilibrium constants for FeS precipitation, acidity constant for H_2S, and rate constant of S^0 disproportionation, respectively.*

Reaction	Rate expression
Sulfide Oxidation	$R_{SOX} = k_{SOX}[O_2][H_2S]$
Sulfate production from R-O-SO₃H	$R_{PSO4} = f_{SO_4} * \frac{S}{C} V_m$; Where S/C is the sulfur to carbon molar ratio; V_m = organic carbon mineralization rate.
Sulfide production from R-SH	$R_{PH2S} = f_{H_2S} * \frac{S}{C} V_m$
Aerobic Respiration	$R_{OX} = \dfrac{V_m[O_2]}{K_i + [O_2]}$
Iron Reduction	$R_{FeOOH} = \dfrac{V_m[FeOOH]}{K_{FeOOH} + [FeOOH]} \dfrac{K_i}{K_i + [O_2]}$
Sulfide Precipitation	$R_{FeS} = k_{FeS}(\dfrac{\Omega}{K_{FeS}} - 1)$ $\Omega = \dfrac{[Fe^{2+}][HS^-]}{[H^+]}$ $[HS^-] = \dfrac{[H_2S]}{1 + [H^+]K_{H_2S}}$
Sulfate Reduction	$R_{SR} = \dfrac{V_m[SO_4^{2-}]}{K_m + [SO_4^{2-}]} \dfrac{K_i}{K_i + [O_2]}$
Elemental Sulfur Formation	$R_{S0} = k_{S0}[FeOOH][H_2S]$
Elemental Sulfur Disproportionation	$R_{Disp} = k_{Disp}[S^0](1 - \frac{[H_2S]}{[H_2S]_{stop}})$ for [H₂S] < [H₂S] stop 0 \qquad\qquad\qquad for [H₂S] ≥ [H₂S] stop

Table 2.3 *Parameters in the reactive transport model. Asterisk (*) indicates parameters that were randomly varied in the sensitivity analysis within their specified expected ranges.*

Parameter	Symbol	Value	Unit	Expected Range	Ref.
*Diffusion coefficient of sulfate	D_{SO4}	300	$cm^2\ yr^{-1}$	200-400	Canfield 2006
*Diffusion coefficient of sulfide	D_{H2S}	500	$cm^2\ yr^{-1}$	400-600	Burdige 2006
*Diffusion coefficient of oxygen	D_{O2}	500	$cm^2\ yr^{-1}$	300-500	Burdige 2006
*Sulfide oxidation rate constant	k_{OXD}	160	$uM^{-1}yr^{-1}$	100-1000	Katsev et al. 2004
*FeS precipitation rate constant	k_{FeS}	10^{-5}	$mol\ g^{-1}\ yr^{-1}$	10^{-6}-10^{-5}	Katsev et al. 2004
FeS equilibrium constant	K_{FeS}	10^{-4}	M	-	Dyrssen & Kremling 1990
*Sulfur-to-carbon ratio in organic matter	S:C	0.005	mol/mol	0.003-0.01	Urban et al., 1999; Hoe et al. 2003
*Fraction of oxidized organic sulfur	f_{SO4}	0.4	-	0.2-0.6	-
*Fraction of reduced organic sulfur	f_{H2S}	0.6	-	0.4-0.8	-
Acid-base equilibrium constant for H_2S	K_{H2S}	2.48×10^{-7}	-	-	Dyrssen & Kremling 1990
*S^0 formation rate constant	k_{S0}	8×10^{-3}	$\mu M^{-1}yr^{-1}$	10^{-4}-10^{-2}	Van Cappellen & Wang 1996
*S^0 disproportionation rate constant	k_{Disp}	0.001	yr^{-1}	10^{-4}-10^{-2}	Jourabchi 2007
Threshold H_2S concentration for disproportionation	$[H_2S]_{stop}$	10	mM	-	Jourabchi 2007
*Monod constant for SO_4^{2-} reduction	K_m	20	uM	5-77	Katsev et al. 2004
*Monod constant for O_2 (inhibition constant)	K_i	1	μM	0.5 – 2	Katsev et al. 2004
Monod constant for FeOOH reduction	K_{FeOOH}	20	$\mu mol/g$	15-30	Katsev et al. 2004
*Sulfate at SWI (sediment water interface)	$[SO_4^{2-}]$	10	μM	1-500	-
Sulfide concentration at SWI	$[H_2S]$	0	μM	-	-
*Oxygen concentration at SWI	$[O_2]$	0	μM	0-30	-
*Fe^{2+} at SWI	$[Fe^{2+}]$	0	μM	0-10	-
*Fe(III) concentration at OPD	$[Fe(OH)_3]_{OPD}$	5	mg/g	0-25	-
Density of dry sediment	ρ_s	2.65	g/cm^3	-	-
Grid size	dz	6.67×10^{-3}	cm	-	-
Flux of elemental sulfur at sediment water interface	$Flux_{S0}$	0.4	$\mu mol/cm^2/year$	0.1-1	
*pH	pH	6	-	6-7	Halevy and Bachan 2017
*Organic carbon content	OC	0.3	wt%	0.1-1	

*Burial velocity	V_{burial}	0.05	cm yr^{-1}	0.05-0.2	-
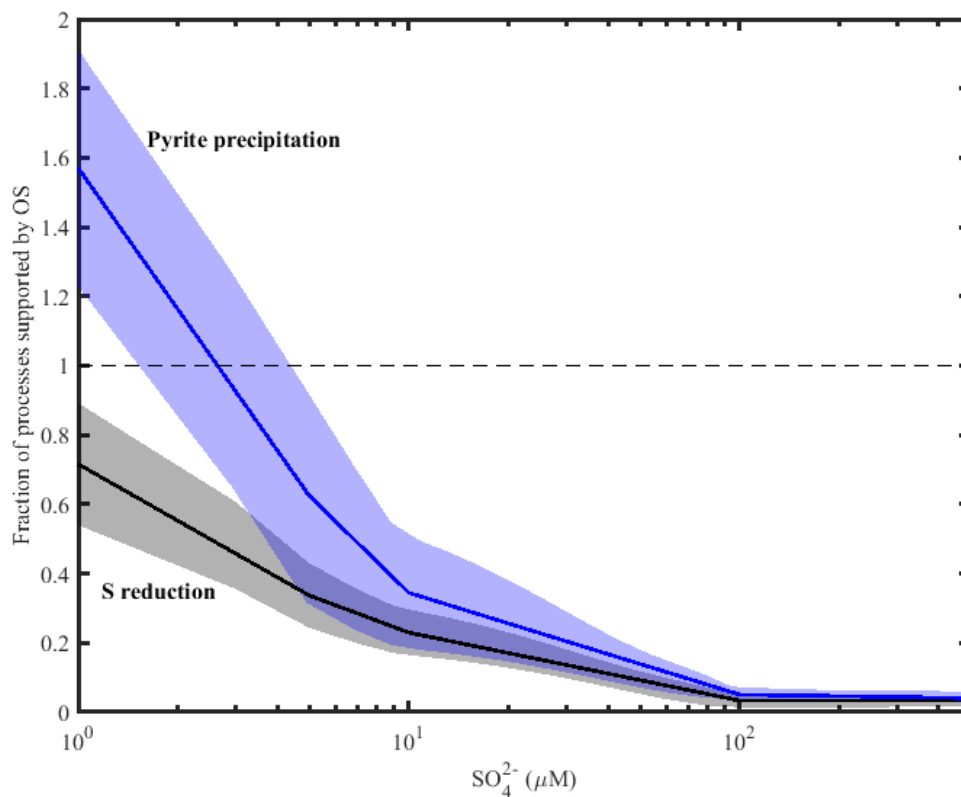
Figure 2.3 *Support of sulfate (or sulfite) reduction and iron sulfide formation by organic matter-sourced sulfur (OS) as a function of sulfate (sulfite) concentration under oxic condition ([O$_2$] = 10 μM). Shaded bands reflect the corresponding ±1σ ranges obtained in the sensitivity analysis.*
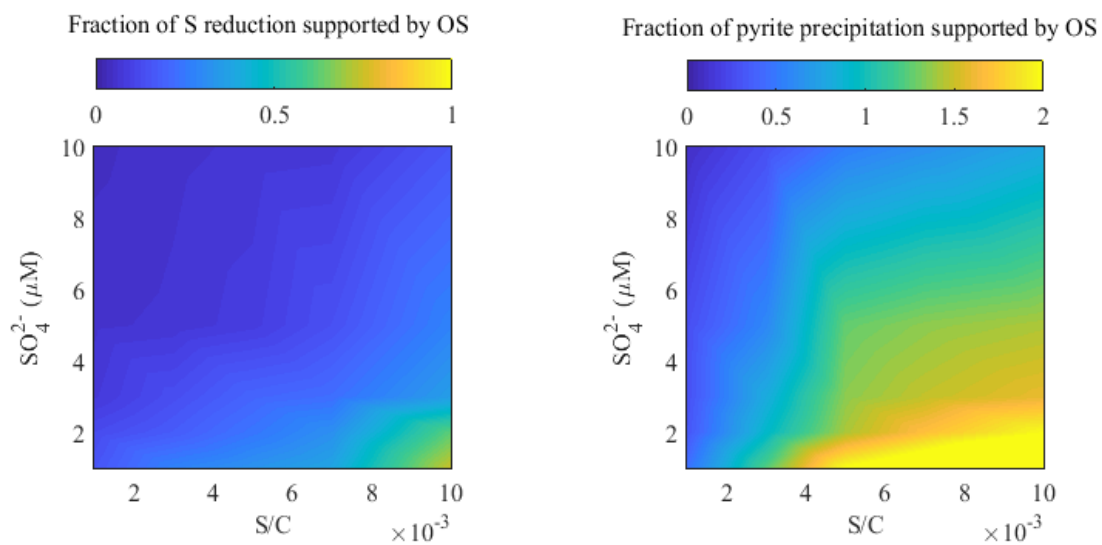
Figure 2.4 *Sensitivity of α (left) and β (right) to the S:C ratio in organic matter, under anoxic conditions.*
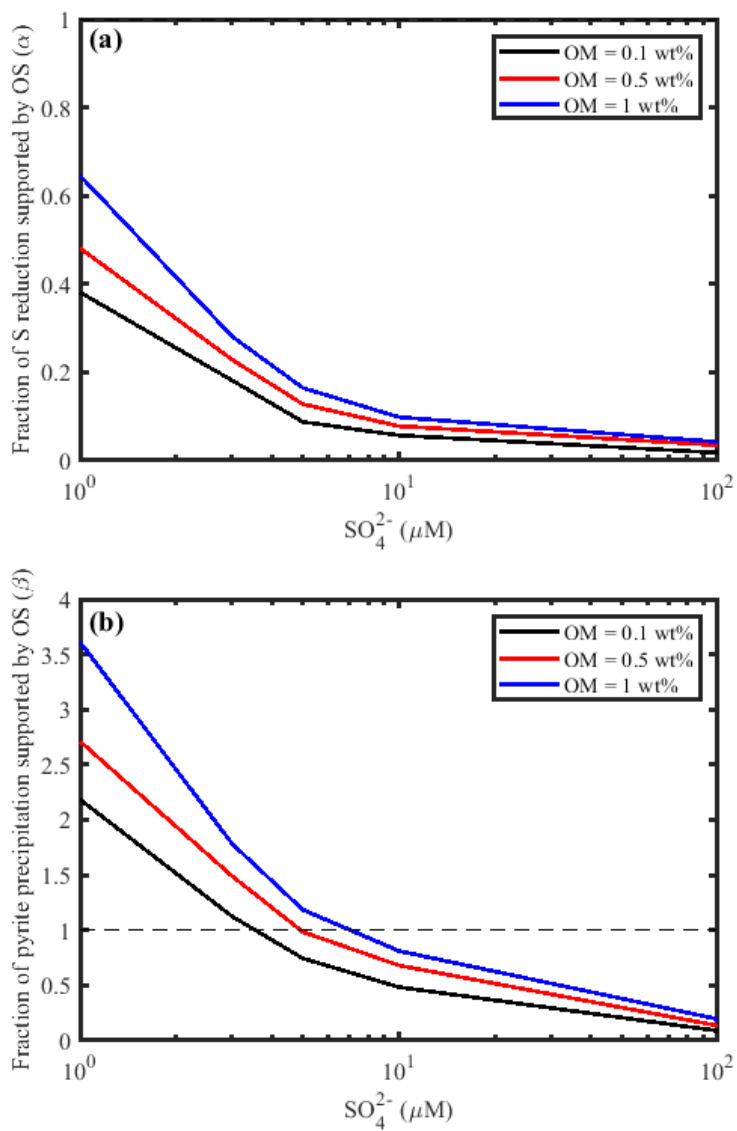
Figure 2.5 *Sensitivity of α (a) and β (b) to organic matter (OM) availability, under anoxic conditions.*

Chapter 3 Sedimentary sulfur isotopes and Neoarchean ocean oxygenation

Results in this Chapter have been published in Fakhraee et al. (2018): Science Advances 4 (2018).

Title: Sedimentary sulfur isotopes and Neoarchean ocean oxygenation

Authors: [1]Mojtaba Fakhraee, [2] Sean A. Crowe, [1, 3]Sergei Katsev

[1] Large Lakes Observatory, University of Minnesota Duluth

[2] Department of Microbiology and Immunology and Department of Earth, Ocean, and Atmospheric Sciences, University of British Columbia, Vancouver

[3] Department of Physics, and Astronomy, University of Minnesota Duluth

3.1 Synopsis

Abrupt disappearance of mass independent fractionation of sulfur isotopes (MIF-S) from the geologic record and an apparent ingrowth in seawater sulfate around 2.45 Ga signal the first large-scale oxygenation of the atmosphere (the Great Oxygenation Event, GOE). Pre-GOE O_2 production is evident from multiple other terrestrial and marine proxies, but oceanic O_2 concentrations remain poorly constrained. Current interpretations of S isotope records, furthermore, do not explain a concurrent expansion in the range of both mass independent S-isotope fractionations (MIF-S) – diagnostic for low atmospheric O_2 – and $\delta^{34}S$ beginning at 2.7 Ga. To address these unknowns, we developed a reaction-transport model to analyze the preservation patterns of sulfur isotopes in Archean sedimentary pyrites, one of the most robust and widely distributed proxies for early Earth biogeochemistry. Our modeling, paradoxically, reveals that micromolar levels of O_2 in seawater enhance the preservation of large MIF-S signals, while concomitant ingrowth of sulfate expands the ranges in pyrite $\delta^{34}S$. The 2.7-2.45 Ga expansion in both $\Delta^{33}S$ and $\delta^{34}S$ ranges thus argues for a widespread and protracted oxygenation of seawater, at least in shallow marine environments. At the micromolar levels predicted, the surface oceans would support a strong flux of O_2 to the atmosphere, where O_2 sinks balanced these fluxes until the GOE. This microoxic seawater would have provided habitat for early aerobic microorganisms and supported a diversity of new O_2 driven biogeochemical cycles in the Neoarchean.

Two key features of sulfur isotope distributions in Archean pyrites underpin assertions for very low Archean atmospheric O_2 concentrations: records of large mass independent sulfur isotope fractionations ($\Delta^{33}S$, MIF-S) (Farquhar et al. 2001; Pavlov and Kasting 2002; Ohmoto et al. 2006) and a narrow range of $\delta^{34}S$ values (Habicht et al. 2002). Mass independent fractionations are produced in an ozone-free atmosphere, and atmospheric photochemical models suggest delivery of MIF-S to the Earth's surface only when atmospheric O_2 concentrations are less than 10^{-5} present atmospheric levels (PAL) (Farquhar et al. 2001; Pavlov and Kasting 2002). The relatively restricted ranges of $\delta^{34}S$ in Archean pyrites, particularly before 2.7 Ga, point to low sulfate concentrations in the oceans reflecting both restricted oxidative weathering of pyrites on land and little oxidative recycling of sulfur in the oceans (Canfield and Farquhar 2009; Reinhard et al. 2009). The broad-scale features of the $\Delta^{33}S$ and $\delta^{34}S$ records thus paint a coherent picture of Archean atmospheric chemistry—low O_2 concentrations that lead both to extensive photochemical sulfur cycling imparting large MIF and limited biogeochemical sulfur cycling at Earth's surface imparting small MDF. There is, however, a more nuanced structure to the Archean S-isotope record including an expansion in the ranges of both $\Delta^{33}S$ and $\delta^{34}S$ between the 2.7 and 2.45 Ga (Fig. 3.1). The $\Delta^{33}S$ expansion was attributed to changes in the oxidation state of volcanic sulfur vented to the atmosphere (Halevy et al. 2010), whereas the $\delta^{34}S$ expansion was thought to reflect increased sulfate concentrations in oceans (Habicht et al. 2002). We show here that the Neoarchean records of $\Delta^{33}S$ and $\delta^{34}S$ both indicate progressive seawater oxygenation beginning at 2.7

Ga, and our models constrain the corresponding levels of O₂ and sulfate in Archean coastal environments.
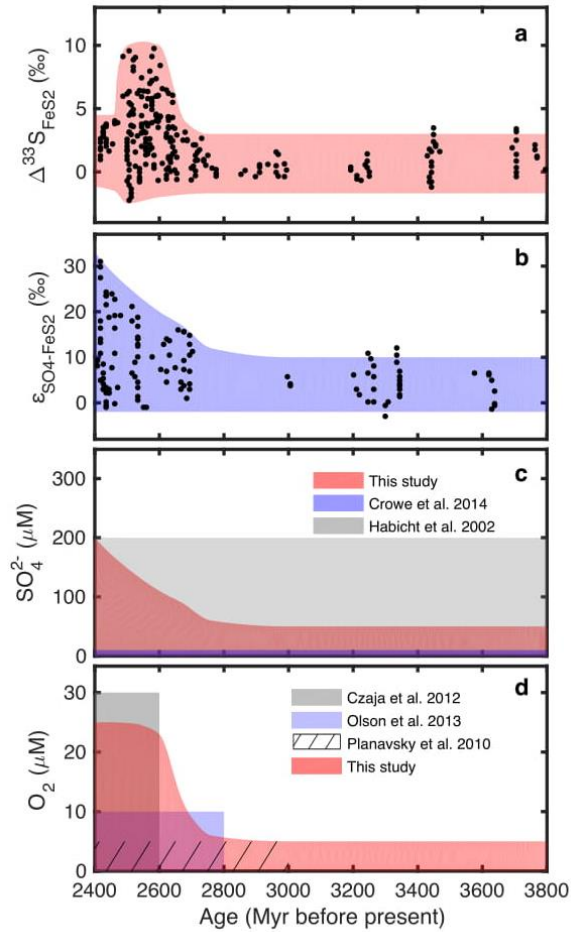
Figure 3.1 *Record of (a) $\Delta^{33}S_{SO4\text{-}FeS2}$ and (b) $\varepsilon_{SO4\text{-}FeS2}$ (assuming seawater sulfate value of 12‰), and the simulated (c) oceanic sulfate and (d) O₂ levels through time. Data points are from Canfield and Farquhar (2009) and Johnston (2011). Simulated outlines for sulfate and O₂ concentrations correspond to values for which our model reproduces the S isotope records.*

The $\delta^{34}S$ and $\Delta^{33}S_{FeS2}$ isotopic records preserved in Archean sedimentary pyrites carry signatures of atmospheric processes as well as information about isotopic alterations taking place in oceanic water column and in sediments after their deposition. The transformations during early diagenesis were investigated here with a 1D reaction-transport model, which traced the differential dynamics of sulfur isotopes through a network of geochemical and biogeochemical reactions (*see Model description*) and provided insights into the preservation patterns of S isotopes and the role of oxygen in them.

The pre-GOE expansion in sulfate-pyrite $\delta^{34}S$ isotopic differences, $\varepsilon_{SO4\text{-}FeS2}$, has been previously ascribed to rising seawater sulfate concentrations, which lead to more intense sedimentary sulfate reduction and generate isotopically lighter pyrite (Habicht et al. 2002; Crowe et al. 2014). Our simulations support this conclusion but additionally suggest that the presence of dissolved O_2 also increases the $\delta^{34}S$ range by intensifying in-sediment sulfate-sulfide redox cycling. Low-micromolar O_2 concentrations, however, only increase $\varepsilon_{SO4\text{-}FeS2}$ by a few permil, as sulfur cycling remains limited and fractionation during sulfide oxidation is minor in comparison to that imparted during sulfate reduction (Fig. 3.12a). The effect of O_2 on the preservation of $\Delta^{33}S$ signatures, in contrast, is pronounced. Oxygen in the atmosphere is generally thought to preclude the formation of MIF-S due to ozone formation and the shielding of the UV radiation needed for SO_2 photolysis (Farquhar et al. 2000; Ono et al. 2003). Our modeling, on the other

hand, reveals that O_2 in the ocean enhances the preservation of MIF-S in pyrite (Fig. 3.12b). Pyrite is
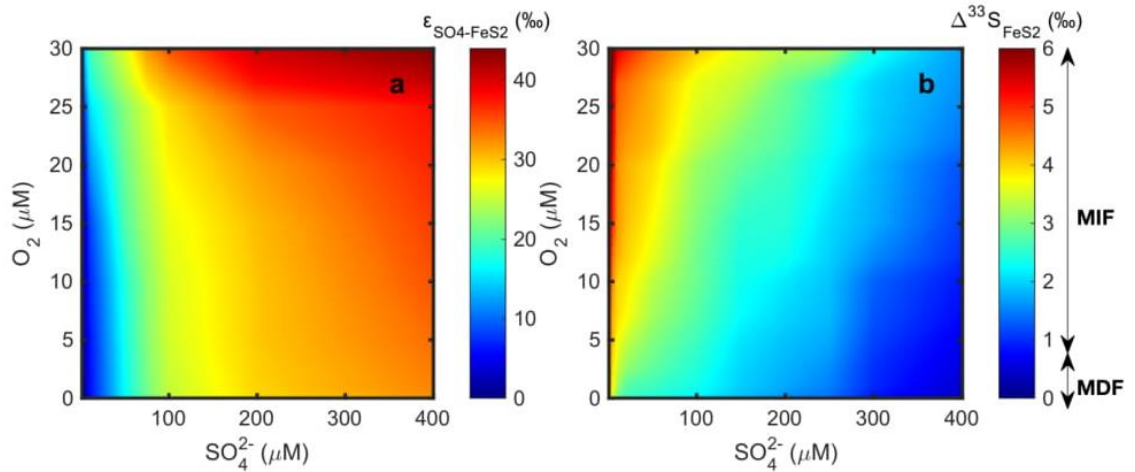
Figure 3.2 *(a) Modeled range of $\delta^{34}S$ isotopic differences between seawater sulfate and sedimentary pyrites ($\varepsilon_{SO4-FeS2}$) for different O_2 and sulfate levels. (b) Modeled range of $\Delta^{33}S_{FeS2}$ for which atmospheric MIF-S signal is preserved in sedimentary pyrites, as a function of seawater O_2 and sulfate levels. Up-down arrows correspond to the respective ranges of mass independent (MIF) and mass dependent fractionations (MDF). Higher resolution details at the low sulfate range are provided in Fig. 3.8.*

typically formed when iron monosulfide reacts with either elemental S or hydrogen sulfide (R_{FeS+S} and R_{FeS+HS} in Table 3.1). When the atmospheric MIF-S signal is transmitted from elemental S into pyrite through diagenesis, it is thus influenced by the isotopic composition of iron monosulfide and porewater hydrogen sulfide (Fig. 3.2). As hydrogen sulfide can be produced from non-MIF-S sulfate through microbially catalyzed

reactions such as sulfate reduction that impart mass-dependent fractionation, its addition to pyrite dilutes the MIF-S signal. Hydrogen sulfide precipitation with ferrous iron generates iron monosulfide, the isotopic composition of which becomes a complex function of the intensity of sulfate reduction, recycling of hydrogen sulfide through redox processes within sediment, and Rayleigh distillation (Jorgensen 1979; Goldhaber and Kaplan 1980). These processes make the MIF-S signatures in pyrite dependent on the rate of sulfate reduction, which is regulated by the availability of sulfate and reactive organic matter (Fakhraee et al. 2017), and several other factors involved in sediment S cycling (Figs. 3.12b, 13 and 3.8). Oxygen plays a key role by controlling oxidative S-cycling and the supply of reactive organic matter available to fuel sulfate reduction. Higher O_2 levels in particular enhance the preservation of MIF-S signals (Fig. 3.12b) by decreasing the sulfate reduction rates through deepening of the depth of the sulfate reduction zone in the sediment and limiting the supply of reactive organic matter reaching that zone. In contrast to the effect of O_2, increased sulfate levels result in more intense sulfate reduction and hydrogen sulfide production, and more intense dilution of MIF-S signal, resulting in lower $\Delta^{33}S$ (Fig. 3.12b, 3.13 and 3.8, 3.9).

Isotopic variability induced by rising marine O_2 and concomitant increases in seawater sulfate provide a self-consistent explanation for the observed Neoarchean expansions in $\Delta^{33}S$ and $\delta^{34}S$ ranges. In Archean rocks, high values of $\Delta^{33}S$ tend to be associated with low values of $\varepsilon_{SO4-FeS2}$, while larger values of $\varepsilon_{SO4-FeS2}$ tend to occur at low $\Delta^{33}S$ (Fig. 3.13). This pattern has been attributed to variability in the atmospheric processes that produce MIF-S (Halevy et al. 2010). Figure 3 illustrates that diagenetic

processes can impart a similar relationship, where $\delta^{34}S$ and $\Delta^{33}S$ co-vary depending on seawater O_2 and sulfate concentrations. The increase in $\Delta^{33}S$ variability in the Neoarchean was previously attributed to changes in the oxidation state of volcanic sulfur emitted to the atmosphere (Halevy et al. 2010), and to the associated shift in photochemical S transformation pathways (Zahnle et al. 2006; Domagal-Goldman et al. 2008; Halevy et al. 2010). This explanation, however, relies on the assumption that atmospherically produced MIF-S signals remain unmodified by diagenesis (Halevy et al. 2010), which requires persistently negligible sediment sulfate reduction. This conflicts with recent evidence for increased microbial sulfate reduction in the Neoarchean (Zhelezinskaia et al. 2014) and with the correlative expansion in $\varepsilon_{SO4-FeS2}$, which is a known indicator for increased sulfate concentrations and enhanced rates of sulfate reduction (Habicht et al. 2002). Furthermore, there remains no known geological process that would induce the inferred shift in the oxidation state of volcanic gases prior to the GOE. Our model suggests instead that the Neoarchean expansion in $\Delta^{33}S$ and $\delta^{34}S$ reflects the protracted oxygenation of seawater and an early ingrowth in marine sulfate (Fig. 3.13).
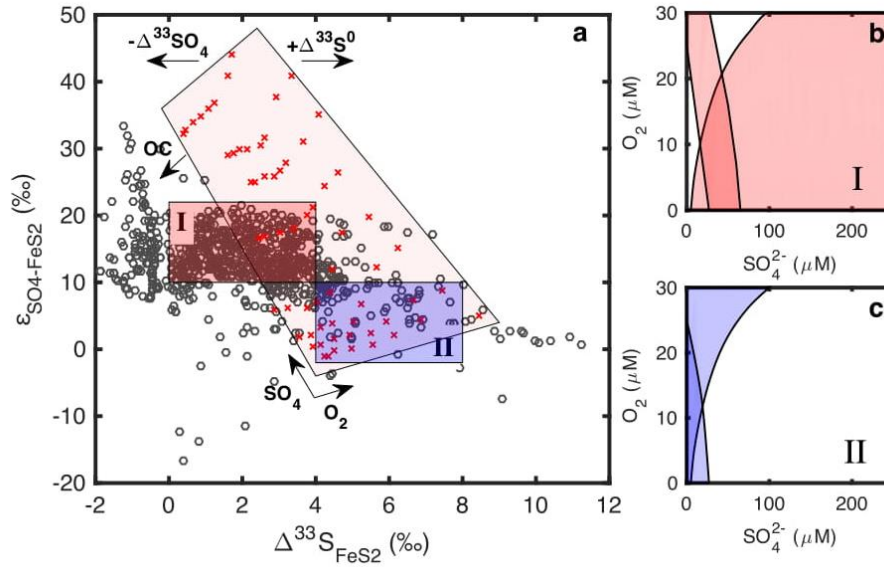
Figure 3.3 *(a) Sulfur isotope data (circles) in Archean pyrites older than 2.4Ga (Johnston et al. 2011). Sulfate-pyrite isotopic differences $\varepsilon_{SO4\text{-}FeS2}$ were calculated from rock $\delta^{34}S$ values for the value of $\delta^{34}S$ in seawater sulfate of 12‰. Shaded region corresponds to model's range in Fig. 3.12, obtained for sediment organic carbon (OC) content of 0.1%, the $\Delta^{33}S^0$ in the deposited elemental sulfur of 10‰, and the $\Delta^{33}SO_4$ in seawater sulfate of zero. Arrows indicate the directions in which the modeled range shifts in response to increases in indicated parameters. (b,c) Ranges (dark shading) of O_2 and sulfate that correspond to the isotopic ranges within the respective outlines I and II in panel (a). Lightly shaded areas correspond to the respective ranges in individual isotopic parameters, $\varepsilon_{SO4\text{-}FeS2}$ and $\Delta^{33}S_{FeS2}$, calculated for the same set of parameters as in Fig. 3.12. The modeled trends indicate that preservation of large $\varepsilon_{SO4\text{-}FeS2}$ values observed after 2.7 Ga (Fig. 3.1) requires high sulfate, whereas preservation of large $\Delta^{33}S_{FeS2}$ values requires the presence of O_2.*

Comparisons of our model results with the $\delta^{34}S$ and $\Delta^{33}S$ compositions of Archean pyrites allow us to constrain the O_2 and sulfate levels of contemporaneous seawater and identify the effects of several diagenetic factors on the preserved sulfur isotopic signatures (Fig 3.13). The concentrations of O_2 and sulfate required to reproduce given $\delta^{34}S$ and $\Delta^{33}S$ ranges depend on factors such as sediment organic matter

concentration and the isotopic values of elemental S and sulfate delivered to the sediment (Fig. 3.13). The narrow mid-Archean ranges of both $\delta^{34}S$ and $\Delta^{33}S$ require pyrite formation under very low O_2 and low sulfate concentrations. The preservation of large values of $\Delta^{33}S$ observed after 2.7 Ga, in contrast, requires a rise in seawater O_2 concentrations to several μM. The correlative increase in $\epsilon_{SO4\text{-}FeS2}$ signals a contemporaneous increase in seawater sulfate to concentrations on the order of 200 μM. Increased sulfate alone, however, does not reproduce the $\epsilon_{SO4\text{-}FeS2}$ record, which also requires enhanced deposition of organic carbon (Fig. 3.13), as even at low sulfate levels sulfate reduction becomes co-limited by organic substrates (Fakhraee et al. 2017). The Neoarchean S isotope expansion, therefore, likely signals not only the onset of marine oxidative sulfur cycling but also an increase in the ocean's biological productivity, at least in localized coastal oxygen oases.

S isotopes thus paint a cogent picture of Neoarchean ocean oxygenation that is supported by insight from other proxies. Abundant evidence implies O_2 production across more than 700 Ma before the GOE (Wille et al. 2007; Czaja et al. 2012; Crowe et al. 2013; Reinhard et al. 2009; Planavsky et al. 2014; Waldbauer et al. 2011). Development of ocean O_2 "oases" at the onset of the Neoarchean with concentrations up to tens of micromolar is supported by inferences from the geochemistries of molybdenum (Czaja et al. 2012), and manganese and iron (Liu et al. 2016; Planavsky et al. 2010), while cerium anomalies in carbonates (Planavsky et al. 2010) imply shallow water O_2 concentrations approaching ~ 5 μM O_2. Our model supports these estimates and shows that micromolar

O_2 concentrations in the ocean are compatible with (Kasting 2001; Bekker et al. 2004; Guo et al. 2009; Olson et al. 2013) and are possibly even required by the MIF-S record. Global biogeochemical models reveal that seawater O_2 concentrations on the order of 1-10 μM (Olson et al. 2013), and possibly up to 25 μM, can exist under an ostensibly anoxic atmosphere, despite large fluxes of O_2 from the ocean (Kasting 1992). Further, the Neoarchean development of coastal euxina (Reinhard et al. 2009) may also reflect an accompanying increase in seawater sulfate concentrations resulting from enhanced oxidative continental weathering. Our results further suggest that broadening of the $\delta^{34}S$ range during the GOE, after the disappearance of the MIF-S signal (~2.5-2.4 Ga; Fig. 3.1), reflects an increase in seawater O_2 from low μM concentrations to beyond a threshold value of 10s of μM. The sensitivity of pyritic $\varepsilon_{SO4-FeS2}$ values to O_2 is dependent on microbial physiology, but increases dramatically in the range of 10 to 15 μM (Fig. 3.7). The approximately 10‰ increase in $\varepsilon_{SO4-FeS2}$ observed at the GOE thus likely indicates a transition from low μM seawater O_2 concentrations to several tens of μM, rather than its first production and accumulation.

The Neoarchean was thus characterized by a major reorganization of the global S cycle that saw an ingrowth of seawater sulfate, the onset of oxidative sediment sulfur cycling, and an increase in the role of sediment sulfate reduction beginning around 2.7 Ga. This reorganization, captured in the isotopic composition of carbonate associated sulfate (Zhelezinskaia et al. 2014), made microbial sulfate reduction an important sink for marine sulfate (Zhelezinskaia et al. 2014). The onset of O_2 driven marine sulfur cycling, as revealed by the sulfur isotope record (Canfield and Farquhar 2009), signals a broader

expansion of the oxic marine biosphere and the proliferation of aerobic microbial metabolisms likely linked to heterotrophic carbon respiration and possibly methanotrophy and oxidative nitrogen cycling in the sea.

3.2 Model Description
3.2.1 Geochemical Model

Vertical distributions of chemical species within the sediment are simulated at steady state with a diagenetic equation (Crowe et al. 2014; Berner 1980):

$$0 = D_i \varphi \frac{d^2 C_i}{dx^2} - v \frac{dC_i}{dx} + \mathring{a}_j R_{ij} \tag{3.1}$$

Here, x is depth below the sediment surface, C_i is the concentration of species i, D_i is the corresponding molecular diffusion coefficient corrected for sediment porosity φ using the Archie's law factor of $\varphi^{1.14}$ (Boudreau 1997), and v is burial velocity which is neglected for solutes. R_{ij} the rates of reactions that consume or produce species i. The included reactions and their rates are listed in Tables 3.1 & 3.2. Model parameter values are listed in Table 3.3. For simplicity, we assume no sediment compaction so that porosity is constant with depth. Bioturbation and bioirigation are neglected, as macrofauna was absent during the simulated geological period.

The rate of sulfate reduction was simulated using the Michaelis-Menten kinetics:

$$R_{SR} = \frac{V_m [SO_4^{2-}]}{K_m + [SO_4^{2-}]} \frac{K_i}{K_i + [O_2]} \tag{3.2}$$

Here, constant K_m, which describes the affinity of enzymes for substrate, was taken as 5 µM for low sulfate environments (Ingvorsen and Jørgensen 1984). K_i describes

the inhibition effect of oxygen on sulfate reduction. V_m is the maximum sulfate reduction rate under sulfate-replete conditions when the reaction rate is limited by the availability of reactive organic matter. This organic carbon (OC) mineralization rate was approximated

Table 3.1 *Reactions included in the model*

Reactions	Rate
$CH_2O + O_2 \Rightarrow CO_2 + H_2O$	R_{OX}
$SO_4 + 2CH_2O \Rightarrow H_2S + 2HCO_3$	R_{SR}
$CH_2O + 4\ FeOOH_{(s)} + 7CO_2 + H_2O \Rightarrow 4Fe^{2+} + 8\ HCO_3^-$	R_{FeOOH}
$H_2S + 2O_2 + 2HCO_3^- \Rightarrow SO_4^{2-} + 2CO_2 + 2H_2O$	R_{SOX}
$Fe^{2+}\ +\ HS^-\ \Rightarrow\ FeS(s) +\ H^+$	R_{FeS}
$2FeOOH_{(s)} + 3H_2S_{(aq)} => S^0_{(s)} + 2FeS_{(s)} + 4H_2O$	R_{S0}
$4\ S^0_{(s)} + 4H_2O => SO_4^{2-} + 3HS^- + 5H^+$	R_{Disp}
$FeS + S^0 => FeS_2$	R_{FeS+S}
$FeS + H_2S => FeS_2 + H_2$	R_{FeS+HS}

Table 3.2 *Kinetics of the reactions included in the model. KFeS, and KH₂S are the equilibrium constants for FeS precipitation and acidity constant for H₂S, respectively.*

Reaction	Rate expression
Sulfide Oxidation	$R_{SOX} = k_{SOX}[O_2][H_2S]$
Aerobic Respiration	$R_{OX} = \dfrac{V_m[O_2]}{K_i + [O_2]}$
Iron Reduction	$R_{FeOOH} = \dfrac{V_m[FeOOH]}{K_{FeOOH} + [FeOOH]} \dfrac{K_i}{K_i + [O_2]}$
Sulfide Precipitation	$R_{FeS} = k_{FeS}(\dfrac{\Omega}{K_{FeS}} - 1)$ $\Omega = \dfrac{[Fe^{2+}][HS^-]}{[H^+]}$ $[HS^-] = \dfrac{[H_2S]}{1 + [H^+]K_{H_2S}}$
FeS₂ precipitation with S⁰	$R_{FeS+S} = k_{FeS+S}[FeS][S^0]$
FeS₂ precipitation with H₂S	$R_{FeS+HS} = k_{FeS+HS}[FeS][H_2S]$
Sulfate Reduction	$R_{SR} = \dfrac{V_m[SO_4^{2-}]}{K_m + [SO_4^{2-}]} \dfrac{K_i}{K_i + [O_2]}$
Elemental Sulfur Formation	$R_{S0} = k_{S0}[FeOOH][H_2S]$
Elemental Sulfur Disproportionation	$R_{Disp} = k_{Disp}[S^0](1 - \frac{[H_2S]}{[H_2S]_{stop}})$ For [H₂S] < [H₂S] stop 0 For [H₂S] ≥ [H₂S] stop

as V_m = k [OC] where the reactivity k was described by the Middelburg power law as a function of carbon age t: $\log_{10}$ k = - (0.95) $\log_{10}$ t – (0.81). This power law was recently shown to hold over a range of conditions including low-sulfate environments (Katsev and Crowe 2015). Our model was set to describe shallow water environments, as most studies

of oxygen in the Archean Ocean suggest them as most likely locations of oxic conditions (Planavsky et al. 2014). Thus, sedimentation rate was assumed at 0.5 g cm^{-2} yr^{-1} which is within the typical range of marine environments with water depth less than 100m (Li et al. 2012; Canfield 1994; Burdige 2007). Global marine productivity in the Archean was estimated at up to 5 x 10^{14} mol C yr^{-1} (Canfield et al. 2006); combining this with an ocean surface area of 3.61 x 10^{14} m^2 yields the average primary production of 1.39 mol C m^{-2} yr^{-1}. As at least 10 percent of produced material was likely delivered to the sediment in shallow waters (water depth< 100m) (Li et al. 2012), the carbon flux to the sediment water interface can be estimated to be on the order of 400 µmol m^{-2} d^{-1}. The initial age of organic matter at the sediment-water interface for the Middelburg power law was calculated at 1.11 year using the Stockes' law, the settling rate of organic matter with particle of the average size of 1 µm and density of 2650 kg m^{-3} (45 m yr^{-1}), and the average water depth of 50m. It was assumed that adsorption of organic matter to particles was the main process in delivering the organic matter to the sediment. The carbon age was converted to depth below sediment surface using constant porosity φ and assumed solid sediment density ρ_x.

For simplicity, the concentration of Fe(OH)$_3$ was defined by using a function that mimics the FeOOH profiles in modern freshwater (low-sulfate) and marine sediments (Li 2014):

$$[FeOOH] = [FeOOH]_1 \left(\frac{1}{1 + e^{x-OPD}} + 2e^{-\frac{(x-OPD)^2}{2}} \right) \tag{3.3}$$

97

where depth x>OPD is in cm and $[FeOOH]_1$ is a constant. The OPD was defined as depth where oxygen level becomes less than 0.1µM.

Disproportionation reactions of sulfur compounds of intermediate oxidation states (S^0, S_2O_3, and SO_3) can contribute to isotopic fractionations and, through a repeated cycle of sulfide oxidation and disproportionation can generate more ^{34}S-depleted sedimentary sulfides (Canfield and Teske 1996; Canfield and Thamdrup 1994). In particular, Canfield and Thamdrup (1994) showed that disproportionation of elemental sulfur results in the isotopic fractionation where the produced sulfate is enriched in ^{34}S by 12.6 to 15.3 per mil and the produced sulfide is depleted in ^{34}S by 7.3 to 8.6‰. Higher concentrations of elemental sulfur were shown to increase the disproportionation rate and result in larger fractionation. In modern sediments, the sulfur compounds of intermediate oxidation state are typically produced through the oxidation of hydrogen sulfide via several potential pathways (Table 3.4), particularly through the oxidation of sulfide by iron oxides. We considered elemental sulfur formation through oxidation of sulfide by iron oxides; however, at the low sulfide level in our model, other proposed reactions that result in the production of elemental sulfur are thermodynamically unfavorable (Table 3.4). That fractionation decreases at low elemental sulfur levels (Canfield and Thamdrup 1994) further suggests that fractionation associated with S^0 cycling should be minor. Although all the reactions in Table 3.4 are unfavorable at the sulfide level in our model, the first two reactions become favorable under higher levels of sulfide (>100µM), and are observed in modern environments (Canfield et al. 2005). The last reaction can become favorable under acidic conditions (pH<6) and high levels of sulfide. Thiosulfate and

sulfite as intermediate products of sulfide oxidation can also generate isotopic fractionations through disproportionation, but, at low sulfide availability, sulfide as growth-limiting substrate for bacteria should be oxidized directly to sulfate without intermediate reactions (Pfennig 1975; Canfield and Teske 1996). The contributions from thiosulfate and sulfide are therefore neglected.

Diagenetic equations (3.1) for sulfate, hydrogen sulfide, and oxygen were iteratively solved in Matlab as a boundary-value problem using the ″bvp4c″ function. The imposed boundary conditions are listed in Table 3.5. Sample results from the model for the sediment profiles of sulfate, sulfide, oxygen, iron, CRS pool including FeS and elemental sulfur, as well as the rates of sulfate reduction (R_{SR}) and sulfide re-oxidation(R_{SOX}) are presented in Fig. 3.2. Model parameter values are summarized in Table 3.3.

Table 3.3 *Parameters for reactive transport modeling and sensitivity analysis.*

Parameter	Symbol	Value	Unit	Range used in sensitivity analysis	Ref.
Diffusion coefficient of sulfate	D_{SO4}	232.87	cm^2/year	200-400	Canfield 2006
Diffusion coefficient of sulfide	D_{H2S}	500	cm^2/year	400-600	Burdige & Lerman 2006
Diffusion coefficient of oxygen	D_{O2}	400	cm^2/year	300-500	Burdige & Lerman 2006
Organic matter content at the sediment-water interface	C_{org}	0.0035	g per g dry weight	-	-
Sulfide oxidation rate constant	k_{SOX}	1600	µM^{-1}year^{-1}	16-1600	Cappellen & Wang 1996
FeS precipitation rate constant	k_{FeS}	10^{-5}	mol g^{-1} yr^{-1}	10^{-7}-10^{-5}	Dyrssen, & Kremling 1996
FeS equilibrium constant	K_{FeS}	10^{-4}	M	-	Dyrssen, & Kremling 1996
Acid-base equilibrium constant for H$_2$S	K_{H2S}	2.48x10^{-7}	-	-	Dyrssen, & Kremling 1996
S^0 formation rate constant	k_{S0}	8x10^{-3}	µM^{-1}year^{-1}	10^{-5}-10^{-1}	Dyrssen, & Kremling 1996
Rate constant for FeS$_2$ precipitation with S^0	k_{FeS+S}	10^4	mol^{-1}g yr^{-1}	-	Dyrssen, & Kremling 1996
Rate constant for FeS$_2$ precipitation with H$_2$S	k_{FeS+HS}	0.003	µM^{-1}year^{-1}	-	Dyrssen, & Kremling 1996
Monod constant for FeOOH reduction	K_{FeOOH}	20	µmol/g	15-30	Dyrssen, & Kremling 1996

S^0 disproportionation rate constant	k_{Disp}	0.01	year^{-1}	0.001-0.1	Jourabchi et al. 2005
Threshold H_2S concentration for disproportionation	$[H_2S]_{stop}$	10	mM	-	Jourabchi et al. 2005
Monod constant for SO_4^{2-} reduction	K_m	5	µM	5-25	Ingvorsen, & Jørgensen 1984
Monod constant for O_2 (inhibition constant)	K_i	1	µM	0.5 – 2	Katsev et al. 2007
Fe^{2+} concentration scale	$[Fe]_1$	20	µM	-	-
$Fe(OH)_3$ concentration scale	$[Fe(OH)_3]_1$	10	mg/g	-	-
Burial Velocity	ν	0.18	cm/yr	-	-
Porosity	ϕ	0.9	-	-	-
Density of dry sediment	ρ_s	2.6	g/cm^3	-	-
Grid size	dz	6.67x10^{-3}	cm	-	-
pH	pH	8	-	7-9	Kempe & Degens 1985

Table 3.4 *Thermodynamic favorability of reactions suggested for elemental sulfur formation.*

Reaction	ΔG^0 (kJ/mol)	ΔG_r(kJ/mol)	[H$_2$S]/[HS$^-$] (µM)	[H$^+$] (µM)	[Fe^{2+}] (µM)	[Mn^{2+}] (µM)	[CO$_2$] (µM)	[HCO$_3^-$] (µM)	[H$_2$] (µM)
2FeOOH$_{(s)}$ + 3H$_2$S$_{(aq)}$ => S$^0_{(s)}$ + 2FeS$_{(s)}$ + 4H$_2$O	-79	-57	10	-	-	-	-	-	-
MnO$_{2(s)}$ + HS$^-_{(aq)}$ + 3H$^+_{(aq)}$ => Mn$^{2+}_{(aq)}$ + S$^0_{(s)}$ + 2H$_2$O	-52	101	1	10^{-2}	-	50	-	-	-
H$_2$S$_{(aq)}$ + 4CO$_2$ + 2Fe(OH)$_{3(s)}$ => 2Fe$^{2+}_{(aq)}$ + S$^0_{(s)}$ + 2H$_2$O + 4HCO$_3^-$	98	126	1	-	50	-	10	1000	-
FeS$_{(s)}$ + 2H$_2$O => FeOOH$_{(s)}$ + 3/2H$_2$ + S$^0_{(s)}$	81	55	-	-	-	-	-	-	1000
Fe$_3$O$_{4(s)}$ + HS$^-_{(aq)}$ + 7H$^+_{(aq)}$ => 3Fe$^{2+}_{(aq)}$ + S$^0_{(s)}$ + 4H$_2$O	171	261	1	10^{-2}	50	-	-	-	-

Table 3.5 *Model boundary conditions for sulfate, sulfide and oxygen*

Boundary conditions	Symbol	Top	Bottom
Sulfate	$[SO_4^{2-}]$	1-1000 µM	$d[SO_4^{2-}]/dx=0$
Sulfide	$[H_2S]$	0	$d[H_2S]/dx=0$
Oxygen	$[O_2]$	0-25 µM	$d[O_2]/dx=0$
Iron	$[Fe^{2+}]$	0	$d[Fe^{2+}]/dx=0$

3.2.2 Isotopic Model

The isotopic model uses results from the geochemical model to calculate the concentrations and rates for individual isotopes and to compute the isotopic ratios of interest. Fractionations during diagenetic reactions are calculated using defined fractionation factors, as described below; these fractionations are used to adjust the reaction rates for individual isotopes; the concentration profiles for each isotope are calculated based on the obtained rates; and the self-consistency of the obtained results is enforced through iteration. Figure 3.4 illustrates the considered reactions and isotopic fractionations associated with each pathway in the model.

Oxic $SO_4, \Delta^{33}S=0$ $S^0, \Delta^{33}S\neq0$

$O_2, 5‰$

Anoxic Fe(OH)$_3$, 5‰

Disp, -12‰ S^0

Disp, 7‰ H$_2$S

SO_4^{2-}

SR, 30‰

Fe^{2+}

FeS

$S^0, \Delta^{33}S\neq0$ H$_2$S, $\Delta^{33}S=0$

& $S^0, \Delta^{33}S=0$

FeS$_2$
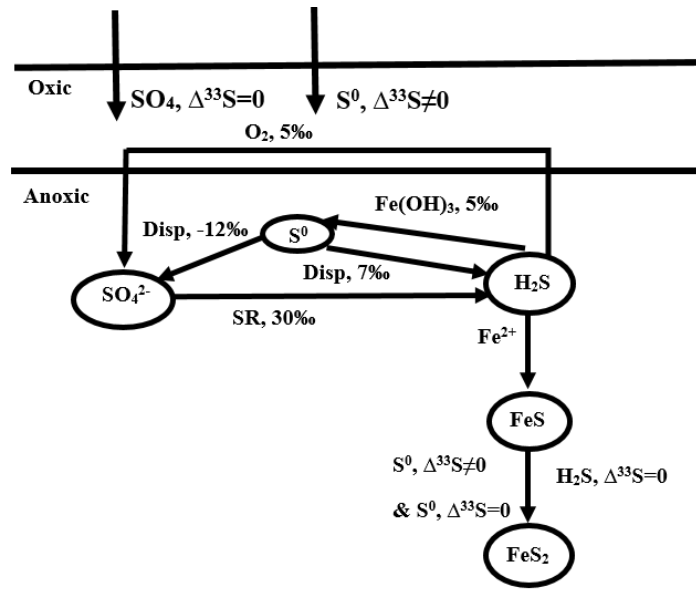
Figure 3.4 Sediment sulfur cycle with isotopic fractionation associated with each reaction

The total rate of sulfate reduction obtained from the geochemical model can be partitioned in terms of the individual isotope rates:

$$R_{32SR} + R_{33SR} + R_{34SR} = R_{SR} \tag{3.4}$$

To calculate the individual rates, the total rate was first approximated as $R_{32SR}+R_{34SR} = 0.9924\ R_{SR}$, as the sediment sulfate pool is dominated by two stable isotopes, $^{32}SO_4$ (96%) and $^{34}SO_4$ (4%). R_{33SR} will then be calculated based on the R_{32SR} value. As sulfate reducing bacteria reduce the isotopically light sulfate at a higher rate, the reduction rates for the two isotopes can be written as:

$$R_{32SR} = \frac{[^{32}SO_4^{2-}]}{[SO_4^{2-}]} n\ 0.9924 R_{SR} \tag{3.5}$$

$$R_{34SR} = \frac{[^{34}SO_4^{2-}]}{[SO_4^{2-}]} m\ 0.9924 R_{SR} \tag{3.6}$$

where $[^{32}SO_4]$ and $[^{34}SO_4]$ are the concentrations of the isotopically light and heavy sulfate respectively and n>1 and m<1 are parameters (Jorgensen 1979) whose ratio, termed the bacterial fractionation factor (α), describes the preferential use of the lighter isotope:

$$\alpha = \frac{n}{m} \tag{3.7}$$

Using Eq. (3.5-3.6), the reduction rates of $^{34}SO_4^{2-}$ and $^{32}SO_4^{2-}$ and the concentrations of $^{34}SO_4^{2-}$ and $^{32}SO_4^{2-}$ are related as

$$\alpha = \frac{R_{32SR}\,[^{34}SO_4^{2-}]}{R_{34SR}\,[^{32}SO_4^{2-}]} \tag{3.8}$$

For α, we conservatively imposed a fractionation factor of 30 ‰ (α=1.030), which is typical for sulfate reducing bacteria (Canfield 2001) and decreased this fractionation linearly below 6 μM, which reflects sulfate limitation (Habicht et al. 1998, Bradley et al. 2016), similarly to previous models (Crowe et al. 2014). Similar approach was used for other reactions: For sulfide oxidation, fractionation was considered constant (1.005) at all concentration levels (Habicht et al. 1998). For elemental sulfur disproportionation, fractionations 0.988 and 1.007 were used respectively for sulfate and sulfide (Canfield and Thamdrup 1994).

For sulfate reduction, defining η = $[^{34}SO_4^{2-}]$: $[^{32}SO_4^{2-}]$, the reduction rates for individual isotopes were calculated from the overall rate R_{SR} as:

$$R_{32SR} = \frac{0.9924 * R_{SR}}{1 + \dfrac{\eta}{\alpha}} \tag{3.9}$$

$$R_{34SR} = \frac{0.9924 * R_{SR}}{1 + \frac{\alpha}{\eta}}$$

(3.10)

The coefficient 0.9924, as discussed above, represents an approximation for the total rate based on the two most abundant ^{32}S and ^{34}S isotopes. At the beginning of iterations, the initial value of η was calculated from the following equation with the initial value of $\delta^{34}SO_4^{2-}$ of 12‰:

$$\eta = \frac{\delta^{34}SO_4^{2-} * \frac{^{34}S_{CDT}}{^{32}S_{CDT}}}{1000} + \frac{^{34}S_{CDT}}{^{32}S_{CDT}}$$

(3.11)

where CDT refers to the $^{34}S/^{32}S$-ratio of the standard troilite, an iron monosulfide from the Canyon Diablo Meteroite.

The isotopic fractionations for the ^{33}S isotope were treated similarly. The fractionation factor (α') for $^{33}SO_4^{2-}$ was written as:

$$\alpha' = \frac{R_{32SR}[^{33}SO_4^{2-}]}{R_{33SR}[^{32}SO_4^{2-}]}$$

(3.12)

and the value of α' (in permil) was defined as $\alpha'=0.515\alpha$, where the coefficient 0.515 reflects the relative mass difference of $^{33}S/^{32}S$ vs $^{34}S/^{32}S$, which defines the mass dependent fractionation (Eq. 3.75 below).

Defining similarly $\eta' = [^{33}SO_4^{2-}]$: $[^{32}SO_4^{2-}]$, the reduction rate for $^{33}SO_4^{2-}$ was calculated as:

$$R_{33SR} = R_{32SR}\frac{\eta'}{\alpha'}$$

(3.13)

The initial value of η' was calculated using the initial value of $\delta^{33}SO_4^{2-}$ of 2.5‰:

$$\eta' = \frac{\delta^{33}SO_4^{2-} * \frac{^{33}S_{CDT}}{^{32}S_{CDT}}}{1000} + \frac{^{33}S_{CDT}}{^{32}S_{CDT}} \tag{3.14}$$

Similarly, for sulfide oxidation, the kinetic fractionation factor (ω) was defined as:

$$\omega = \frac{R_{32SOX}\,[H_2{}^{34}S]}{R_{34SOX}\,[H_2{}^{32}S]} \tag{3.15}$$

Using $f_{H2S} = [H_2{}^{34}S]: [H_2{}^{32}S]$, the specific rates of sulfide oxidation were calculated from the overall oxidation rate:

$$R_{32SOX} = \frac{0.9924 * R_{SOX}}{1 + \frac{f_{H_2S}}{\omega}} \tag{3.16}$$

$$R_{34SOX} = \frac{0.9924 * R_{SOX}}{1 + \frac{\omega}{f_{H_2S}}} \tag{3.17}$$

Similarly, to Eq. (3.11), the initial value of f_{H2S} for iterations was calculated as:

$$f_{H_2S} = \frac{\delta H_2{}^{34}S * \frac{^{34}S_{CDT}}{^{32}S_{CDT}}}{1000} + \frac{^{34}S_{CDT}}{^{32}S_{CDT}} \tag{3.18}$$

The fractionation factor (ω') for $H_2{}^{33}S$ was written analogously as:

$$\omega' = \frac{R_{32SOX}\,[H_2{}^{33}S]}{R_{33SOX}\,[H_2{}^{32}S]} \tag{3.19}$$

The value of ω' was defined as $\omega'=0.515\omega$.

With $f'_{H2S}= [H_2{}^{33}S]: [H_2{}^{32}S]$, the oxidation rate for $H_2{}^{33}S$ was calculated from the R_{32SOX} as:

$$R_{33SOX} = R_{32SOX}\,\frac{f'_{H_2S}}{\omega'} \tag{3.20}$$

The initial value of f'_{H2S} was calculated with the initial value of $\delta H_2{}^{33}S$ of 2.5‰:

$$f'_{H_2S} = \frac{\delta H_2{}^{33}S * \frac{{}^{33}S_{CDT}}{{}^{32}S_{CDT}}}{1000} + \frac{{}^{33}S_{CDT}}{{}^{32}S_{CDT}} \tag{3.21}$$

For elemental sulfur disproportionation, the kinetic fractionation factors for the generated sulfate and sulfide were defined, respectively, as:

$$\sigma = \frac{R_{32Disp(SO_4)}[{}^{34}S^0]}{R_{34Disp(SO_4)}[{}^{32}S^0]} \tag{3.22}$$

$$\sigma' = \frac{R_{32Disp(H_2S)}[{}^{34}S^0]}{R_{34Disp(H_2S)}[{}^{32}S^0]} \tag{3.23}$$

For $f_{S0} = [{}^{34}S^0]:[{}^{32}S^0]$, the specific rates of sulfate and sulfide production were calculated from the overall disproportionation rate:

$$R_{32Disp(SO_4)} = \frac{0.25 * 0.9924 * R_{Disp}}{1 + \frac{f_{S^0}}{\sigma}} \qquad \text{(for sulfate)} \tag{3.24}$$

$$R_{34Disp(SO_4)} = \frac{0.25 * 0.9924 * R_{Disp}}{1 + \frac{\sigma}{f_{S^0}}} \tag{3.25}$$

$$R_{32Disp(H_2S)} = \frac{0.75 * 0.9924 * R_{Disp}}{1 + \frac{f_{S^0}}{\sigma'}} \qquad \text{(for sulfide)} \tag{3.26}$$

$$R_{34Disp(H_2S)} = \frac{0.75 * 0.9924 * R_{Disp}}{1 + \frac{\sigma'}{f_{S^0}}} \tag{3.27}$$

Here, coefficients 0.25 and 0.75 correspond to the stoichiometry of the sulfate and sulfide production during sulfur disproportionation.

Similarly to Eqs. (3.11), (3.18) and (3.21), the initial value of f_{S0} was calculated as:

$$f_{S^0} = \frac{\delta^{34}S^0 * \frac{^{34}S_{CDT}}{^{32}S_{CDT}}}{1000} + \frac{^{34}S_{CDT}}{^{32}S_{CDT}} \qquad (3.28)$$

The initial value of $\delta^{34}S^0$ for the model's iterations was taken as 5‰. This choice did not affect the final value achieved on convergence.

Similarly to Eqs. (3.12) and (3.19), the fractionation factors (φ, φ') for $^{33}S^0$ disproportionation were written as:

$$\varphi = \frac{R_{32Disp(SO_4)}[^{33}S^0]}{R_{33Disp(SO_4)}[^{32}S^0]} \qquad \text{(for sulfate)} \qquad (3.29)$$

$$\varphi' = \frac{R_{32Disp(H_2S)}[^{33}S^0]}{R_{33Disp(H_2S)}[^{32}S^0]} \qquad \text{(for sulfide)} \qquad (3.30)$$

The value of φ was defined as $\varphi = 0.515\sigma$.

For $f'_{S^0} = [^{33}S^0]:[^{32}S^0]$, the specific rates of ^{33}S sulfate and sulfide production during elemental sulfur disproportionation were calculated as:

$$R_{33Disp(SO_4)} = R_{32Disp(SO_4)} \frac{f'_{S^0}}{\varphi} \qquad (3.31)$$

$$R_{33Disp(H_2S)} = R_{32Disp(H_2S)} \frac{f'_{S^0}}{\varphi'} \qquad (3.32)$$

The initial value of f'_{S^0} for model iterations was calculated with the initial value of $\delta^{33}S^0$ of 2.5‰:

$$f'_{S^0} = \frac{\delta^{33}S^0 * \frac{^{33}S_{CDT}}{^{32}S_{CDT}}}{1000} + \frac{^{33}S_{CDT}}{^{32}S_{CDT}} \qquad (3.33)$$

No fractionations were considered associated with the formation of Fe sulfides and elemental sulfur:

$$R_{32FeS} = \frac{[H_2{}^{32}S]}{[H_2S]} 0.9924 * R_{FeS} \tag{3.34}$$

$$R_{34FeS} = \frac{[H_2{}^{34}S]}{[H_2S]} 0.9924 * R_{FeS} \tag{3.35}$$

$$R_{33FeS} = \frac{[H_2{}^{33}S]}{[H_2S]} R_{32FeS} \tag{3.36}$$

$$R_{32S^0} = \frac{[H_2{}^{32}S]}{[H_2S]} 0.9924 * R_{S0} \tag{3.37}$$

$$R_{34S^0} = \frac{[H_2{}^{34}S]}{[H_2S]} 0.9924 * R_{S0} \tag{3.38}$$

$$R_{33S^0} = \frac{[H_2{}^{33}S]}{[H_2S]} R_{32S^0} \tag{3.39}$$

Reactions of iron sulfide with elemental sulfur and hydrogen sulfide to form pyrite were also assumed to have no fractionation. As pyrite includes two sulfur atoms, the probabilities of choosing different sulfur isotopes from iron sulfide, elemental sulfur and hydrogen sulfide were expressed as:

$$P_{FeS}(34) = \frac{f_{FeS}}{1 + f_{FeS} + f'_{FeS}} \tag{3.40}$$

$$P_{FeS}(33) = \frac{f'_{FeS}}{1 + f_{FeS} + f'_{FeS}} \tag{3.41}$$

$$P_{FeS}(32) = 1 - P_{FeS}(34) - P_{FeS}(33) \tag{3.42}$$

For elemental sulfur:

$$P_{S^0}(34) = \frac{f_{S^0}}{1 + f_{S^0} + f'_{S^0}} \tag{3.43}$$

$$P_{S^0}(33) = \frac{f'_{S^0}}{1 + f_{S^0} + f'_{S^0}} \tag{3.44}$$

$$P_{S^0}(32) = 1 - P_{S^0}(34) - P_{S^0}(33) \tag{3.45}$$

And for hydrogen sulfide:

$$P_{H_2S}(34) = \frac{f_{H_2S}}{1 + f_{H_2S} + f'_{H_2S}} \tag{3.46}$$

$$P_{H_2S}(33) = \frac{f'_{H_2S}}{1 + f_{H_2S} + f'_{H_2S}} \tag{3.47}$$

$$P_{H_2S}(32) = 1 - P_{H_2S}(34) - P_{H_2S}(33) \tag{3.48}$$

Here, f and f' are the ratios of $^{34}S/^{32}S$, and $^{33}S/^{32}S$ in each species respectively.

The ratios of heavy to light isotopes ($^{34}S/^{32}S$, and $^{33}S/^{32}S$) in pyrite resulted from each of the two pathways – via reactions of iron monosulfide with hydrogen sulfide or elemental sulfur -- then were calculated from the corresponding probabilities as:

$$f_{FeS_2(H_2S)} =$$

$$\frac{P_{FeS}(32)*P_{H_2S}(34)+P_{FeS}(34)*P_{H_2S}(32)+2*P_{FeS}(34)*P_{H_2S}(34)+P_{H_2S}(33)*P_{FeS}(34)+P_{FeS}(33)*P_{H_2S}(34)}{2*P_{FeS}(32)*P_{H_2S}(32)+P_{FeS}(33)*P_{H_2S}(32)+P_{H_2S}(33)*P_{FeS}(32)+P_{FeS}(34)*P_{H_2S}(32)+P_{FeS}(32)*P_{H_2S}(34)} \tag{3.49}$$

$$f'_{FeS_2(H_2S)} =$$

$$\frac{P_{FeS}(32)*P_{H_2S}(33)+P_{FeS}(33)*P_{H_2S}(32)+2*P_{FeS}(33)*P_{H_2S}(33)+P_{H_2S}(33)*P_{FeS}(34)+P_{FeS}(33)*P_{H_2S}(34)}{2*P_{FeS}(32)*P_{H_2S}(32)+P_{FeS}(33)*P_{H_2S}(32)+P_{H_2S}(33)*P_{FeS}(32)+P_{FeS}(34)*P_{H_2S}(32)+P_{FeS}(32)*P_{H_2S}(34)} \tag{3.50}$$

And for reaction of iron suflide with elemental sulfur:

$$f_{FeS_2(S^0)} =$$

$$\frac{P_{FeS}(32)*P_{S^0}(34)+P_{FeS}(34)*P_{S^0}(32)+2*P_{FeS}(34)*P_{S^0}(34)+P_{S^0}(33)*P_{FeS}(34)+P_{FeS}(33)*P_{S^0}(34)}{2*P_{FeS}(32)*P_{S^0}(32)+P_{FeS}(33)*P_{S^0}(32)+P_{S^0}(33)*P_{FeS}(32)+P_{FeS}(34)*P_{S^0}(32)+P_{FeS}(32)*P_{S^0}(34)} \quad (3.51)$$

$$f'_{FeS_2(S^0)} =$$

$$\frac{P_{FeS}(32)*P_{S^0}(33)+P_{FeS}(33)*P_{S^0}(32)+2*P_{FeS}(33)*P_{S^0}(33)+P_{S^0}(33)*P_{FeS}(34)+P_{FeS}(33)*P_{S^0}(34)}{2*P_{FeS}(32)*P_{S^0}(32)+P_{FeS}(33)*P_{S^0}(32)+P_{S^0}(33)*P_{FeS}(32)+P_{FeS}(34)*P_{S^0}(32)+P_{FeS}(32)*P_{S^0}(34)} \quad (3.52)$$

The rates of pyrite precipiation for individual isotopes and individual reactions were then written as follows. For the reaction of iron sulfide with hydrogen sulfide (Table 3.1):

$$R_{32FeS+HS} = \frac{0.9924 * R_{FeS+HS}}{1 + f_{FeS_2(H_2S)}} \quad (3.53)$$

$$R_{34FeS+HS} = \frac{0.9924 * f_{FeS_2(H_2S)} * R_{FeS+HS}}{1 + f_{FeS_2(H_2S)}} \quad (3.54)$$

$$R_{33FeS+HS} = R_{32FeS+HS} * f'_{FeS_2(H_2S)} \quad (3.55)$$

And for the reaction of iron sulfide with elemental sulfur (Table 3.1):

$$R_{32FeS+S} = \frac{0.9924 * R_{FeS+S}}{1 + f_{FeS_2(S^0)}} \quad (3.56)$$

$$R_{34FeS+S} = \frac{0.9924 * f_{FeS_2(S^0)} * R_{FeS+S}}{1 + f_{FeS_2(S^0)}} \quad (3.57)$$

$$R_{33FeS+S} = R_{32FeS+S} * f'_{FeS_2(S^0)} \quad (3.58)$$

These rates were used in the model to calculate the isotopic ratios in the precipitated pyrite, as described below.

To calculate the vertical concentration profiles for $[^{34}SO_4^{2-}]$, $[^{33}SO_4^{2-}]$, $[^{32}SO_4^{2-}]$, $[H_2^{34}S]$, $[H_2^{33}S]$, $[H_2^{32}S]$, $[^{34}S^0]$, $[^{33}S^0]$, and $[^{32}S^0]$, net rates were expressed as follows:

$$NR^{32}SO_4^{2-} = R_{32SR} - R_{32SOX} - R_{32Disp(SO_4)} \tag{3.59}$$

$$NR^{33}SO_4^{2-} = R_{33SR} - R_{33SOX} - R_{33Disp(SO_4)} \tag{3.60}$$

$$NR^{34}SO_4^{2-} = R_{34SR} - R_{34SOX} - R_{34Disp(SO_4)} \tag{3.61}$$

$$NRH_2{}^{32}S = R_{32SOX} + R_{32FeS} + R_{32S^0} + R_{32FeS+HS} - R_{32SR} - R_{32Disp(H_2S)} \tag{3.62}$$

$$NRH_2{}^{33}S = R_{33SOX} + R_{33FeS} + R_{33S^0} + R_{33FeS+HS} - R_{33SR} - R_{33Disp(H_2S)} \tag{3.63}$$

$$NRH_2{}^{34}S = R_{34SOX} + R_{34FeS} + R_{34S^0} + R_{34FeS+HS} - R_{34SR} - R_{34Disp(H_2S)} \tag{3.64}$$

$$NR^{32}S^0 = R_{32S^0} - (R_{32Disp(H_2S)} + R_{32Disp(SO_4)}) - R_{32FeS+S} \tag{3.65}$$

$$NR^{33}S^0 = R_{33S^0} - (R_{33Disp(H_2S)} + R_{33Disp(SO_4)}) - R_{33FeS+S} \tag{3.66}$$

$$NR^{34}S^0 = R_{34S^0} - (R_{34Disp(H_2S)} + R_{34Disp(SO_4)}) - R_{34FeS+S} \tag{3.67}$$

The vertical gradients and concentrations for each isotope were then computed by integrating Eq. (3.1) with rates given by Eqs. (3.59-3.67) over depth. The concentrations, rates, and isotopic ratio parameters (η, η', f, f', σ, σ', φ, φ', α, α', ω, ω') were then recalculated iteratively until convergence was reached.

The isotopic composition of FeS_2 was found after the convergence of iterations by integrating the FeS_2 precipitation rates for individual isotopes. Based on Eq. (1) with $D_i=0$:

$$[Fe^{34}S_2] = \frac{\int_0^l (R_{34FeS+S} + R_{34FeS+HS}) \cdot dx}{v} \tag{3.68}$$

$$[Fe^{33}S_2] = \frac{\int_0^l (R_{33FeS+S} + R_{33FeS+HS}) \cdot dx}{v} \tag{3.69}$$

$$[Fe^{32}S_2] = \frac{\int_0^l (R_{32FeS+S} + R_{32FeS+HS}) \cdot dx}{v} \tag{3.70}$$

The isotopic fractionations are reported in the manuscript relative to international standards, according to the conventional δ-notation (‰):

$$\delta^{34}SO_4^{2-} = \left(\frac{\frac{^{34}SO_4}{^{32}SO_4}}{\frac{^{34}S_{CDT}}{^{32}S_{CDT}}} - 1 \right) . 1000 \tag{3.71}$$

$$\delta Fe^{34}S_2 = \left(\frac{\frac{Fe^{34}S_2}{Fe^{32}S_2}}{\frac{^{34}S_{CDT}}{^{32}S_{CDT}}} - 1 \right) . 1000 \tag{3.72}$$

$$\delta Fe^{33}S_2 = \left(\frac{\frac{Fe^{33}S_2}{Fe^{32}S_2}}{\frac{^{33}S_{CDT}}{^{32}S_{CDT}}} - 1 \right) . 1000 \tag{3.73}$$

The values of $\varepsilon_{SO4\text{-}FeS2}$ and, $\Delta^{33}S_{FeS2}$ are defined as follows:

$$\varepsilon_{FeS_2 - SO_4^{2-}} (‰) = \delta^{34}SO_4^{2-} (‰) - \delta Fe^{34}S_2(‰) \tag{3.74}$$

$$\Delta^{33}S_{FeS_2} (‰) = \delta Fe^{33}S_2(‰) - 0.515 * \delta Fe^{34}S_2(‰) \tag{3.75}$$

The isotope enrichment factor ($\varepsilon_{SO4\text{-}FeS2}$) describes the isotopic enrichment in the source substrate relative to the products. Negative values indicate that the product is depleted in the heavy isotope ^{34}S relative to the source; positive values indicate that the product is enriched in the heavy isotope ^{34}S compared to the source sulfur compound. The δ^{33}S and δ^{34}S values of most Earth materials typically fall on the terrestrial fractionation line: δ^{33}S = 0.515*δ^{34}S. Such relationships occur because the magnitude of isotope fractionation during most (bio)chemical reactions depends primarily on differences in isotope mass, which is termed mass-dependent fractionation. Deviation from the terrestrial fractionation line is commonly expressed as: Δ^{33}S = δ^{33}S - 0.515*δ^{34}S.

A $\Delta^{33}S$ range of $0 \pm 0.5‰$ has been suggested for mass-dependent fractionation (Farquhar and Wing 2003); $\Delta^{33}S$ values outside this range reflect mass independent fractionation of sulfur (MIF-S).
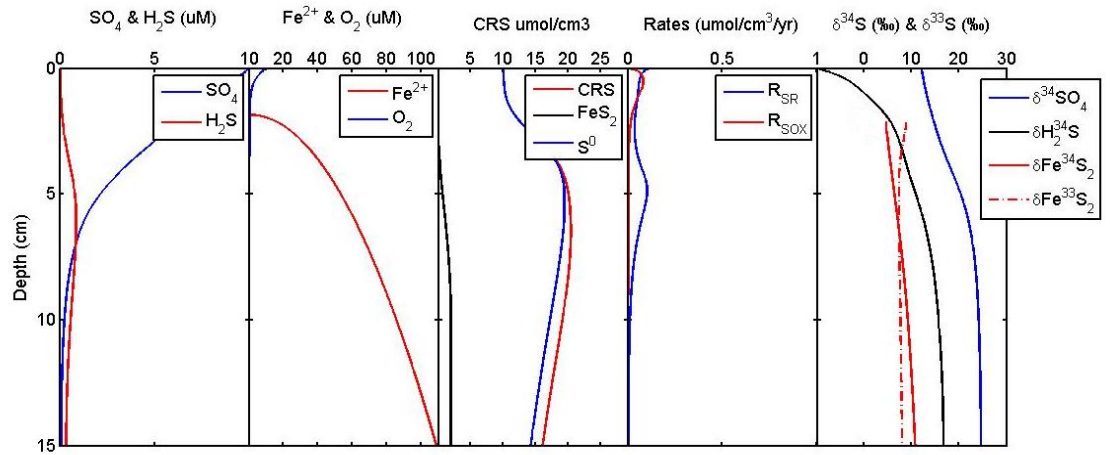
Figure 3.5 *Typical Sediment Profiles of Sulfate, Sulfide, Oxygen, Iron, CRS pool including FeS and elemental sulfur and rates of reduction(R_{SR}), and re-oxidation(R_{SOX}) along with isotopic fractionation of sulfate, sulfide and pyrite for Archean Condition.*

3.2.3 Sensitivity Analysis

To investigate the sensitivity of our results to the values of model parameters, we conducted a sensitivity analysis. Model parameters were varied within their reasonable ranges (specified in Table 3.3), and changes in $\varepsilon_{SO4-FeS2}$ between maximum and minimum of each parameter were recorded. The results are shown in Fig. 3.3. Our conclusions presented in the main manuscript are essentially insensitive (<2‰ change in $\varepsilon_{SO4-FeS2}$) to most parameters including pH, initial age of organic matter, diffusion coefficients, porosity, burial velocity, and elemental sulfur disproportionation rate constant. The parameters that affect the isotopic composition of the precipitated sulfides stronger (2-9‰) include the organic matter content, rate constants for oxidation of sulfide and FeS precipitation, and Monod constants for sulfate reduction and inhibition by oxygen. The sensitivity to organic matter content is illustrated in Fig. 3.4 and 3.5. A greater supply of organic matter increases the sulfate reduction rates and the $\delta^{34}S$ values of sulfides become closer to the seawater sulfate value (Crowe et al. 2014). As ours is the first isotopic model for the Archean conditions to include elemental sulfur disproportionation, and the kinetics of Fe sulfides precipitation, we varied the disproportionation and precipitation rates constants to investigate their effects on the isotopic composition of the resultant pyrites. Increasing the S^0 disproportionation rate constant results in an isotopically lighter pyrite, however, this change is not significant (~2‰) within its reasonable range presented in Table 3. Increasing the kinetics of precipitation (k_{FeS}) also results in an isotopically lighter pyrite and a greater $\varepsilon_{SO4-FeS2}$. At higher rate of precipitation, sulfides

become lighter, and $\varepsilon_{SO4\text{-}FeS2}$ increases. The Monod/inhibition constant (K_i) can also affect the $\varepsilon_{SO4\text{-}FeS2}$: Increasing K_i results in a greater isotopic difference of sulfate to sulfides (Fig. 3.6). This difference is greater at higher oxygen levels: an inflection points around $[O_2] = 10$ µM in Fig. 5 implies that for higher O_2 levels, $\varepsilon_{SO4\text{-}FeS2}$ has a stronger dependence on oxygen. This increased sensitivity suggests that an expansion in the $\varepsilon_{SO4\text{-}FeS2}$ range (such as around GOE), does not need to have resulted from an equivalently higher increase in oxygen levels. Increases in $\varepsilon_{SO4\text{-}FeS2}$ can come from increases in either sulfate or oxygen concentrations (Fig. 3.6). Negative $\varepsilon_{SO4\text{-}FeS2}$ can be obtained for oxygen and sulfate levels below 5µM.

We also investigated the sensitivity of $\Delta^{33}S_{FeS2}$ to model parameters. To investigate the homogenization of the atmospherically produced MIF signal, the model imposed the flux of elemental sulfur with predetermined $\Delta^{33}S$ values, and the diagenetic effect on homogenization of this MIF-S signal was recorded in sedimentary pyrite. The corresponding values of $\delta^{33}S$ and $\delta^{34}S$ are not well constrained for the Archean. The $\delta^{33}S$ and $\delta^{34}S$ values in the deposited elemental sulfur were chosen in our model at $\delta^{33}S=20‰$ and $\delta^{34}S=20‰$ ($\Delta^{33}S_{S0} = 10‰$), based on the trends in Archean pyrites interpreted to reflect mixing between atmospheric S^0 and atmospheric SO_4 sulfur sources (Ono et al. 2003). To address the potential uncertainty, these values were varied in sensitivity analysis (Fig. 3.3). The seawater sulfate was assumed to carry no MIF signal ($\delta^{34}S=12‰$ (Canfield and Farquhar 2009), $\delta^{33}S=6‰$; $\Delta^{33}S_{SO4} = 0$). To investigate the sensitivity of the results to this choice, the model was also run for an alternative set of values ($\delta^{33}S=$-

15‰, $\delta^{34}S=-15$‰; $\Delta^{33}S_{SO4} = -7$‰) (Ono et al. 2003). As S^0 becomes incorporated into pyrite through a reaction with hydrogen sulfide, its MIF signal becomes affected by two processes: parting the system as efflux of sulfide, produced through elemental sulfur disproportionation reaction, and dilution by the pyrites that precipitate from the biologically cycled sulfides without the participation of S^0. The first process is a function of the intensity of sulfate reduction, elemental sulfur disproportionation, redox recycling, and Rayleigh distillation (Jorgensen et al. 1979; Goldhaber and Kaplan 1980). The second process reflects the intensity of sulfate reduction and the fraction of the produced hydrogen sulfide that precipitates as iron monosulfide and subsequently forms pyrite. Change in sulfate, organic matter supply, and oxygen levels affect the value of $\Delta^{33}S_{FeS2}$ (Fig. 3.7, 3.8, 3.9, 3.10). Increased sulfate level results in more intense sulfate reduction, higher biological production of pyrite, and more intense dilution of MIF-S signal (Fig. 3.7, 3.8). Increased organic matter also results in less MIF-S signal preservation. Higher organic matter content increases the sulfate reduction rate but the sulfate reduction zone and pyrite formation zone become shallower and the efflux of sulfide, including sulfide produced through disproportionation of elemental sulfur with MIF-signal (Fig. 3.8), is increased. Change in oxygen level, however played a different role on $\Delta^{33}S_{FeS2}$. As oxygen level increases and oxygen penetration deepens, both the amount and reactivity of organic matter that reaches the sulfate reduction zone decrease, and this results in lower reaction rates (Fig. 3.7, 3.8, 3.9). In consequence, decreased reaction rates attenuate sulfur cycling, efflux of sulfide, rate of biologically produced pyrite, and eventually increase the $\Delta^{33}S_{FeS2}$ value.
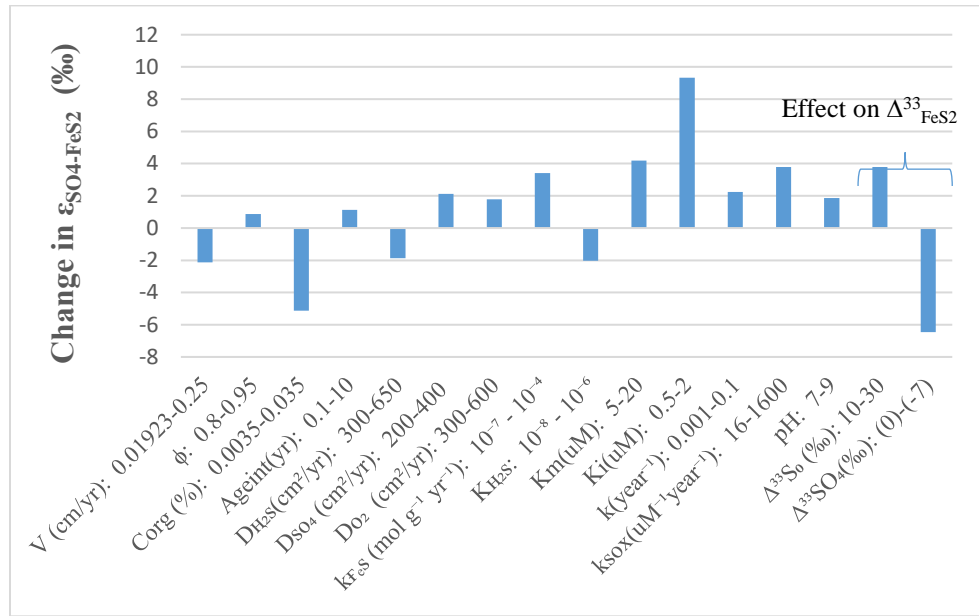
Figure 3.6 *Change in ε$_{SO4-FeS}$ (‰) in response to changes in model parameter values.*
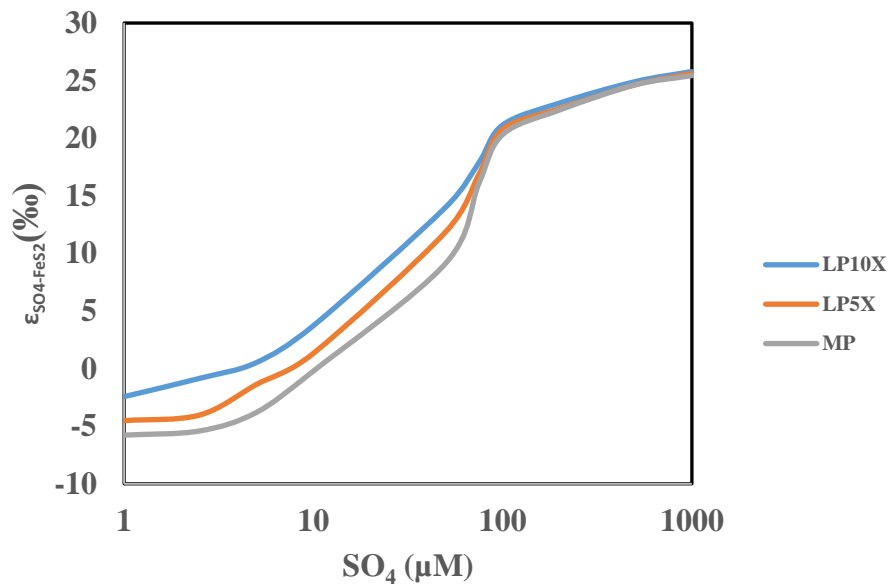
Figure 3.7 *Sensitivity of model outputs to organic matter availability at [O$_2$] = 1µM. MP corresponds to modern levels of productivity (C$_{org}$ = 2%), LP5x and LP10x correspond to 5 and 10 times lower productivity.*
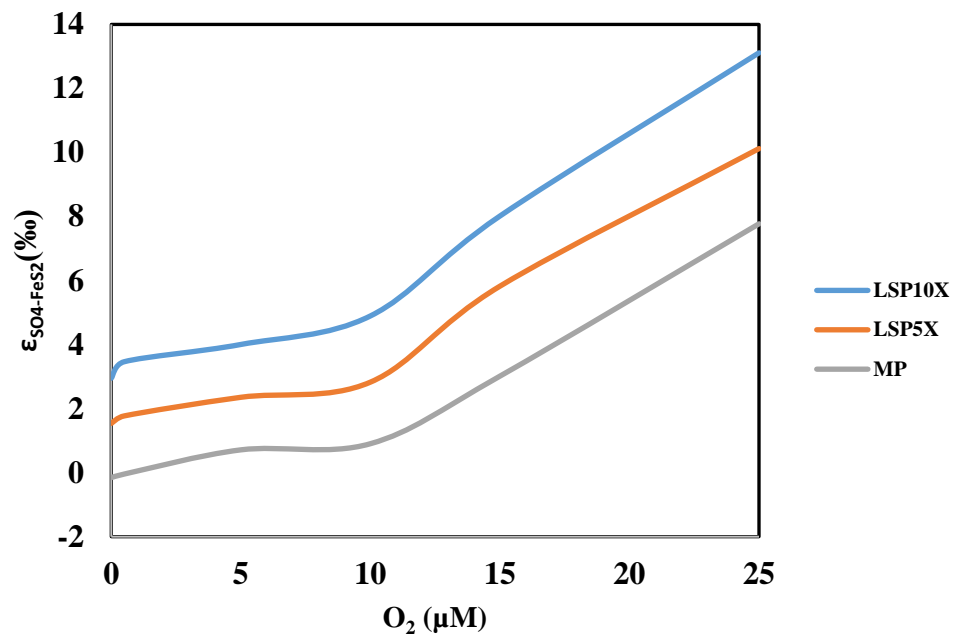
Figure 3.8 *Sensitivity of model outputs to organic matter availability at [SO₄] = 10μM. MP corresponds to modern levels of productivity, LP5x and LP10x correspond to 5 and 10 times lower productivity.*
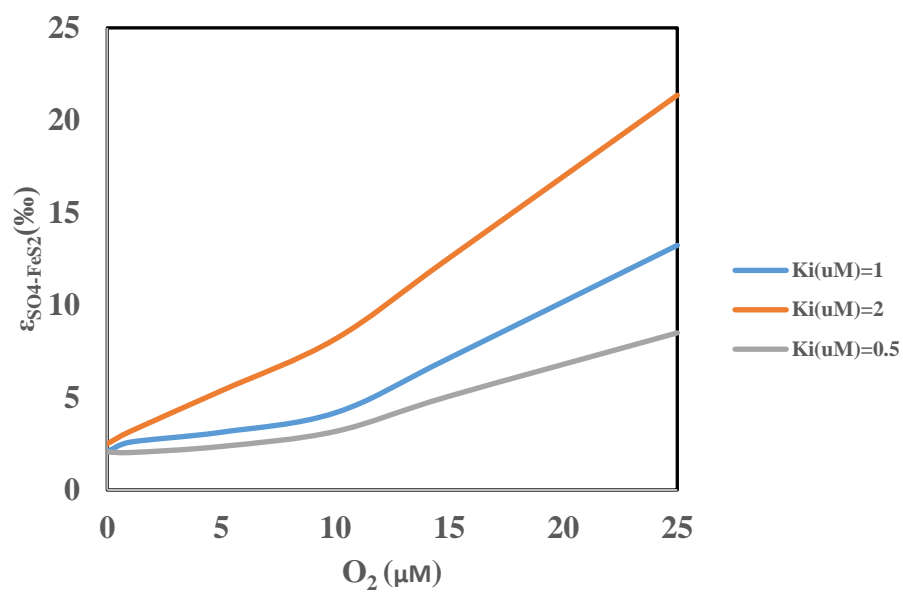
Figure 3.9 *Effect of oxygen inhibition constant (K_i) on $\varepsilon_{SO4\text{-}FeS}$ at $[SO_4] = 10\mu M$.*
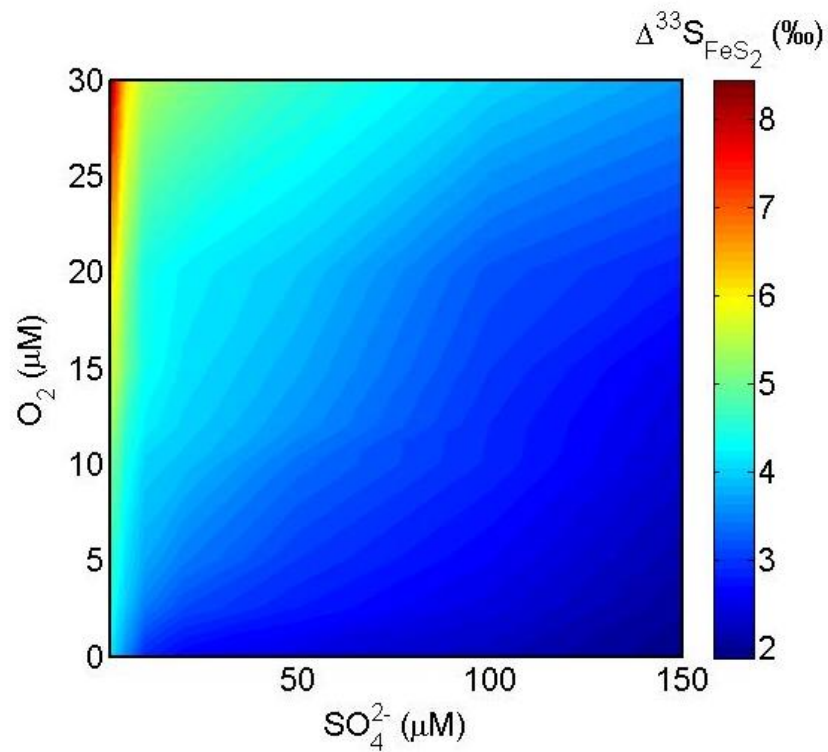
Figure 3.10 *Modeled range of* $\Delta^{33}S_{FeS2}$ *for which atmospheric MIF-S signal is preserved in sedimentary pyrites, as a function of seawater oxygen and sulfate levels. This is similar to Fig. 12b in the results and discussion but provides more resolution in the low sulfate region.*
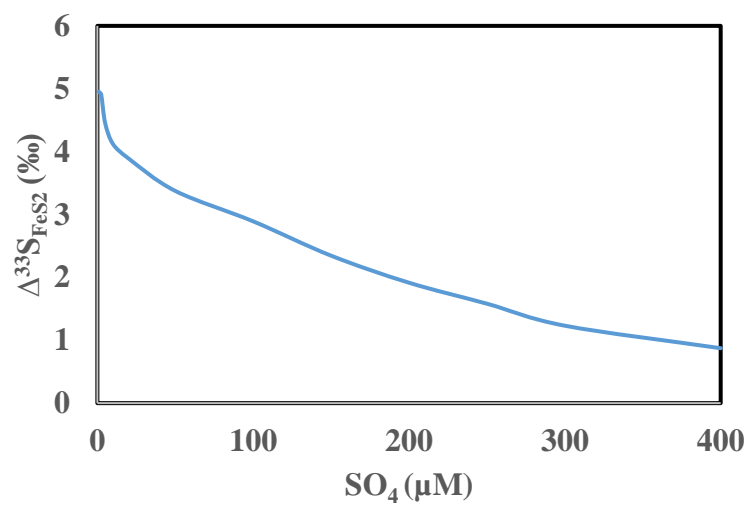
Figure 3.11 *Effect of sulfate concentration on $\Delta^{33}S_{FeS2}$ at [O_2] = 10μM*
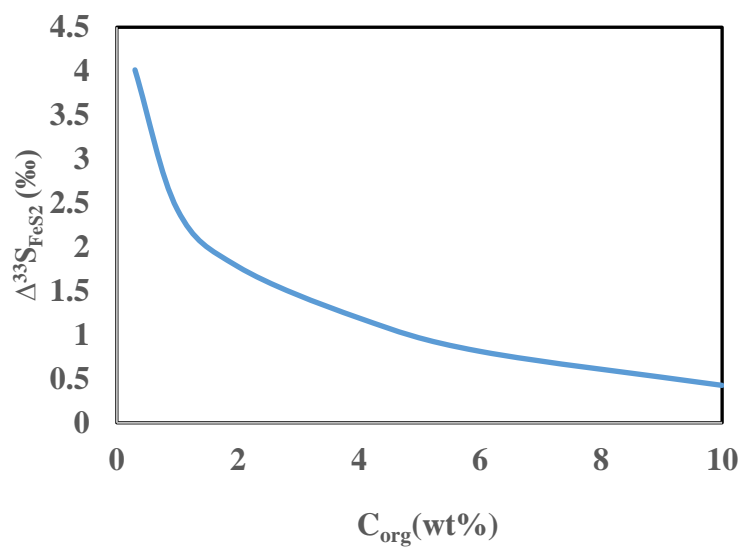
Figure 3.12 *Effect of organic matter availability on $\Delta^{33}S_{FeS2}$ at [SO_4] = 10μM, and [O_2] = 10μM.*
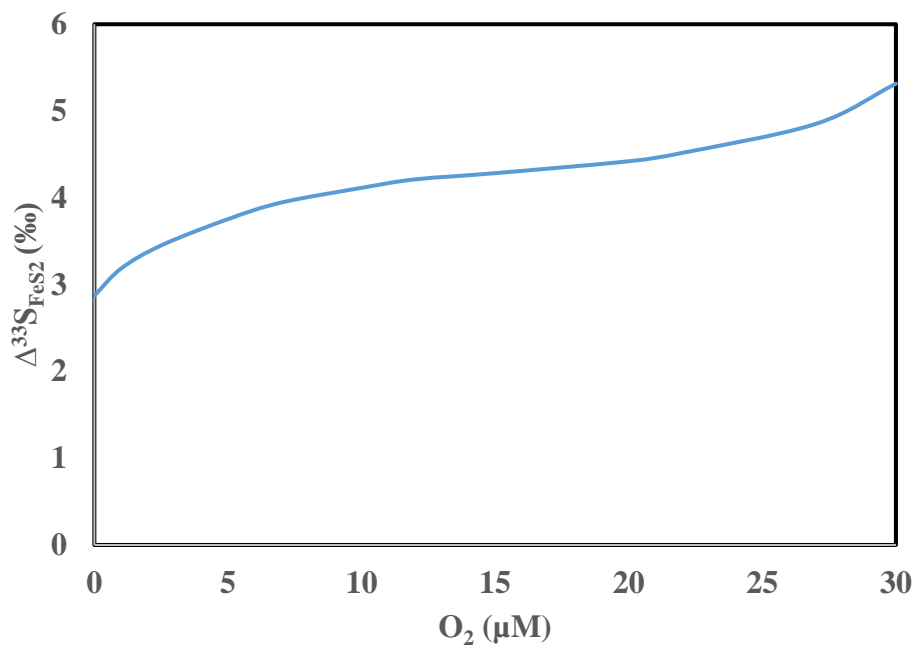
Figure 3.13 *Effect of oceanic level on $\Delta^{33}S_{FeS2}$ at $[SO_4] = 10\mu M$.*

Chapter 4 Seawater sulfate scarcity, ferruginous oceans, and a methane-rich Proterozoic atmosphere

Results in this Chapter are currently in revision for resubmission to Nature Geoscience

Title: Seawater sulfate scarcity, ferruginous oceans, and a methane-rich Proterozoic atmosphere

Authors: [1] Mojtaba Fakhraee, [2] Olivier Hancisse, [3] Donald E. Canfield, [4] Sean A. Crowe, and [1,5] Sergei Katsev

[1]*Large Lakes Observatory, University of Minnesota Duluth*

[2]*Department of Earth, Ocean, and Atmospheric Sciences, University of British Columbia, Vancouver, BC, Canada*

[3]*Danish Center for Earth System Science (DCESS) and Institute of Biology, University of Southern Denmark*

[4]*Department of Microbiology and Immunology and Department of Earth, Ocean, and Atmospheric Sciences, University of British Columbia, Vancouver, BC, Canada*

[5]*Department of Physics and Astronomy, University of Minnesota Duluth*

4.1. Synopsis

Oceanic sulfate is widely assumed to have reached mM concentrations during the Proterozoic Eon (0.6-2.5 Ga). Indeed, an increase in the range of marine sulfide $\delta^{34}S$ values following the Great Oxidation Event (GOE) around 2.3-2.5 billion years ago is thought to reflect an increase in seawater sulfate concentrations induced by enhanced oxidative weathering on land and the onset of marine sulfur redox cycling. The resulting increase in seawater sulfate concentrations, however, remains largely unquantified and is broadly inconsistent with the persistence of ferruginous (Fe-rich) Proterozoic deep oceans. We use global S budgets to show that seawater sulfate concentrations remained below 1.5 % of modern values (<500 µM), and possibly as low as 100 µM throughout much of the Proterozoic Eon. At these low sulfate concentrations, the relatively large sulfate-sulfide S-isotopic differences cannot be explained by sulfate reduction alone and are thus only possible through oxidative sediment S cycling, requiring tens of µM of oxygen in shallow Proterozoic seawater. Seawater sulfate concentrations less than 500 µM would have promoted ferruginous deep ocean conditions, carbon degradation through methanogenesis, a large methane efflux to the atmosphere, and greenhouse warming across much of the Proterozoic eon.

At 28 mM, sulfate is the second most abundant anion in modern seawater, and plays key roles in global carbon cycling and climate (Jørgensen 1982; Reeburgh 1983; Knittel & Boetius 2009). More than 90% of methane produced in the ocean's sediments, for example, is consumed through microbially catalyzed anaerobic oxidation with sulfate, effectively attenuating methane effluxes from the ocean to the atmosphere and mitigating corresponding greenhouse effects (Reeburgh 1983; Knittel & Boetius 2009). In contrast, under the low seawater sulfate concentrations of the Archean Eon, marine methane effluxes were likely large (Habicht et al. 2002; Crowe, S. A. et al. 2014; Fakhraee et al. 2018). The rise of atmospheric oxygen during the Great Oxidation Event (GOE) (2.3-2.5 Ga) is thought to have enhanced oxidative weathering of pyrite on land, leading to larger inputs of sulfate to the ocean and a corresponding increase in seawater sulfate concentrations (Cameron 1982; Canfield & Farquhar 2009). Low seawater sulfate concentrations before the GOE, <200 µM (Habicht et al. 2002; Fakhraee et al. 2018) and possibly as low as <5 µM (Crowe, S. A. et al. 2014), are reflected in a narrow range of sulfur isotope values (δ^{34}S <10‰) in sedimentary sulfides (Crowe, S. A. et al. 2014; Canfield 1998; Canfield et al. 2000). The apparent expansion of sulfur isotope fractionation following the GOE was previously attributed to rising seawater sulfate concentrations (>1mM) (Schopf 1992; Holland 1994; Karhu & Holland 1996; Petsch & Berner 1998; Farquhar et al. 2000; Farquhar & Wing 2003; Bekker et al. 2004), given that larger S-isotope fractionations generally develop at higher sulfate concentrations in both laboratory and field experiments (Habicht et al. 2002; Crowe, S. A. et al. 2014; Habicht & Canfield 1996; Canfield et al. 2010; Sim et al. 2011). Such relatively high

concentrations of seawater sulfate, however, are at least qualitatively inconsistent with pervasive ferruginous deep oceans throughout much of the Proterozoic Eon (Canfield et al. 2008; Planavsky et al. 2011), given that sulfate reduction promoted by widespread sulfate availability would have favored euxinic conditions (Canfield 1998), unless oceanic primary production and marine carbon export were unusually low (Planavsky et al. 2011). In natural environments, however, large S-isotope fractionations may also be generated at low sulfate concentrations by the repeated redox cycling of S, promoted by oxygen, and by disproportionation of elemental sulfur (Fakhraee et al. 2018; Canfield & Thamdrup 1994), providing a possible means of reconciling the sulfur isotope record with ferruginous Proterozoic oceans. While oxygen concentrations in shallow Proterozoic environments could have reached 10s of µM (Lyons et al. 2014; Zhang et al. 2016; Knoll et al. 2016), the effect of oxygen on diagenetic sulfur cycling and sedimentary sulfur isotopic compositions in the Proterozoic eon remains unexplored.

To reconstruct sulfate concentrations in Proterozoic seawater, we set up mass-balance and diagenetic reaction-transport models, which address the constraints imposed by both fluxes of sulfur from weathering and volcanism and the observed range of isotopic compositions in marine sedimentary pyrites. The mass balance model (*see Model Description*) considers three compartments that correspond to coastal, surface pelagic, and deep-ocean settings. The inputs include fluxes of sulfate from weathering and volcanic sources, and hydrothermal inputs of hydrogen sulfide. Outputs include removal of sulfate through microbial sulfate reduction and the resulting precipitation of iron sulfides from sediments and the anoxic deep ocean. Organic matter degradation coupled

to microbial sulfate reduction was scaled to account for lower biological productivity in the Proterozoic oceans (*see Model Description*). The shallow coastal environments and surface pelagic oceans were modeled as weakly oxygenated (Lyons et al. 2014; Sperling et al. 2015; Zhang et al. 2016; Knoll et al. 2016; Tostevin et al. 2016; Stolper & Keller 2018), while we considered an anoxic deep pelagic ocean in line with the redox state of Fe in Proterozoic basalts (Canfield & Thamdrup 1994). Oxidation of sulfide at the oxic-anoxic boundary between pelagic compartments recycled sulfate into the surface ocean. The effect of sulfide recycling on sulfate concentrations was examined by eliminating sulfide oxidation at the oxic anoxic boundary and assuming all sulfide produced was removed as FeS, as would be expected under the widespread ferruginous conditions that characterized the Proterozoic deep oceans (Canfield et al. 2008; Michiels et al. 2017; Planavsky et al. 2014). To assess the possible range of sulfate concentrations in Proterozoic seawater, parameters were varied within ranges thought possible for the Proterozoic Eon (Table 4.1) and sulfate concentrations within the model's three compartments were obtained as outputs in steady-state solutions.
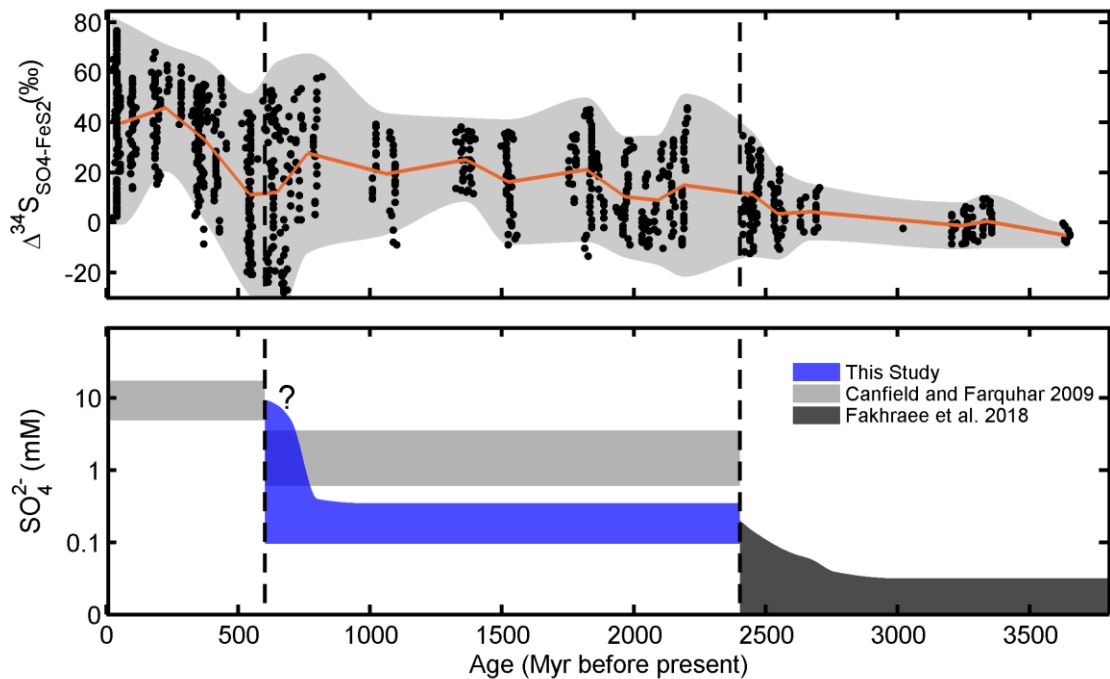
Figure 4.1 *Changes through time in $\Delta^{34}S_{SO4\text{-}FeS2}$ (a) and oceanic sulfate (b). Grey outline represents $\pm 2\sigma$ range; brown line is the mean. Data points are from Canfield and Farquhar (2009). Blue box represents the sulfate concentration consistent with S isotope records based on current study.*

Irrespective of the values for most model parameters, the inputs of oxidized sulfur to the ocean were insufficient to raise the sulfate concentrations above several hundred μM (100-500 μM) (Figs. 4.2, 4.3). The strongest limitation on oceanic sulfate levels was imposed by the removal of sulfate through its reduction in the anoxic deep ocean. The seawater sulfate concentrations, accordingly, were most sensitive to factors that characterized the strength of this sink, such as the area of the pelagic ocean regions, and maximum sulfate reduction rate in deep anoxic water (Fig 4.6). Our sensitivity analyses also suggest that removing sulfide oxidation from the pelagic oxic-anoxic boundary,

which assumes quantitative sulfide removal as FeS, can result in even lower sulfate concentrations, decreasing steady-state sulfate concentrations in surface pelagic compartment from 200 µM (the most probable value; Fig. 4.3) to 130µM. While marine sulfate concentrations were previously thought to depend strongly on the supply rate of sulfate from weathering (Canfield & Farquhar 2009), which would be expected to increase as oxygen accumulated in the atmosphere to around 1% present atmospheric level (PAL) (Lyons et al. 2014; Zhang et al. 2016; Knoll et al. 2016), our results suggest that the strong sink of sulfate in deep ocean would preclude any dramatic increase in seawater sulfate concentration, resulting in only a weak sensitivity of seawater sulfate concentrations to weathering fluxes. Varying weathering fluxes in the model from zero to modern values increased seawater sulfate concentrations by less than 200 µM, from 50 µM to around 250 µM (Fig 4.6).
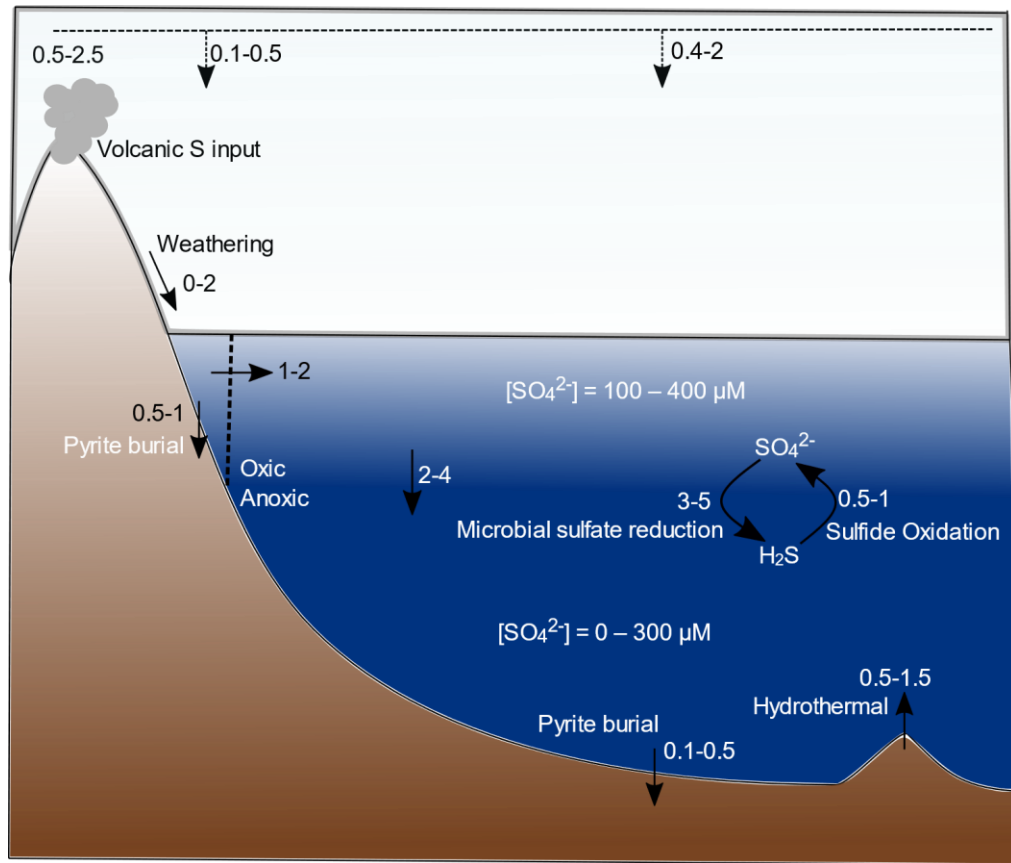
Figure 4.2 *Schematic depiction of sulfate cycle during Proterozoic eon. Dark and light blue boxes represent coastal and deep oceans respectively. Arrows correspond to the fluxes of sulfate and curved left arrow correspond to depth integrated sulfate reduction rate in the water column. All fluxes are in Tmol/year.*
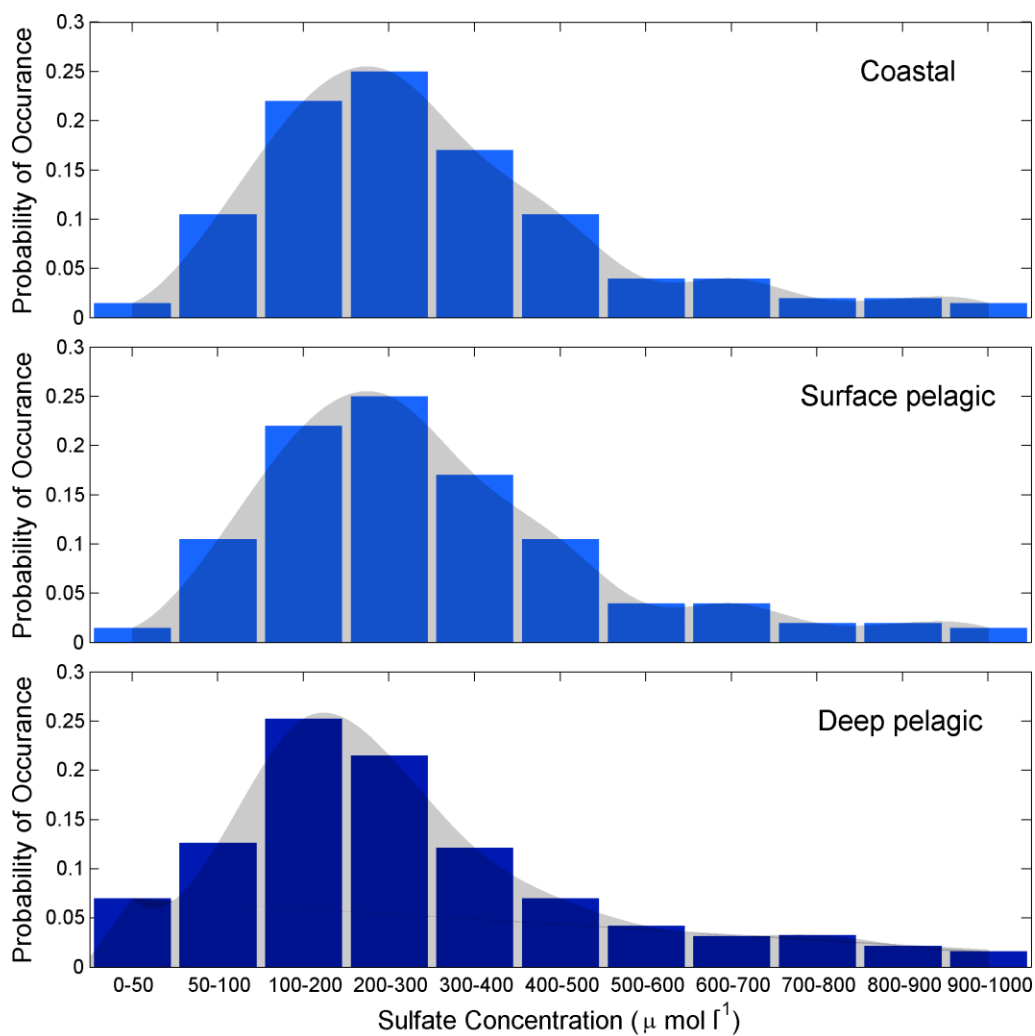
Figure 4.3 *Probability of occurrence of different sulfate ranges, based on the sensitivity analysis of mass balance model, in coastal, surface pelagic, and deep pelagic compartments during Proterozoic eon.*

While we did not explicitly simulate transient, weak oxygenation of the deep ocean (Stolper & Keller 2018), such events are unlikely to dramatically affect sulfate concentrations. At low atmospheric oxygen, mid-water depths would remain anoxic, analogous to modern-day oxygen-minimum zones (OMZs) (Devol & Hartnett 2001), but likely much more geographically expansive. Based on modern OMZs (Devol & Hartnett 2001; Andersson et al. 2004), between 70 and 90% of anaerobic mineralization of organic matter that could be coupled to sulfate reduction would take place in anoxic mid-ocean waters (200 < Depth (m) < 1000), with only 10 to 30% of mineralization occurring below OMZ depth. We thus tested the effect of deep ocean oxygenation by decreasing maximum sulfate reduction rate in anoxic compartment by 30%; this increased the steady state sulfate concentration by less than 150 µM. Hence, for all likely scenarios, Proterozoic seawater sulfate concentrations would have remained at sub-mM concentrations even if riverine sulfate fluxes were as high as today.

To test the seawater sulfate concentrations implied by our sulfur mass balance against the isotopic records in Proterozoic sulfides, we constructed a reaction-diffusion model (see *Model description*) that simulates S isotopic fractionation during sediment diagenesis. The model was applied to coastal ocean environments where iron sulfide minerals form in sediments below a weakly oxygenated water column. In contrast to previous isotopic models (Habicht et al. 2002; Crowe et al. 2014), our model considered the redox cycling of S through sulfate, sulfide, and elemental sulfur pools, and the disproportionation of elemental sulfur. The interplay of these oxidative processes has the capacity to increase the isotopic difference between sulfate and sedimentary sulfides

($\Delta^{34}S_{SO4-FeS}$), relative to sulfate reduction alone (Canfield & Thamdrup 1994). In modern sediments, sulfur compounds of intermediate oxidation state are typically produced through the oxidation of hydrogen sulfide. We only considered the formation of elemental sulfur through the oxidation of sulfide by iron oxides, as the other oxidative reactions (Table 4.4) are thermodynamically unfavorable at the low concentrations of hydrogen sulfide that would be expected in sediment pore waters with low-sulfate (<200 μM) concentrations. The $\Delta^{34}S_{SO4-FeS2}$ values were calculated for sulfate concentrations between 1 and 1000 μM.

Our diagenetic model yielded large $\Delta^{34}S_{SO4-FeS}$ values for oxygenated shallow coastal environments (Fig. 4.4). In contrast to previous suggestions that Proterozoic seawater had mM concentrations of sulfate based on observed $\Delta^{34}S_{SO4-FeS}$ (Luo et al. 2015), our results show that the S isotope fractionations needed to impart the 10-40‰ $\Delta^{34}S_{SO4-FeS}$ observed in the rock record are entirely possible at seawater sulfate concentrations less than 500 μM (0.5 mM). Notably, however, the range of $\Delta^{34}S_{SO4-FeS}$ observed in Proterozoic rocks is only reproduced at these sulfate concentrations if contemporaneous O_2 concentrations are >5 μM in shallow coastal environments (Fig. 4.4). Such O_2 concentrations are indeed supported by multiple other lines of evidence, and at various times throughout the Proterozoic eon (Lyons et al. 2014; Sperling et al. 2015; Zhang et al. 2016; Knoll et al. 2016; Tostevin et al. 2016; Stolper & Keller 2018). For instance, enrichments of redox-sensitive trace metals 1,400 million years ago (Zhang et al. 2016), cerium enrichments preserved in carbonate rocks ($\sim$1,000–541 million years ago) (Tostevin et al. 2016), and iron-based proxies from shales 2,300 million years old to

137

the end of the Proterozoic (Sperling et al. 2015), altogether, signify multiple punctuated intervals, if not the persistence, of at least several µM oxygen in Proterozoic surface oceans. Oxygen influences sedimentary sulfur cycling by fueling sulfide oxidation (Canfield & Thamdrup 1994) and by attenuating the supply of reactive organic matter available for sulfate reduction. Oxygenation of surface sediment, in particular, decreases sulfate reduction rates by deepening the sulfate reduction zone and decreasing availability of organic matter delivered to this zone. This decreases vertical gradients in porewater $^{32}SO_4$ and $^{34}SO_4$, allowing for a greater relative drawdown of the lighter isotope in proportion to the heavier isotope (Fakhraee et al. 2018), and resulting in lighter sulfides and increased $\Delta^{34}S_{SO4-FeS}$ (Fakhraee et al. 2018).
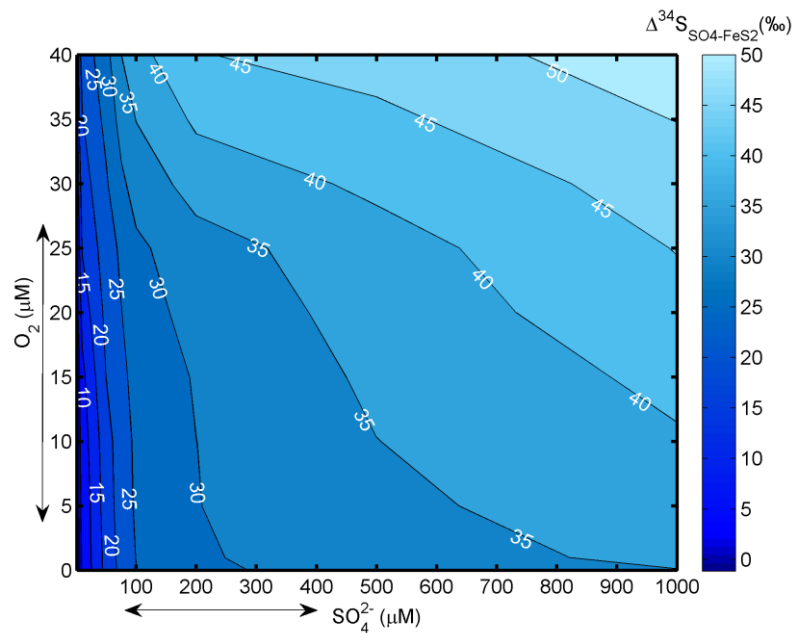
Figure 4.4 *Modeled range of $\Delta^{34}S_{SO4-FeS2}$, showing that high $\Delta^{34}S_{SO4-FeS2}$ values are possible for low sulfate and oxygen concentrations. The $\Delta^{34}S_{SO4-FeS2}$ values are also increased by lower organic matter fluxes (Fakhraee et al. 2018). Arrows correspond to most probable ranges of sulfate and oxygen, suggested by our model.*

Together, our modeling suggests that marine sulfate concentrations ranged between 100-500 µM throughout most of the Proterozoic Eon, despite enhanced oxygen-induced pyrite weathering after the GOE. Importantly, our results imply that the increased range in the S isotopic composition of sedimentary sulfides and the larger $\Delta^{34}S_{SO4\text{-}FeS}$ observed after the GOE could be predominantly the result of coastal seawater oxygenation since: 1) the only evidence for increased seawater sulfate concentrations comes from increased $\Delta^{34}S_{SO4\text{-}FeS}$; Canfield and Farquhar 2009) increased $\Delta^{34}S_{SO4\text{-}FeS}$ can be achieved through diagenesis in sediments overlain by oxic seawater with low sulfate concentration; and 3) increased sulfate concentrations to mM levels are not supported by sulfur mass balance models (Fig. 4.4). The sub-mM sulfate concentrations implied by our modeling are in line with other features of the Proterozoic rock record. For instance, our estimate for seawater sulfate is consistent with rare bedded gypsum in the Proterozoic eon, except during the Paleoproterozoic Lomagundi interval (Planavsky et al. 2012), and apparent deposition of halite before gypsum (Kah et al. 2001). Lower sulfate concentrations would have presumably resulted in only isolated occurrences of gypsum, and more frequent gypsum deposition would have not been expected to occur until the Neoproterozoic, when sulfate concentrations may have reached several mM (Kah et al. 2001). Higher sulfate concentrations implied for the late Neoproterozoic may thus have been a response to a more strongly oxygenated ocean (Sahoo et al. 2012; Lenton et al. 2014), conditions under which microbial sulfate reduction would have been relegated from the water column into sediments thereby reducing the pelagic sulfate sink and allowing sulfate accumulation. We tested this within our mass balance model: when the

139

entire marine water column was oxygenated, the sedimentary sinks of sulfate were insufficient to balance the inputs, and sulfate could accumulate to mM concentrations.

The development of mid-water euxinia overlying ferruginous deep waters is another feature of the mid-Proterozoic oceans previously attributed to high rates of microbial sulfate reduction (Canfield 1998; Michiels et al. 2017). At the 100s of µM sulfate concentrations found in our models, however, sulfate reduction rates are more sensitive to the availability of organic matter than sulfate (Fakhraee et al. 2017). Mid-water euxinia caused by enhanced sulfate reduction rates could thus reflect increased delivery of organic matter exported from surface production rather than elevated sulfate concentrations. Such a scenario goes hand in hand with the increased ratio of organic to inorganic C in sediments during the mid-Proterozoic era, which is thought to have resulted from enhanced tectonic activity that stimulated primary production by supplying P to the oceans (Garrels & Mackenzie 1971), increasing organic C burial (Hayes et al. 1999).

Measurements in modern lake sediments show that sulfate reduction rates at µM concentrations of sulfate are suppressed compared to rates at mM sulfate (Holmer & Storkholm 2001, Fakhraee et al. 2017). At 100s of µM sulfate, microbial sulfate reduction becomes quantitatively less important than methanogenesis and re-mineralizes a correspondingly smaller fraction of organic material, channeling anaerobic carbon mineralization through methanogenesis (Habicht et al. 2002, Katsev & Dittrich 2013). Previous Earth system modeling revealed that low seawater sulfate and oxygen concentrations could have led to large-scale marine methane production throughout the

Proterozoic eon (Olson et al. 2016), but concluded that with more than 1mM sulfate in seawater, methane effluxes to the atmosphere would have been strongly attenuated leading to atmospheric methane concentrations of less than 10 ppmv (Olson et al. 2016). With 100-500 µM sulfate in early and mid-Proterozoic seawater, however, methane effluxes would have been sufficient to sustain atmospheric methane concentrations of ~30 ppmv (Olson et al. 2016), which, depending on atmospheric photochemistry, could have had a strong warming effect. Oxygenation of the deep ocean during the late Neoproterozoic could have shifted sulfate reduction from water column into sediments, reduced the pelagic sulfate sink, and thus allowed the accumulation of oceanic sulfate to higher levels. Increased seawater sulfate concentrations at the end of the Proterozoic Eon would then have enhanced anaerobic methane oxidation, decreased the oceanic methane flux to the atmosphere, and given rise to the first ''snowball'' glaciation (Hoffman et al. 1998). Together, our analyses imply that the sub-mM seawater sulfate concentrations characteristic of the Archean oceans extended well into the Proterozoic Eras, the Lomagundi interval excepted, supporting pervasive and persistent deep ocean ferruginous conditions and a role for high atmospheric methane in climate regulation throughout the Precambrian.

4.2. Model Description
4.2.1 The Mass Balance Model

Sulfur mass balance model was constructed by considering fluxes in three compartments: coastal, surface pelagic, and deep ocean. A diagrammatic presentation of model is shown in Fig. 4.5.
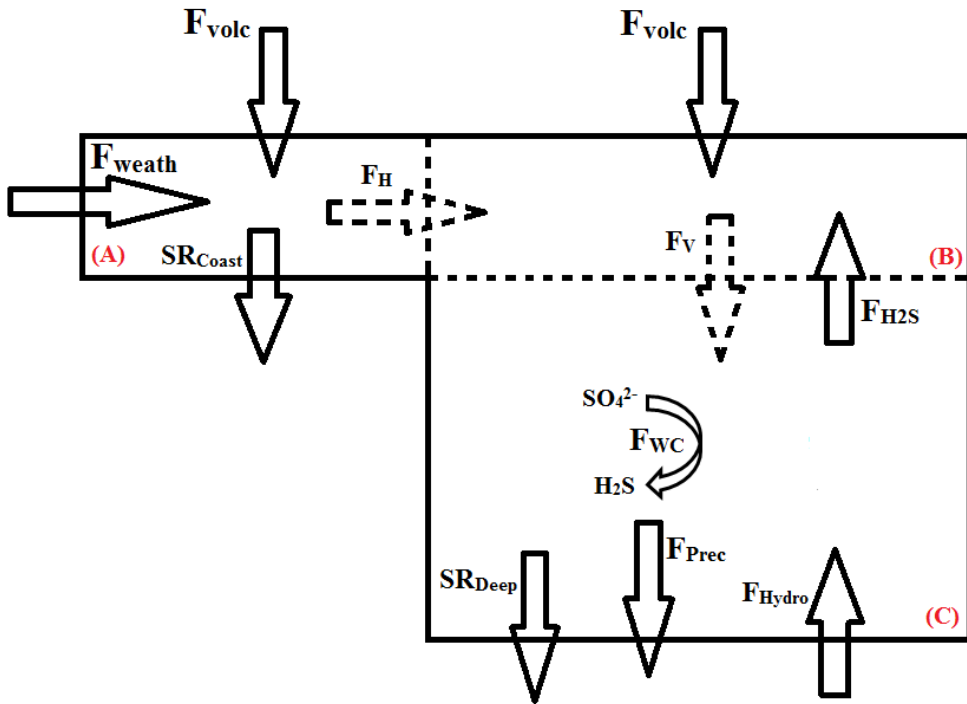
Figure 4.5 *Diagrammatic presentation of mass balance model*

Compartment ''A'' includes sulfate influxes from volcanic source and weathering and the sulfate export by horizontal diffusion and to sulfate reduction in weakly oxygenated coastal sediments. The differential expression for sulfate concentration in box A (C_A) is, thereby:

$$V_A \frac{dC_A}{dt} = F_{volc} + F_{weath} - F_H - F_{Coastal} \tag{4.1}$$

Here $F_{volc,}$ is the flux of sulfate from volcanic sources, scaled proportionally to the area of the coastal compartment. F_{weath} is the flux of sulfate from weathering, and F_H represents the removal of sulfate through horizontal transport.

The removal of sulfate by sulfate reduction in coastal sediments, $F_{Coastal}$, was calculated with a Michaelis-Menten-type term that accounts for the decrease in sulfate reduction rates at low sulfate concentrations:

$$F_{Coastal} = \frac{SR_{Coast}\, C_A}{K_m + C_A} A_{Coast} f_{prod} \qquad (4.2)$$

Here, the Monod parameter K_m describes the affinity of enzymes for substrate. SR_{Coast} is the depth integrated sulfate reduction rate, obtained from the relationship in Canfield (1989) for integrated sulfate reduction rate vs sedimentation rate. Sedimentation rate was assumed at 0.5 g cm^{-2} yr^{-1} which is within the typical range in modern marine environments with water depth less than 200m (Li et al. 2012; Canfield 1994; Burdige 2007). To account for differences in organic sedimentation flux due to a presumably lower productivity in Proterozoic oceans, the integrated rate obtained from the modern sediments is multiplied by f_{prod}, a factor of productivity. A_{Coast} is the area of the coastal ocean, calculated based on the total area (A_{Total}) and the fraction of total area covered by the coastal ocean (1-$f_{areadeep}$).

The horizontal transport flux of sulfate is calculated as:

$$F_H = A_{Cross}(C_A - C_B)\frac{K_h}{L_{h1}} \qquad (4.3)$$

where A_{Cross} is the cross-sectional area between coastal and surface pelagic oceans, calculated by multiplying the coastline length ($L_{coastline}$) by the depth of coastal ocean (H-$_{coastal}$). K_h and L_{h1} are the effective horizontal diffusion coefficient and the length scale for

horizontal diffusion respectively. C_A and C_B are the concentration of sulfate in coastal and surface pelagic compartments.

Surface pelagic part (box ''B'') includes inputs from volcanic sources and horizontal transport, and removal flux by vertical turbulent eddy diffusion to deep pelagic Box C. Sulfate concentration in this box (C_B) is calculated as:

$$V_B \frac{dC_B}{dt} = F_{volc} + F_H - F_V + F_{H_2S}$$ (4.4)

where F_V is the vertical diffusion flux. Similarly, to horizontal diffusion flux, the vertical diffusion flux of sulfate is calculated as:

$$F_V = A_{Deep}(C_B - C_C)\frac{K_v}{L_{v1}}$$ (4.5)

Where A_{Deep} is the area of surface pelagic ocean, calculated based on the total area (A_{Total}) and the fraction of total area covered by the deep ocean ($f_{areadeep}$). K_v and L_{v1} are the vertical turbulent diffusion coefficient and the length scale for vertical diffusion respectively. Similarly, to the vertical flux of sulfate, F_{H2S}, the turbulent diffusion flux of sulfide, was calculated by considering the vertical turbulent diffusion coefficient, area of deep ocean and sulfide gradient across the oxic anoxic boundary.

Finally, sulfate enters the deep ocean, box ''C'', through vertical turbulent diffusion and is removed through sulfate reduction in deep anoxic water column and sediments. Thus, sulfate concentration in deep ocean, C_C, is estimated as:

$$V_C \frac{dC_C}{dt} = F_V - F_{SedDeep} - F_{WC}$$ (4.6)

where F_{WC} and $F_{SedDeep}$ are the removal fluxes of sulfate through sulfate reduction in anoxic deep-water column and sediment respectively. The removal flux of sulfate in

anoxic deep sediments was calculated similarly to flux in coastal sediments, with the sedimentation rate adjusted to values in deep ocean (Canfield 1989). F_{WC} was also calculated based on the Michaelis-Menten kinetics:

$$F_{WC} = \frac{V_m \, C_C}{K_m + C_C} A_{Deep} f_{prod} \tag{4.7}$$

Here V_m is the depth integrated sulfate reduction rate when sulfate supply is unlimited and sulfate reduction rates are limited by the availability of organic matter. We take modern open ocean respiration rates, adjusted by a stoichiometric coefficient of 0.5, (Andersson et al. 2004) as a starting point for the estimation of V_m (Table 4.1). The rate is decreased further by 25% to account for slower anaerobic respiration in a stratified Proterozoic water column. Finally, to account for lower productivity during Proterozoic and a correspondingly lower amount of organic matter delivered to deep ocean, the rate V_m is multiplied by f_{prod}.

Concentration of sulfide in the deep ocean compartment was calculated by considering inputs from hydrothermal sources and removal of sulfide through iron sulfide precipitation and sulfide oxidation:

$$V_C \frac{dH_2S}{dt} = (1 - f_{Prec})F_{WC} + F_{Hydro} - F_{H_2S} \tag{4.8}$$

Here F_{Hydro} represents the hydrothermal flux of sulfide. $(1 - f_{prec}) F_{WC}$ is the production of sulfide produced from sulfate reduction in the anoxic water column where f_{prec} is a fraction of the produced sulfide that is precipitated as pyrite in anoxic water column. We did not consider the flux of sulfide from the deep sediment, as in deep anoxic ocean the rate of sulfate reduction in sediment would be much lower than in water column, as only

a small fraction of organic matter is delivered to the sediment. The concentrations of sulfate and sulfide species were calculated by solving Eqs (4.1-4.8) simultaneously, using Matlab ODE solver.

The parameter values used in mass balance model are summarized in Table 4.1.

4.2.2 Sensitivity Analysis of the Mass Balance Model

To investigate the sensitivity of our results to the values of mass balance model parameters, we conducted a sensitivity analysis. Model parameters were changed within their expected ranges (specified in Table 4.1), and changes in sulfate concentration ($\Delta[SO_4^{2-}]$) between maximum and minimum levels of each parameter were recorded. The results are shown in Fig. 4.6. Our conclusions presented in the main manuscript are essentially insensitive (<30 µM change in sulfate concentration) to most parameters including mean depth of coastal ocean, horizontal and vertical diffusion coefficients, and integrated sulfate reduction rate in anoxic sediment. The parameters that affect the sulfate concentration in surface pelagic compartment most strongly include the inputs due to weathering flux, volcanic and hydrothermal sources, mean depth of deep ocean, maximum sulfate reduction rate (V_m), Monod constant for SO_4^{2-} reduction, integrated sulfate reduction rate in oxic sediment, and fraction of total area covered by deep ocean. Among these parameters, the model showed the highest sensitivity to the Monod constant for the SO_4^{2-} reduction rate (K_m), with around 350 µM change in sulfate concentration. However, within the expected range of K_m, sulfate level still falls below 1mM. Increased maximum sulfate reduction in the deep ocean (V_m), and integrated sulfate reduction rate in sediments, in particularly coastal sediment, also result in a stronger sulfate drawdown

and lower sulfate level in surface pelagic compartment. Probabilities of occurrence for sulfate (Fig. 4.7) in different compartments as well as sulfide (Fig. 4.7) in deep compartment were calculated by randomly and independently varying the model parameters within their typical ranges (Table 4.1), with uniform probability distributions for each parameter.

Table 4.1 *Parameters for mass balance modeling and sensitivity analysis*

Parameter	Symbol	Value	Unit	Typical Range	Ref.
Flux from volcanic sources	F_{volc}	2.5	Tmol/yr	0.5-2.5	Holland 2002; Poulton & Canfield 2011
Flux from weathering	F_{weath}	2	Tmol/yr	0-2	Holland 2002; Poulton & Canfield 2011
Flux from hydrothermal inputs	F_{Hydro}	1.5	Tmol/yr	0.5-1.5	Holland 2002; Kump & Seyfried 2005
Monod constant for SO_4^{2-} reduction	K_m	77	uM	5-200	Canfield 2006
Vertical turbulent diffusion coefficient	K_v	3×10^{-5}	m^2/s	10^{-4}-10^{-6}	Canfield 2006
Horizontal diffusion coefficient	K_h	1800	m^2/s	500-5000	Canfield 2006, Milliman, & Meade 1983
Length scale for vertical diffusion	L_{v1}	60	m	10-100	
Length scale for horizontal diffusion	L_{h1}	100	km	50-200	
Maximum sulfate reduction in water column	V_m	50	mmol m^{-2} d^{-1}	10-100	Canfield 1989
Fraction of total area covered by deep oceans	$f_{areadeep}$	0.7	-	0.6-0.9	Parsons & Sclater 1977
Integrated sulfate reduction rate in modern coastal sediment	SR_{Coast}	10	mmol m^{-2} d^{-1}	10-100	Canfield 1989
Integrated sulfate reduction rate in modern deep sediment	SR_{Deep}	0.001	mmol m^{-2} d^{-1}	0.001-0.01	Canfield 1989
Total area of oceans	A_{Total}	3.6×10^{14}	m^2	-	Parsons &

					Sclater 1977
Precipitation factor	f_{prec}	0.6	-	0.1-0.9	Jorgensen 1979
Productivity factor	f_{prod}	0.1	-	0.1-1	Schopf & Klein 1992
Mean depth of deep ocean	H_{deep}	3000	m	2000-4000	Kitajima et al. 2001 , Burdige 2006
Mean depth of coastal ocean	$H_{coastal}$	150	m	100-200	Kitajima et al. 2001 , Burdige 2006
Length of coastline	$L_{coastline}$	356 x10^6	m		Kitajima et al. 2001 , Burdige 2006
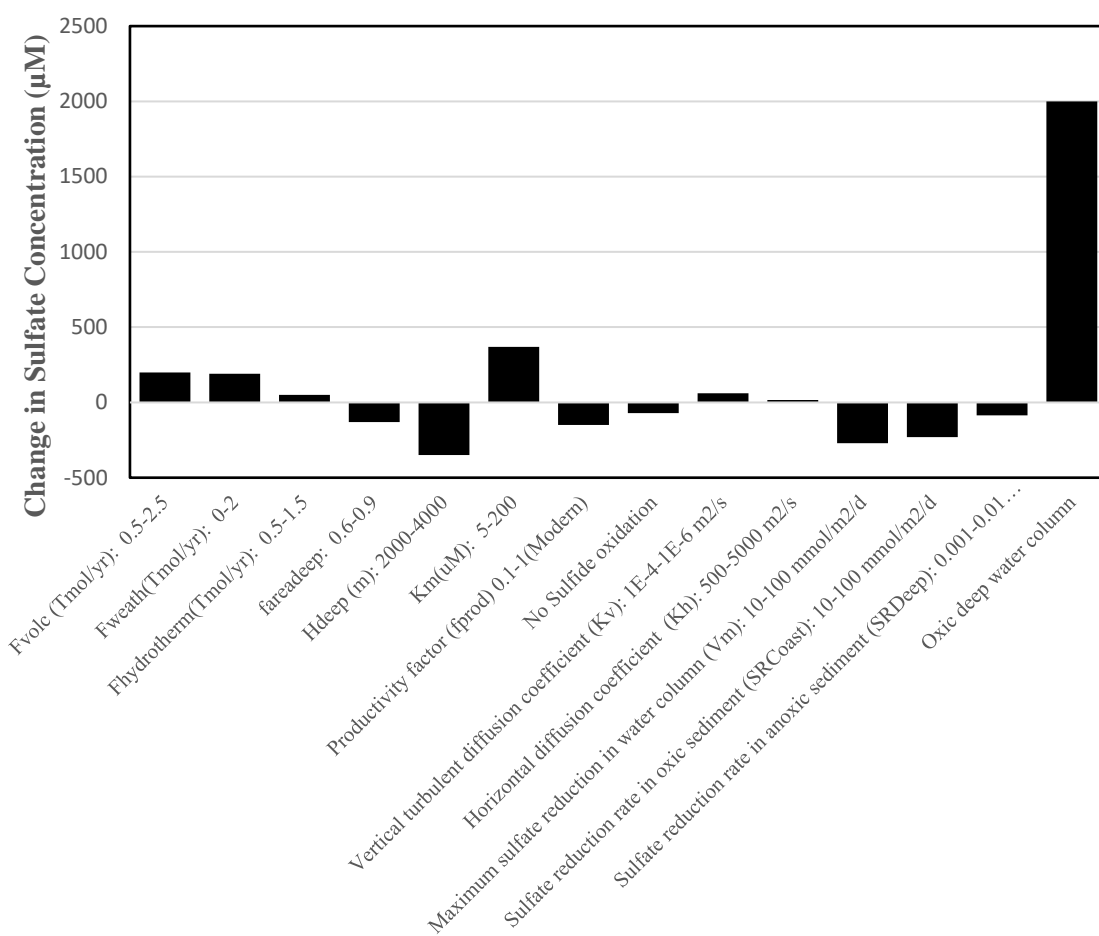
Figure 4.6 *Change in sulfate concentration in surface pelagic compartment in response to changes in box model parameter values from lowest to highest values.*
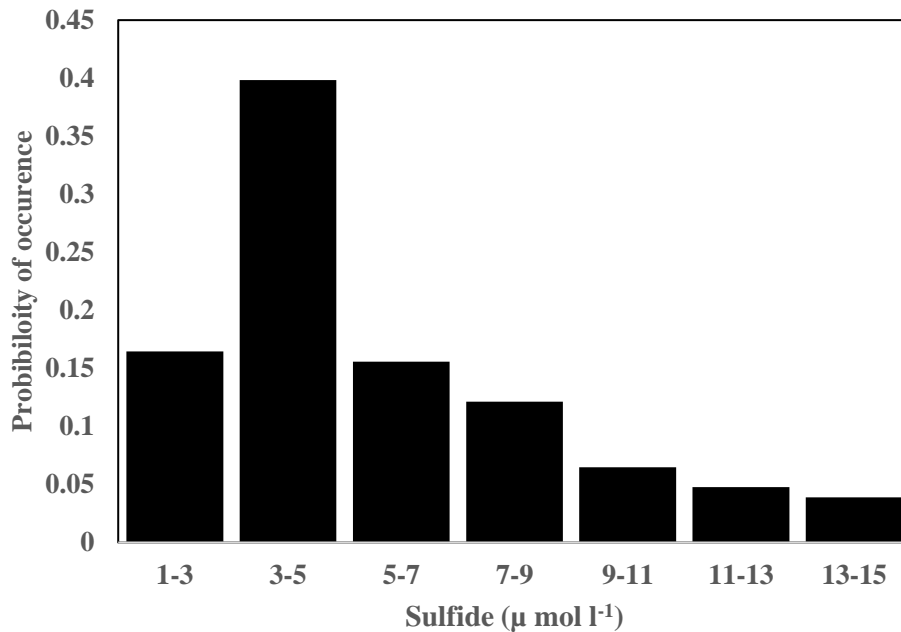
Figure 4.7 *Probability occurrence of sulfide ranges, from sensitivity analysis of mass balance model*

4.3. The Sediment Geochemical Model

Sediment geochemical model is similar to the model described in Chapter 3.

4.3.1. Isotopic Model

The isotopic model for S diagenetic transformations is based on previously published models (Crowe et al. 2014; Fakhraee et al. 2018). The sediment S pool is dominated by two stable isotopes, $^{32}SO_4$ (96%) and $^{34}SO_4$ (4%). Sulfate reducing bacteria reduce the isotopically light sulfate at a higher rate than the heavy isotope. For the total rate of bacterial sulfate reduction, R_{SR}, the $^{32}SO_4$ reduction rate is:

$$R_{32SR} = \frac{[^{32}SO_4^{2-}]}{[SO_4^{2-}]} n \, R_{SR} \tag{4.9}$$

and $^{34}SO_4$ reduction rate is:

$$R_{34SR} = \frac{[^{34}SO_4^{2-}]}{[SO_4^{2-}]} m \, R_{SR} \tag{4.10}$$

where $[^{32}SO_4]$ and $[^{34}SO_4]$ are the concentrations for light and heavy isotope respectively and $n>1$ and $m<1$ are parameters (Jorgensen 1979) whose ratio, termed the bacterial fractionation factor (α), describes the preferential use of the lighter isotope:

$$\alpha = \frac{n}{m} \tag{4.11}$$

Using Eq. (4.10) & (4.11), the reduction rates of $^{34}SO_4^{2-}$ and $^{32}SO_4^{2-}$ and the concentrations of $^{34}SO_4^{2-}$ and $^{32}SO_4^{2-}$ can be related as

$$\alpha = \frac{R_{32SR} [^{34}SO_4^{2-}]}{R_{34SR} [^{32}SO_4^{2-}]} \tag{4.12}$$

For α, we conservatively imposed a fractionation factor of 30 ‰, which is typical for sulfate reducing bacteria (Canfield 2001) and decreased this fractionation linearly below 6 µM, which reflects sulfate limitation (Habicht et al. 1998; Bradley et al. 2016). Fractionation for sulfide oxidation was considered constant (1.005) at all concentration levels (Bradley et al. 2016). Also, for elemental sulfur disproportionation, fractionations associated with sulfate and sulfide were considered as 0.988, and 1.007 respectively (Habicht et al. 1998).

For $\eta = [^{34}SO_4^{2-}] : [^{32}SO_4^{2-}]$, the reduction rates for individual isotopes were calculated from the overall rate R_{SR} as:

$$R_{32SR} = \frac{R_{SR}}{1 + \frac{\eta}{\alpha}} \tag{4.13}$$

$$R_{34SR} = \frac{R_{SR}}{1 + \frac{\alpha}{\eta}} \tag{4.14}$$

The initial value of ''η'' for model's iterations was calculated from the following equation, with initial value of $\delta^{34}SO_4^{2-}$ of 5‰.

$$\eta = \frac{\delta^{34}SO_4^{2-} * \frac{^{34}S_{CDT}}{^{32}S_{CDT}}}{1000} + \frac{^{34}S_{CDT}}{^{32}S_{CDT}} \tag{4.15}$$

where CDT refers to the $^{34}S/^{32}S$-ratio of the standard troilite, an iron monosulfide from the Canyon Diablo Meteroite.

Similarly, for sulfide oxidation, the kinetic fractionation factor (α') was defined as:

$$\alpha' = \frac{R_{32SOX}[H_2{}^{34}S]}{R_{34SOX}[H_2{}^{32}S]} \tag{4.16}$$

For $\gamma = [H_2{}^{34}S] : [H_2{}^{32}S]$, the specific rates of sulfide oxidation were calculated from the overall oxidation rate:

$$R_{32SOX} = \frac{R_{SOX}}{1 + \frac{\gamma}{\alpha'}} \tag{4.17}$$

$$R_{34SOX} = \frac{R_{SOX}}{1 + \frac{\alpha'}{\gamma}} \tag{4.18}$$

Similarly to Eq. (4.16), the initial value of γ was calculated as:

$$\gamma = \frac{\delta H_2{}^{34}S * \frac{^{34}S_{CDT}}{^{32}S_{CDT}}}{1000} + \frac{^{34}S_{CDT}}{^{32}S_{CDT}} \qquad (4.19)$$

For elemental sulfur disproportionation, the kinetic fractionation factors for sulfate and sulfide were defined as:

For sulfate:

$$\sigma = \frac{R_{32Disp(SO_4)}[^{34}S^0]}{R_{34Disp(SO_4)}[^{32}S^0]} \qquad (4.20)$$

And for sulfide:

$$\sigma' = \frac{R_{32Disp(H_2S)}[^{34}S^0]}{R_{34Disp(H_2S)}[^{32}S^0]} \qquad (4.21)$$

For $\tau = [^{34}S^0]:[^{32}S^0]$, the specific rates of sulfate and sulfide production during elemental sulfur disproportionation were calculated from the overall disproportionation rate:

For sulfate:

$$R_{32Disp(SO_4)} = \frac{0.25R_{Disp}}{1+\frac{\tau}{\sigma}} \qquad (4.22)$$

$$R_{34Disp(SO_4)} = \frac{0.25R_{Disp}}{1+\frac{\sigma}{\tau}} \qquad (4.23)$$

And for sulfide:

$$R_{32Disp(H_2S)} = \frac{0.75R_{Disp}}{1+\frac{\tau}{\sigma'}} \qquad (4.24)$$

$$R_{34Disp(H_2S)} = \frac{0.75 R_{Disp}}{1 + \frac{\sigma'}{\tau}}$$ (4.25)

where "0.25" and "0.75" correspond to the stoichiometry of the sulfate and sulfide production during disproportionation reaction respectively.

Similarly to Eqs. (4.16) and (4.20), the initial value of τ was calculated as:

$$\tau = \frac{\delta^{34}S^0 * \frac{^{34}S_{CDT}}{^{32}S_{CDT}}}{1000} + \frac{^{34}S_{CDT}}{^{32}S_{CDT}}$$ (4.26)

The initial value of $\delta^{34}S^0$ for the model's iterations was taken as 5‰. This choice did not affect the final value of $\Delta^{34}S_{SO4\text{-}FeS}$ achieved on convergence.

No fractionations were considered associated with the formation of Fe sulfides and elemental sulfur:

For FeS:

$$R_{32FeS} = \frac{[H_2{}^{32}S]}{[H_2S]} R_{FeS}$$ (4.27)

$$R_{34FeS} = \frac{[H_2{}^{34}S]}{[H_2S]} R_{FeS}$$ (4.28)

And for elemental sulfur:

$$R_{32S^0} = \frac{[H_2{}^{32}S]}{[H_2S]} R_{S0}$$ (4.29)

$$R_{34S^0} = \frac{[H_2{}^{34}S]}{[H_2S]} R_{S0}$$ (4.30)

To calculate the vertical concentration profiles for $[^{34}SO_4{}^{2-}]$, $[^{32}SO_4{}^{2-}]$, $[H_2{}^{34}S]$, $[H_2{}^{32}S]$, $[^{34}S^0]$, and $[^{32}S^0]$, net rates were expressed as follows:

154

$$NR^{32}SO_4^{2-} = R_{32SR} - R_{32SOX} - R_{32Disp(SO_4)} \tag{4.31}$$

$$NR^{34}SO_4^{2-} = R_{34SR} - R_{34SOX} - R_{34Disp(SO_4)} \tag{4.32}$$

$$NRH_2{}^{32}S = R_{32SOX} + R_{32FeS} + R_{32S^0} - R_{32SR} - R_{32Disp(H_2S)} \tag{4.33}$$

$$NRH_2{}^{34}S = R_{34SOX} + R_{34FeS} + R_{34S^0} - R_{34SR} - R_{34Disp(H_2S)} \tag{4.34}$$

$$NR^{32}S^0 = R_{32S^0} - (R_{32Disp(H_2S)} + R_{32Disp(SO_4)}) \tag{4.35}$$

$$NR^{34}S^0 = R_{34S^0} - (R_{34Disp(H_2S)} + R_{34Disp(SO_4)}) \tag{4.36}$$

The vertical gradients and concentrations for each isotope were then computed by integrating Eq. (3.1) with rates given by Eqs. (4.31-4.36) over depth. The concentrations, rates, η, γ, and τ were then recalculated iteratively until convergence was reached.

The isotopic composition of FeS was found after the convergence of iterations by integrating the FeS precipitation rates (Eqs. 4.27-4.28) for the individual isotopes based on Eq. (3.1) with $D_i=0$:

$$[Fe^{34}S] = \frac{\int_0^l R_{34FeS} \cdot dx}{v} \tag{4.37}$$

$$[Fe^{32}S] = \frac{\int_0^l R_{32FeS} \cdot dx}{v} \tag{4.38}$$

The isotopic fractionations are reported in plots relative to international standards according to the conventional δ-notation (‰):

$$\delta^{34}SO_4^{2-} = \left(\frac{\frac{^{34}SO_4}{^{32}SO_4}}{\frac{^{34}S_{CDT}}{^{32}S_{CDT}}} - 1 \right) \cdot 1000 \tag{4.39}$$

155

$$\delta Fe^{34}S = \left(\frac{\frac{Fe^{34}S}{Fe^{32}S}}{\frac{^{34}S_{CDT}}{^{32}S_{CDT}}} - 1 \right) . 1000 \qquad (4.40)$$

The isotope enrichment factor (Δ) describes the isotopic enrichment in the source (substrate relative to the products. Negative values indicate that the product is depleted in the heavy isotope ^{34}S relative to the source; positive values indicate that the product is enriched in the heavy isotope ^{34}S compared to the source sulfur compound:

$$\Delta^{34}S_{FeS-SO_4^{2-}} (‰) = \delta^{34}SO_4^{2-} (‰) - \delta\, Fe^{34}S(‰) \qquad (4.41)$$

The parameter values used in our model are summarized in Table S6.

The isotope enrichment factor (Δ) describes the isotopic enrichment in the source (substrate relative to the products. Negative values indicate that the product is depleted in the heavy isotope ^{34}S relative to the source; positive values indicate that the product is enriched in the heavy isotope ^{34}S compared to the source sulfur compound:

4.3.2. Sensitivity Analysis of Sediment Diagenesis Model

To investigate the sensitivity of our results to the values of model parameters, we conducted a sensitivity analysis. Model parameters were varied within their reasonable ranges, and changes in $\Delta^{34}S_{SO4-FeS}$ between maximum and minimum of each parameter were recorded. The results are shown in Fig. 4.8. Our conclusions presented in the main manuscript are essentially insensitive (<2‰ change in $\Delta^{34}S_{SO4-FeS}$) to most parameters including pH, initial age of organic matter, diffusion coefficients, porosity, burial

velocity, and elemental sulfur disproportionation rate constant. The parameters that affect the isotopic composition of the precipitated sulfides stronger (2-9‰) include the organic matter content, rate constants for oxidation of sulfide and FeS precipitation, and Monod constants for sulfate reduction and inhibition by oxygen. The sensitivity to organic matter content is illustrated in Fig. 4.9 and 4.10. A greater supply of organic matter increases the sulfate reduction rates and the $\delta^{34}S$ values of sulfides become closer to the seawater sulfate value (Crowe et al. 2014; Fakhraee et al. 2018). As ours is the first isotopic model for the Archean conditions to include elemental sulfur disproportionation, and the kinetics of Fe sulfides precipitation, we varied the disproportionation and precipitation rates constants to investigate their effects on the isotopic composition of the resultant pyrites. Increasing the S^0 disproportionation rate constant results in an isotopically lighter pyrite, however, this change is not significant (~2‰) within its reasonable range. Increasing the kinetics of precipitation (k_{FeS}) also results in an isotopically lighter pyrite and a greater $\Delta^{34}S_{SO4-FeS}$. At higher rate of precipitation, sulfides become lighter, and $\Delta^{34}S_{SO4-FeS}$ increases. A similar effect imparted by porewater iron concentration is shown in Fig. 4.11. The Monod/inhibition constant (K_i) can also affect the $\Delta^{34}S_{SO4-FeS}$: Increasing K_i results in a greater isotopic difference of sulfate to sulfides (Fig. 4.12). This difference is greater at higher oxygen levels: an inflection points around $[O_2] = 10\ \mu M$ in Fig. 4.12 implies that for higher O_2 levels, $\Delta^{34}S_{SO4-FeS}$ has a stronger dependence on oxygen.
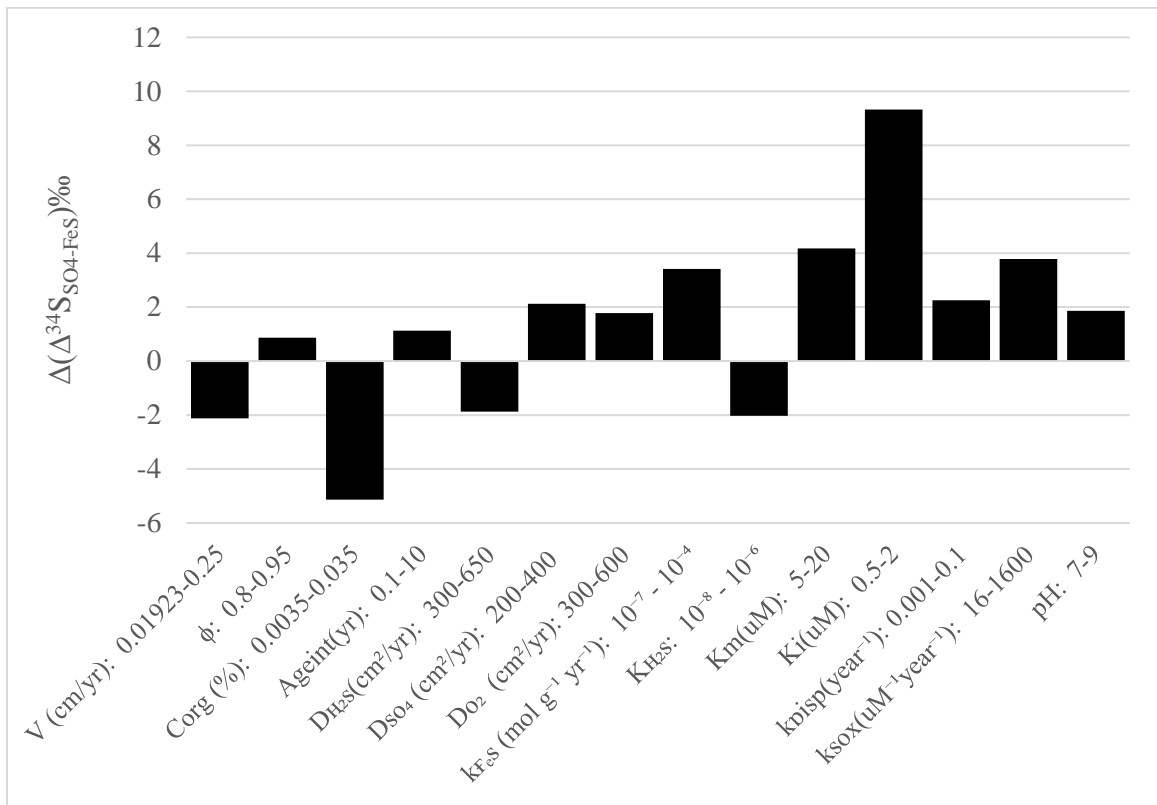
Figure 4.8 *Change in ε*$_{SO4\text{-}FeS}$ *(‰) in response to changes in diagenetic model parameter values from lowest to highest values.*
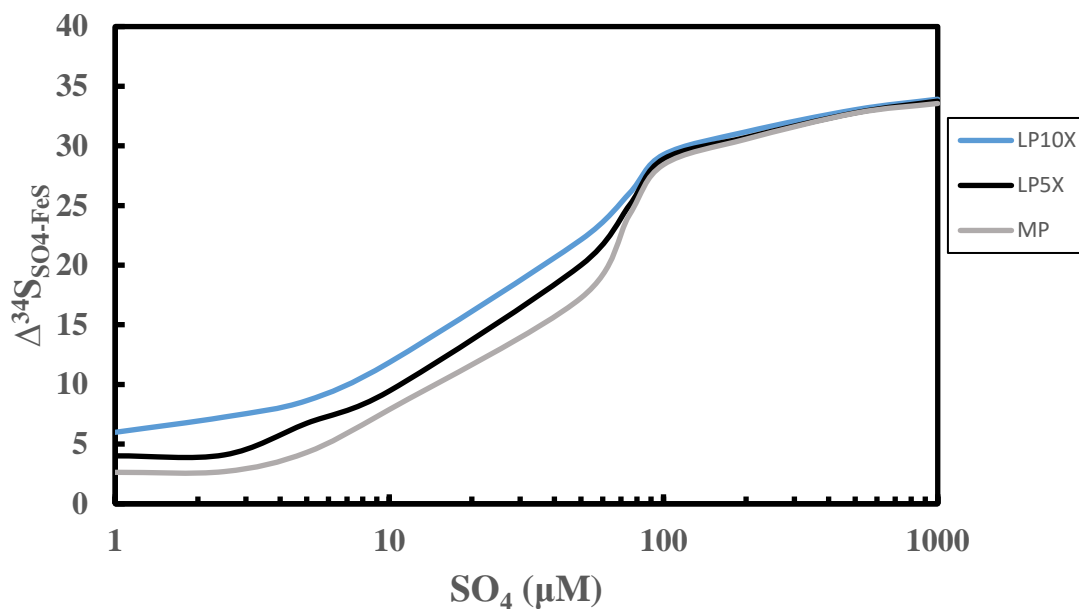
Figure 4.9 *Sensitivity of model outputs to organic matter availability at [O₂] = 10uM. MP corresponds to modern levels of productivity (C_org = 3%), LP5x and LP10x correspond to 5 and 10 times lower productivity.*
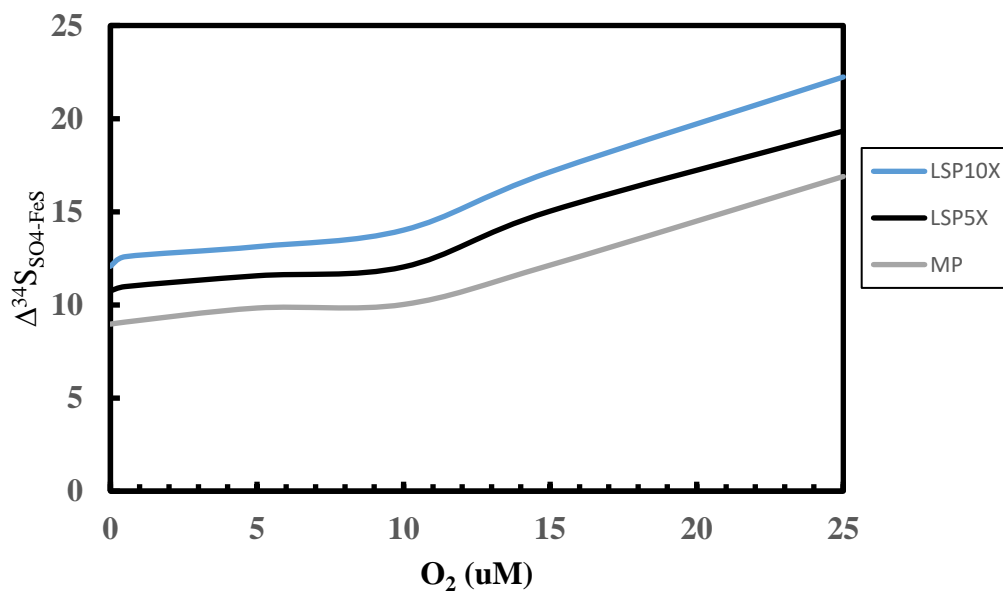
Figure 4.10 *Sensitivity of model outputs to organic matter availability at [SO₄] = 100uM. MP corresponds to modern levels of productivity, LP5x and LP10x correspond to 5 and 10 times lower productivity.*
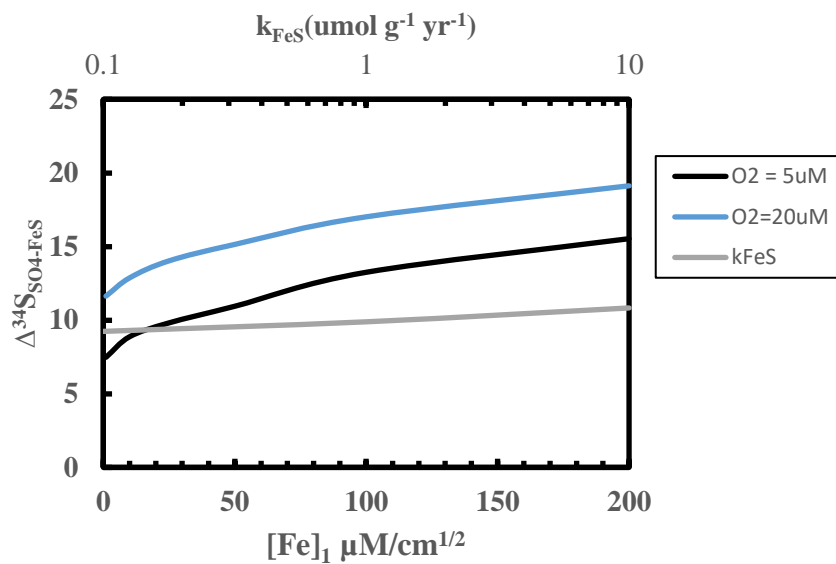
Figure 4.11 *Black and blue lines show the effect of $[Fe]_1$ under low and high oxygen conditions at $[SO_4] = 100 \ \mu M$, and grey line shows the effect of k_{FeS} on $\Delta_{SO4\text{-}FeS}$ at $[SO_4] = 100 \ \mu M$, and $[O_2] = 5 \ \mu M$.*
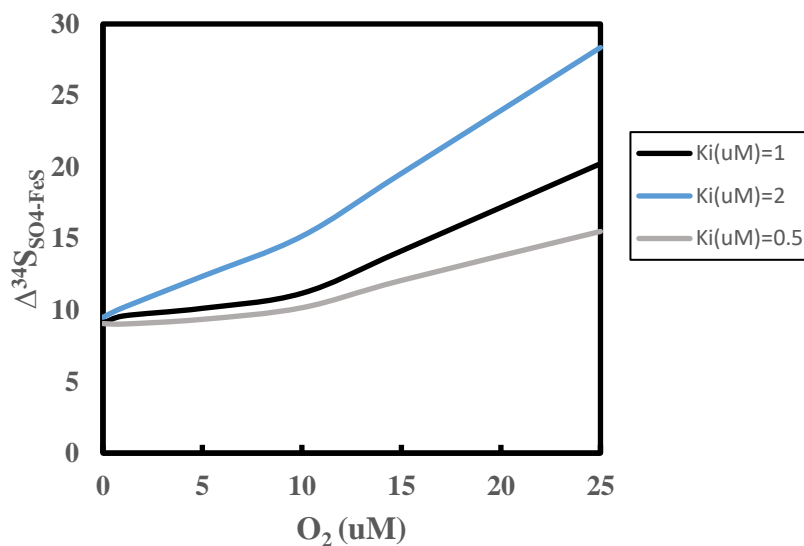
Figure 4.12 *Effect of oxygen inhibition constant (K_i) on $\Delta_{SO4\text{-}FeS}$ at $[SO_4] = 100 \ \mu M$*

Chapter 5 Geochemical constraints on methylmercury fluxes from sediments

Results in this chapter are being prepared for submission to Environmental Science and Technology

Title: Geochemical constraints on methylmercury flux from sediments

Authors: [1]Mojtaba Fakhraee, [2]Amber White, [3]Nathan W. Johnson, [1, 4]Sergei Katsev

[1] *Large Lakes Observatory, University of Minnesota Duluth*

[2] *Water Resources Science Graduate Program, University of Minnesota*

[3] *Department of Civil Engineering, University of Minnesota Duluth*

[4] *Department of Physics, and Astronomy, University of Minnesota Duluth*

5.1. Synopsis

Methylation of inorganic mercury converts it to methylmercury, an organic form that is highly toxic to humans and ecosystems. While past phenomenological studies identified several factors that regulate the production of methylmercury in sediments, the underlying mechanisms and their quantitative effects on the magnitude of methylmercury fluxes remain poorly constrained. Using a reaction-transport model, we investigated the methylmercury cycling under a wide range of sediment conditions. The model was calibrated to data from the St. Louis River estuary, a freshwater estuary upstream of Lake Superior, and cross-validated to marine sediments. The model captured the functional trends and concentrations of inorganic mercury, methylmercury, and hydrogen sulfide in sediments at multiple locations. Sensitivity analysis implicates oxygen, sulfate, and organic matter as leading geochemical parameters that control the diffusive flux of methylmercury to overlying water. In particular, sediments become sources of methylmercury when oxygen concentration drops below a critical threshold level. This threshold, below which the rate of methylation rate exceeds that of demethylation, is a strong function of the sediment organic content, and for organic-rich sediments is predicted to be around 50 μM O_2, for a wide range of sulfate concentrations.

5.2. Introduction

Mercury (Hg) is a pervasive contaminant that affects human and ecosystem health through the production and bioaccumulation of the neurotoxic organic form of mercury, methylmercury (MeHg; CH_3Hg^+) (He et al. 2008; Cleckner et al. 1999). Unlike inorganic forms of Hg, which originate from atmospheric deposition and point discharges, methylmercury is generated in the environment, predominantly by anaerobic microorganisms (Gilmour et al. 1992). Sulfate-reducing bacteria (SRB) are, in many cases, the primary producers of MeHg (King et al. 2000, Benoit et al. 1999, Park et al. 2013), although iron-reducing bacteria (Si et al. 2015; Yu et al. 2012; Warner et al. 2003; Wiatrowski et al. 2006) and methanogens (Kronberg et al. 2018; Yu et al. 2013; Park et al. 2013) were also suggested to mediate the methylation process. Methylation thus commonly occurs within the oxygen depleted bottom waters and sediments of lakes, rivers, reservoirs, and oceans, where rates of anaerobic microbial respiration are high. Wetlands (Zillioux et al. 1993; Marvin et al. 2003; Hoggarth et al. 2015) and sediments of productive lakes (Furutani & Rudd1980; Lockhart et al. 1998) are important hotspots, and their spatial extent influences the total ecosystem methylation rate (Gilmour & Henry 1991). As a result of MeHg slow expulsion from organisms, it is biomagnified in aquatic food chains. Understanding the factors that regulate the cycling of Hg and its toxic organic form, MeHg, is thus critical to comprehending the mechanisms of MeHg enrichment in aquatic systems.

While there is a wealth of information on MeHg content in aquatic systems and site-specific rates of methylmercury production, there is no clear picture of how individual characteristics of the environment affect methylmercury fluxes. This lack of comprehensive mechanistic understanding confounds our ability to predict MeHg fluxes. Earlier studies identified a large number of environmental factors that may affect methylation rates. The availability of sulfur, organic carbon, and sediment structure and composition all affect methylmercury production by regulating the amount of bioavailable inorganic mercury and microbial activity (Merritt and Amirbahman 2009). Sources, concentrations and spatial distributions of Hg could be controlled by factors such as pH, temperature, redox conditions, and availability of nutrients and complexing agents (He et al. 2008; Eckley & Hintelmann, 2006; Cleckner et al. 1999). Binding of methylmercury in sediments depends on grain size, pH, and dissolved oxygen concentration (He et al. 2008; Eckley & Hintelmann, 2006; Cleckner et al. 1999). In coastal marine sediments, sulfate-reducing bacteria, which populate sediments below the zone of oxygen penetration (Noelle 2009), are thought to be the principal agents responsible for MeHg production (Bridou et al. 2011; King et al. 2001). In lakes, high concentrations of MeHg are similarly found in the oxic-anoxic transition zones where SO_4^{2-} is the most available electron acceptor (Furutani & Rudd 1980; Gilmour, et al. 1992; Watrus et al. 1995a & 1995b). While high sulfate levels are thought to stimulate MeHg production by enhancing the activity of SRBs (Gilmour et al. 1992; Jeremiason et al. 2006), MeHg production is limited under conditions where the produced sulfide accumulates in the porewater. Sulfide inhibition has been speculated to be a result of

164

removal of Hg from solution via enhanced precipitation of HgS(s) (Benoit et al. 1999; Han et al. 2008) or attributed to the formation of volatile dimethylmercury from reaction of MeHg with H_2S (Craig & Bartlett 1978; Craig & Moreton 1983). In contrast to methylation where the end-product poses an acute environmental concern, demethylation degrades MeHg into inorganic mercury, mitigating the MeHg sediment content. Carried out by a number of aerobic and anaerobic microbes, demethylation is thought to be predominantly performed by aerobic organisms (Spangler et al. 1973; Taylor & Gilchrist 1991; Visscher & Taylor, 1994; Ndu et al. 2016; Pfeifenschneider et al. 2017). Aerobic demethylation in both freshwater and estuarine sediments is accompanied by production of carbon dioxide, suggesting an oxidative pathway. While demethylation is critical in mitigating the efflux of methylmercury, its controlling factors and ecological contributions are largely unknown.

Scores of investigations generated a patchwork of site-specific information on MeHg cycling, but a comprehensive and mechanistic quantitative description of MeHg fluxes from sediments is lacking. This task, which involves deconvoluting the contributions from individual reactions and physical processes, is commonly performed by modeling. Predictive extrapolations beyond calibration conditions can be obtained in an exploratory fashion (e.g. Katsev et al. 2006), whereby model solutions are investigated for a range of conditions and model parameter values. While calibration datasets are rarely, if ever, complete, such exploratory modeling provides utility beyond the numerical values of its predictions, as it identifies characteristic trends, control parameters, and transitions in diagenetic regimes. It also identifies knowledge gaps and

can guide future experimental studies by offering falsifiable predictions. To mechanistically describe the fluxes of methylmercury in aquatic sediments, we constructed a diagenetic diffusion-reaction model. The model is first calibrated to sediment conditions in the freshwater Saint Louis River estuary (SLRE), and the results are then extrapolated to a broader range of aquatic environments. Using the simulation results, we identify a small number of physico-chemical parameters that most strongly affect the fluxes of MeHg from sediments and calculate the expected variations in those fluxes. We identify the typical ranges and threshold values for sulfate concentrations, organic matter content, and oxygen concentrations that determine the direction and magnitude of methylmercury fluxes.

5.3. Methods
5.3.1. Sampling and analyses

Mercury geochemistry was characterized in sediments, collected by a gravity core, from four relatively low sulfate sites located in the St. Louis River estuary, Minnesota, USA (Fig. 1). The St. Louis River Estuary (SLRE) is a large (50 km^2) freshwater estuary that is used extensively for recreation and serves as an important nursery habitat for western Lake Superior (Hoffman et al., 2010). The estuary contains diverse habitat, ecology, and geomorphology, and the lower portions of the SLRE remain one of the busiest ports on the Laurentian Great Lakes. Habitat Zones – areas delineated by local resource managers as having similar ecological significance (St. Louis River Alliance, 2002) – were used in

this study to select sites that encompass the range of solid phase organic carbon quantity present in the open-water estuary sediment (2 – 8%, Beck and Johnson 2014).

Collected cores were sectioned at 0-2 cm, 2-4 cm, and 4-8 cm sections into borosilicate glass jars. Jars were filled to the top with saturated sediment, sealed with electrical tape, stored in a cooler on ice while in the field, and transferred to an anaerobic chamber (98 % N, 2 %H) in the lab within 6 hours of collection. Analytical methods for sediment organic carbon content and acid volatile sulfide (AVS) as well as porewater sulfide are described in Beck and Johnson (2014). Briefly, zinc acetate-preserved sediment samples were stored frozen and analyzed for acid-volatile sulfide (AVS) by acidifying samples with 1 N HCl and flushing H_2S into an alkaline trapping solution that was analyzed using an automated methylene blue method (4500-$S2^-$ E, Eaton et al., 2005). The organic carbon content was determined in freeze-dried sediment samples by coulometry on a CM150 total carbon (TC), total organic carbon (TOC), total inorganic carbon (TIC) analyzer. Total- and methyl- mercury content was measured through digestion and isotope-dilution mass spectroscopy at Gustavus Adolphus College using methods described in Bailey et al. (2017).

Figure 5.1 *Sampling locations in St. Louis River Estuary (SLRE)*

5.3.2. Diagenetic model

Diagenetic transformations of oxygen, sulfur, iron, and carbon and their effects on mercury cycling are described with a coupled set of reactive-transport equations. If x is the depth below the sediment-water interface and $C_i(x)$ is the concentration of a chemical species i in porewater (in mol per porewater volume) at quasi-steady state (negligible accumulation relative to advection/diffusion/reaction):

$$0 = \frac{\partial}{\partial x}\left(\varphi D_i \frac{\partial C_i}{\partial x}\right) - \frac{\partial}{\partial x}(\varphi v C_i) + \varphi \alpha_{irr}(C_i^0 - C_i^{burr}) + \varphi \sum_j R_{ij} \tag{5.1}$$

For solid phase species including total organic carbon (TOC), elemental sulfur (S^0), and iron mono-sulfide (FeS):

$$0 = \frac{\partial}{\partial x}\left(\psi D_b \frac{\partial C_i}{\partial x}\right) - \frac{\partial}{\partial x}(\psi v C_i) + \varphi \sum_j R_{ij} \tag{5.2}$$

Here, x is the depth below the sediment-water interface and $C_i(x)$ is the concentration of a chemical species i in porewater (in mol per porewater volume) or solid sediment (in mol per gram dry weight). D_i is the diffusion coefficient, v is the advection (burial) velocity, R_{ij} are the rates of all reactions that affect the species i, and the factor ψ is equal to $(1-\phi)\rho$, where ρ is the density of dry sediment, and ϕ is the porosity. The coefficient α_{irr} (Table. 3) describes bioirrigation, which is a fauna-mediated, non-local (nondiffusive) exchange of fluids between the sediment surface (concentration C_i^0) and bioirrigated burrows (C_i^{burr}). In non-permeable sediments, diffusion typically dominates over advection, so the advection term for solutes in Eq. 5. 1 can be neglected. The diffusion of solid particles is due to bioturbation (Berner 1980; Meysman et al. 2005), described by the bioturbation coefficient D_b which was imposed as the exponential function $D_b = (D_{b\text{-top}})*e^{-x/H\_scale}$; where $D_{b\text{-top}}$, and H-scale are the bioturbation coefficient value at the sediment water interface, and a depth scale factor.

For simplicity, the concentration of FeOOH was defined by using a function that mimics the FeOOH profiles in modern freshwater (low-sulfate) and marine sediments (Li 2014):

$$[FeOOH] = [FeOOH]_1 \left(\frac{1}{1 + e^{x-OPD}} + 2e^{-\frac{(x-OPD)^2}{2}} \right) \tag{5.3}$$

where depth x>OPD is in cm and $[FeOOH]_1$ is a constant. The OPD was defined as depth where oxygen level becomes less than 0.1μM. Based on the modeling results, oxygen penetration depths (OPD) for CB1, CHN, SB1, and SB2 sites are 1, 1.6, 1.1, 1.05 cm respectively.

169

The geochemical reactions included in the model and their rate formulations are listed in Tables 5.1 and 5.2. Model parameter values are listed in Table 5.3. The boundary conditions for hydrogen sulfide, oxygen, sulfate, dissolved iron, and methane were chosen as fixed-concentration at the sediment-water interface (SWI) and zero-gradient in the bottom of the integration domain. Equations (5.1-5.2) were iteratively solved in Matlab as a boundary-value problem using the ″bvp4c″ function, to obtain the vertical distributions of concentrations and the rates of individual reactions (Table 5.2).

Table 5.1 *Reactions included in the model*

Reactions	Rate
$CH_2O + O_2 \Rightarrow CO_2 + H_2O$	R_{OX}
$CH_2O + 4\ FeOOH_{(s)} + 7CO_2 + H_2O \Rightarrow 4Fe^{2+} + 8\ HCO_3^{-}$	R_{FeOOH}
$SO_4^{2-} + 2CH_2O \Rightarrow H_2S + 2HCO_3$	SRR
$H_2S + 2O_2 + 2HCO_3^{-} \Rightarrow SO_4^{2-} + 2CO_2 + 2H_2O$	R_{SOX}
$Fe^{2+} + HS^{-} \Rightarrow FeS(s) + H^{+}$	R_{FeS}
$2FeOOH_{(s)} + 3H_2S_{(aq)} => S^0_{(s)} + 2FeS_{(s)} + 4H_2O$	R_{S0}
$2CH_2O => CH_4 + CO_2$	R_{CH4}
$CH_4 + 2O_2 => CO_2 + 2H_2O$	R_{CH4_O2}
$SO_4^{2-} + CH_4 => H_2S + CO_2 + H_2O$	R_{CH4_SO4}
$SO_4^{2-} \Rightarrow R\text{-}SH$	R_{Assim}
$4\ S^0_{(s)} + 4H_2O => SO_4^{2-} + 3HS^{-} + 5H^{+}$	R_{Disp}

170

Table 5.2 *Kinetics of the reactions included in the model.*

Reaction	Rate expression
Sulfide Oxidation	$R_{SOX} = k_{SOX}[O_2][H_2S]$
Aerobic Respiration	$R_{OX} = \dfrac{V_m[O_2]}{K_i + [O_2]}$
Organic carbon (OC) mineralization rate	$V_m = k\,[OC]$ Where $\log_{10} k = -(0.95)\log_{10} t - (0.81)$
Iron Reduction	$R_{FeOOH} = \dfrac{V_m[FeOOH]}{K_{FeOOH} + [FeOOH]}\dfrac{K_i}{K_i + [O_2]}$
Sulfate Reduction	$SRR = \dfrac{V_m[SO_4^{2-}]}{K_m + [SO_4^{2-}]}\dfrac{K_i}{K_i + [O_2]}$
Methane Production	R_{CH_4} $= K_{CH_4}\dfrac{V_m[CH_4]}{K_{methane} + [CH_4]}\dfrac{K_i}{K_i + [O_2]}\dfrac{K_m}{K_m + [SO_4^{2-}]}$
Oxic methane oxidation	$R_{SOX} = k_{CH4-O2}[O_2][CH_4]$
Sulfate-driven oxidation of methane	$R_{SOX} = k_{CH4-SO4}[SO_4][CH_4]$
Sulfide Precipitation	$R_{FeS} = k_{FeS}(\dfrac{\Omega}{K_{FeS}} - 1)$ $\Omega = \dfrac{[Fe^{2+}][HS^-]}{[H^+]}$ $[HS^-] = \dfrac{[H_2S]}{1 + [H^+]K_{H_2S}}$
Assimilatory Sulfate Reduction	$R_{Assim} = k_{Assim}(R_{FeOOH} + R_{OX} + R_{SR})$
Elemental Sulfur Formation	$R_{S0} = k_{S0}[FeOOH][H_2S]$

Elemental Sulfur Disproportionation	$R_{Disp} = k_{Disp}[S^0](1 - \frac{[H_2S]}{[H_2S]_{stop}})$ For $[H_2S] <$ [H₂S] stop 0 For $[H_2S] \geq [H_2S]$ stop

5.3.3. Mercury cycling modeling

Sulfate reduction rate, sulfide concentration, and organic matter mineralization rate calculated by the above model were used as inputs for the mercury and methylmercury model. Figure 5.2 illustrates the sediment mercury cycling that includes porewater mercury methylation and demthylation, and organic and inorganic mercury adsorption/desorption.
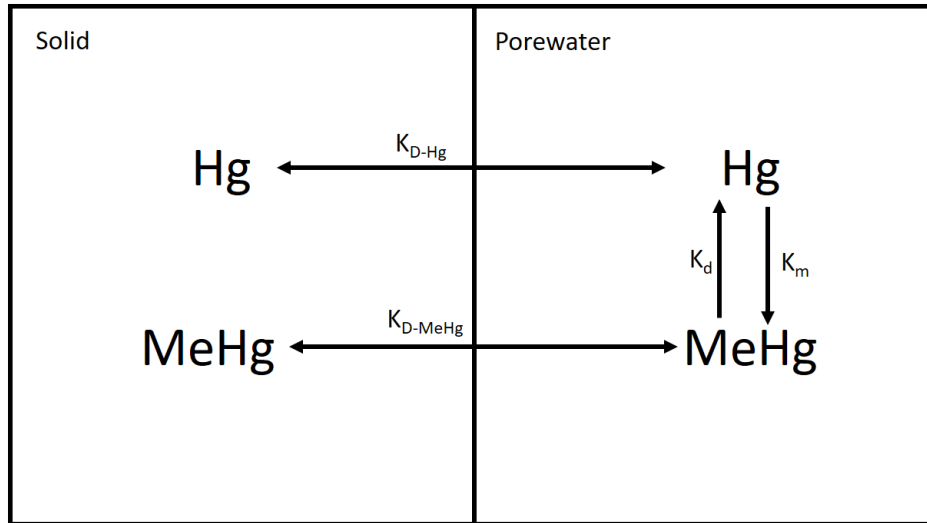
Figure 5.2 *Schematic presentation of sediment mercury cycle*

The distributions of organic (CH₃Hg) and inorganic (iHg) mercury were described, respectively, for solute and solid species as follows:

172

$$0 = \frac{\partial}{\partial x}\left(\varphi D_i \frac{\partial C_{pw_i}}{\partial x}\right) + k_{ads}\left(\frac{C_{S_i}}{K_{D_i}} - C_{pw_i}\right) + \varphi \alpha_{irr}(C_{pw_i}^{0} - C_{pw_i}^{burr}) \pm \varphi R_{meth}$$

$$\pm \varphi R_{demeth} \tag{5.4}$$

$$0 = \frac{\partial}{\partial x}\left(\psi D_b \frac{\partial C_{S_i}}{\partial x}\right) - \frac{\partial}{\partial x}(\psi v C_{S_i}) - k_{ads}\left(\frac{C_{S_i}}{K_{D_i}} - C_{pw}\right) \tag{5.5}$$

Here k_{ads}, K_D, R_{meth} and R_{demeth} are, respectively, the adsorption/desorption coefficients, solid-liquid partitioning factors, and the rates of methylation and demethylation (Table 5.3). The rate of methylation (R_{Meth}) is defined as proportional to the methylmercury concentration:

$$R_{meth} = k_{meth} C_{pw-Hg} \tag{5.6}$$

Where the reaction rate constant k_{meth} is:

$$k_{meth} = \alpha(SRR + \beta(R_{FeOOH} + R_{CH_4}))e^{-\left(\frac{[H_2S]}{[H_2S]_1}\right)} \tag{5.7}$$

Here, α is a rate proportionality factor obtained as a fitting parameter, SRR is the sulfate reduction rate, the parameter β describes the production of methylmercury through other anaerobic pathways, R_{FeOOH} is the iron reduction rate, R_{CH4} is the methanogenesis rate, and the last term accounts for the inhibition of methylation at high sulfide concentrations, suggested by the literature (Janina et al. 1999). The de-methylation rate is assumed to depend on carbon degradation rate and porewater methylmercury concentration:

$$R_{demeth} = k_{demthyl} V_m C_{pw-MeHg} \tag{5.8}$$

The reaction rate constant $k_{demthyl}$ was obtained by fitting the data. The organic carbon mineralization rate V_m was approximated as $V_m = k$ [OC] where the reactivity k was described by the Middelburg power law (Middelburg, 1989) as a function of carbon age t:

173

$\log_{10} k = - (0.95) \log_{10} t - (0.81)$. This power law was recently shown to hold over a range of conditions including low-sulfate environments including Lake Superior (Katsev and Crowe 2015; O'Beirne et al. 2017).

Finally, diffusive fluxes of dissolved mercury and methylmercury across the sediment-water interface were calculated using the Fick's law of diffusion:

$$Flux_{Diff} = -\varphi D_i \frac{\partial C_i}{\partial x} \tag{5.9}$$

The boundary conditions for mercury, and methylmercury were chosen as fixed-concentration at the sediment-water interface (SWI) and zero-gradient in the bottom of the integration domain. Equations (5.4), and (5.5) were iteratively solved in Matlab as a boundary-value problem. When fitting the observational data at multiple locations in the SLRE, parameters were selected to provide a satisfactory fit against the entire dataset, rather than to fit specific features of individual depth profiles.

Table 5.3 *Parameters for sediment diagenesis model. Asterisk (*) indicates parameters that were randomly varied in the sensitivity analysis within their specified expected ranges.*

Parameter	Symbol	Value	Unit	Typical Range	Ref.
*Diffusion coefficient of sulfate	D_{SO4}	300	cm^2/year	200-400	Canfield 2006
*Diffusion coefficient of sulfide	D_{H2S}	500	cm^2/year	400-600	Burdige 2006
*Diffusion coefficient of oxygen	D_{O2}	500	cm^2/year	300-500	Burdige 2006
*Diffusion coefficient of methane	D_{CH4}	300	cm^2/year	200-500	Burdige 2006
*Sulfide oxidation rate constant	k_{OXD}	160	$\mu M^{-1}year^{-1}$	16-1600	Katsev et al. 2004
*Oxic methane oxidation rate constant	K_{CH4-O2}	500	$\mu M^{-1}year^{-1}$	10-1000	Katsev et al. 2004
*Anoxic methane oxidation rate constant	$K_{CH4-SO4}$	0.1	$\mu M^{-1}year^{-1}$	0.001-10	Katsev et al. 2004
*Bioirrigation coefficient	α_{irr}	5	$year^{-1}$	1-10	Canavan et al. 2006

*Bioturbation coefficient at SWI	$D_{b\text{-}top}$	5	cm²/year	1-10	Burdige 2006
*Depth scale for bioturbation	H-scale	1	cm	1-3	
*FeS precipitation rate constant	k_{FeS}	10^{-5}	mol g⁻¹ yr⁻¹	10^{-7}-10^{-5}	Katsev et al. 2004
*FeS equilibrium constant	K_{FeS}	10^{-4}	M	-	Dyrssen & Kremling 1990
Acid-base equilibrium constant for H₂S	K_{H2S}	2.48×10^{-7}	-	-	Dyrssen & Kremling 1990
*S⁰ formation rate constant	k_{S0}	8×10^{-3}	$\mu M^{-1}year^{-1}$	10^{-5}-10^{-1}	Van Cappellen & Wang 1996
Assimilatory reduction of sulfate rate constant	k_{Assim}	10^{-4}	-	-	-
*S⁰ disproportionation rate constant	k_{Disp}	0.01	year⁻¹	0.001-0.1	Jourabchi 2007
Threshold H₂S concentration for disproportionation	$[H2S]_{stop}$	10	mM	-	Jourabchi 2007
*H₂S scale factor for methylation	$[H2S]_1$	50	μM	10-100	Janina et al. 1999
*Monod constant for SO₄²⁻ reduction	K_m	20	μM	5-25	Katsev et al. 2004
*Monod constant for O₂ (inhibition constant)	K_i	1	μM	0.5 – 2	Katsev et al. 2004
*Monod constant for FeOOH reduction	K_{FeOOH}	20	$\mu mol/g$	15-30	Katsev et al. 2004
Density of dry sediment	ρ_s	2.65	g/cm³	-	-
Grid size	dz	6.67×10^{-3}	cm	-	-
*Adsorption/desorption coefficient Hg	$k_{ads\text{-}Hg}$	1	year⁻¹	0.1-10	Dyrssen & Kremling 1990; Beck and Johnson. 2014
*Adsorption/desorption coefficient MeHg	$k_{ads\text{-}MeHg}$	0.1	year⁻¹	0.01-1	Dyrssen & Kremling 1990; Beck and Johnson. 2014
*solid-liquid partitioning coefficient for Hg	$K_{D\text{-}Hg}$	10^4		10^4-10^5	Dyrssen & Kremling 1990
*solid-liquid partitioning coefficient for MeHg	$K_{D\text{-}MeHg}$	10^3		10^3-10^4	
Fitting parameter	α	0.05	μM^{-1}	0.01-0.1	
Coefficient for other anaerobic pathways	β	0.01		0.01-0.1	

Table 5.4 *Model boundary conditions for solutes and solid species in St. Louis River Estuary (SLRE).*

Boundary conditions	Symbol	Top (concentration at sediment water interface)
Sulfate	$[SO_4^{2-}]$	120 µM
Sulfide	$[H_2S]$	0
Oxygen	$[O_2]$	150-350 µM
Iron	$[Fe^{2+}]$	0
Methane	$[CH_4]$	0
MeHg	$[MeHg]$	0.75-1.4 pM
Hg	$[Hg^{2+}]$	12-45 pM
MeHg(solid)	$[MeHg]s$	$[MeHg]* K_{D-Hg}$
Hg(solid)	$[Hg^{2+}]s$	$[Hg^{2+}]* K_{D-MeHg}$
S^0	$[S^0]$	0
FeS	$[FeS]$	0

5.4. Results and Discussion
5.4.1. Hg in SLRE sediments

The vertical distributions of mercury and methylmercury in the porewater of SLRE sediments (Fig. 5.3) exhibited strong spatial heterogeneity. Porewater inorganic mercury concentrations at the sediment-water interface (SWI) were between 12 and 42 pM with the maximum value at site CB1. Porewater methylmercury concentrations at

SWI were between 0.75 and 1.4 pM with the maximum observed at site CHN at 1.4 pM. Depth distribution of porewater methylmercury showed an increase at around 2cm depth, coincident with a decrease in the porewater inorganic mercury concentration at the same depth.

5.4.2. Model calibration in SLRE

When applied to the Saint Louis River estuary, the model captured the functional trends and concentrations ranges in the distributions of dissolved inorganic mercury, methylmercury, and sulfide at sites with a range of organic C content (Fig. 5.3). It successfully reproduced the observed peaks in the methylmercury depth profiles (~3cm). These peaks are concurrent with the peaks in sulfide, which correspond to maximum sulfate reduction rates, and correspond to the depths of the maximum methylation rates (Fig. 5.3). Peaks in the methylmercury concentration at around 3 cm imply the dominance of methylation over demethylation and are consistent with the calculated rates, where the rates of methylation exceed the rates of demethylation. The simulated profiles were used to calculate the sediment fluxes of methylmercury and inorganic mercury and the rates of methylation and demethylation.

The calculated fluxes and depth integrated rates are presented in Table 5.5. Except at SB1, the directions of the diffusive methylmercury fluxes are into the sediment, with the maximum flux of 0.814 pmol cm^{-2} yr^{-1} at SB2. Fluxes of inorganic mercury, except at CHN site, are also directed into the sediment, with the maximum calculated flux at CB1 at 0.5 pmol cm^{-2} yr^{-1}. The depth integrated methylation and demethylation rates range from 2.56 to 5.49 pmol cm^{-2} yr^{-1} and 4.02 to 5.87 pmol cm^{-2} yr^{-1} respectively.

Maximum methylation rates are concurrent with maximum sulfate reduction rates, indicating that microbial sulfate reduction is the main anaerobic process promoting methylation. Modeled sulfate reduction rates (SRR) range from 11.85 µmol cm^{-2} yr^{-1} (Sta. CHN) to 36.38 µmol cm^{-2} yr^{-1} (Sta. SB2), with the average of 25.63 µmol cm^{-2} yr^{-1}. Comparing the depth integrated sulfate reduction rates and sulfide oxidation rates shows that about half of the sulfide produced by microbial sulfate reduction becomes oxidized to sulfate. Depth integrated sulfide oxidation rates (R_{SOX}) range from 5 µmol cm^{-2} yr^{-1} (Sta. CHN) to 24 µmol cm^{-2} yr^{-1} (Sta. SB2), with the average of 14.5 µmol cm^{-2} yr^{-1}.

Modeling results reveal that sediment can act as a sink for MeHg at most sites, or as a source at one site (SB1). The direction of the flux varies among sediments with different availability of oxygen, sulfate, and organic matter (Fig. 5.5), and the concentrations of organic and inorganic mercury (Fig. 5.6). The direction depends on the balance between the area-specific rates of methylation and demethylation. Demethylation dominates in the oxic sediment zone where the low activity of anaerobes restricts methylation. Lower oxygen level and shallower oxic zone suppress demethylation.

The direction of the flux (Eq. 5.9) is often inferred observationally from the direction of the concentration gradient in the immediate vicinity of the interface. While resolving the fine structure of the gradients is feasible in modeled profiles (Fig. 5.3), measured profiles are typically collected at coarser resolution (cm-scale) and the fluxes inferred from such measured gradients may be misleading. Interestingly, the MeHg flux measured in a sediment incubation at the CB site (White 2018) indicated the flux of

methylmercury into the sediment, contrary to the measured coarse-scale gradient but consistent with the simulated fine-scale structure of the profile.

Table 5.5 *Calculated rates and fluxes in St. Louis River Estuary (SLRE). Negative values correspond to the flux from water column to the sediment whereas positive correspond to the flux from the sediment to the overlying water.*

Site	$*R_{meth}$ (pmol cm^{-2} yr^{-1})	$*R_{demeth}$ (pmol cm^{-2} yr^{-1})	$*SRR$ (μmol cm^{-2} yr^{-1})	$Flux_{MeHg}$ (pmol cm^{-2} yr^{-1})	$Flux_{Hg}$ (pmol cm^{-2} yr^{-1})	R meth – Rdemeth
CB1	4.86	5.03	25.76	-0.327	-5.35E-01	-0.17
CHN	2.56	4.31	11.85	-1.99	1.36	-1.75
SB1	4.66	4.02	28.52	+0.0133	-3.65E-01	0.64
SB2	5.49	5.87	36.38	-0.814	-1.92E-01	-0.38
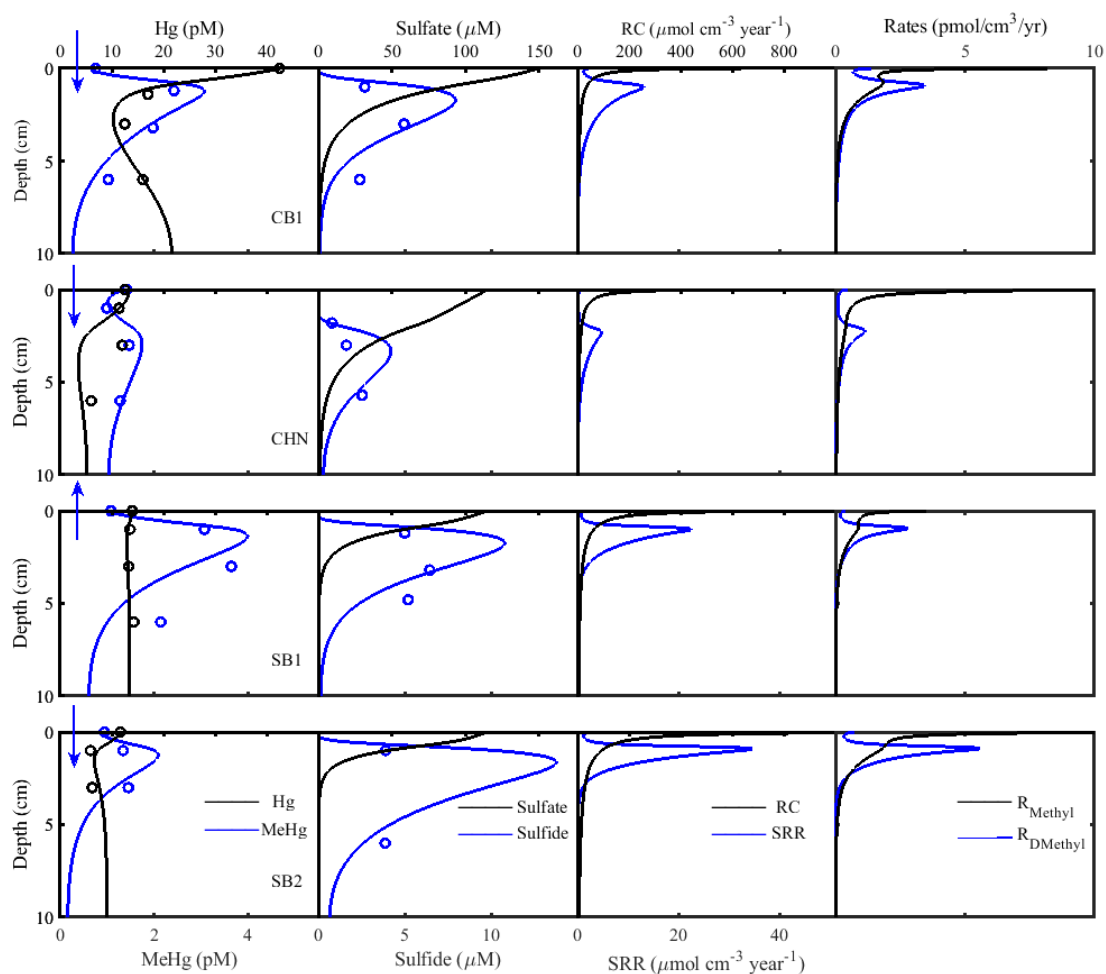
Figure 5.3 *Sediment profiles of mercury (Hg), methylmercury (MeHg), sulfate, sulfide organic matter degradation rate (RC), sulfate reduction rate (SRR), and methylation (R_{Methyl}) and demethylation ($R_{DMethyl}$) rates for four stations in St. Louis River Estuary (SLRE). Symbols correspond to measured values and lines are results from the model. Blue arrows correspond to the direction of MeHg flux at the sediment water interface, resulted from the model.*

5.4.3. Application to marine sediments

To assess the power of the model in describing mercury cycling over a range of conditions, we applied the model to a marine sediment dataset. The only parameters that were varied in order to fit the marine dataset were the geochemical environmental

parameters, including oxygen, sulfate, organic matter content, solid and porewater Hg and MeHg concentrations at the sediment water interface. The internal model parameters such as reaction rate constants and adsorption equilibrium constants were the same as in the SLRE. The model successfully captured the distributions of mercury and methylmercury, both in porewater and solid phases (Fig. 5.4). Similarly to the results in SRLE, calculated methylmercury fluxes indicate that sediments are acting as methylmercury sinks. The decrease in the concentration of solid phase methylmercury below 5 cm at both marine sites reflects desorption of MeHg, which increases the methylmercury concentration in porewater. Porewater MeHg becomes demethylated to inorganic mercury near the sediment-water interface. Simulated demethylation rate at the second site has two peaks, reflecting the respective maxima in the porewater methylmercury concentration and the carbon degradation rate (Fig. 5.4). As in the SRLE, our modeling results indicate that an increase in methylmercury concentration occurs at the depths (~6cm St.1; ~3cm St.2) where the rate of methylation outcompetes that of demethylation. The MeHg increase is concurrent with the increase in the rate of microbial sulfate reduction, in agreement with the idea that methylation is stimulated by sulfate reduction (Gilmour et al. 1992).
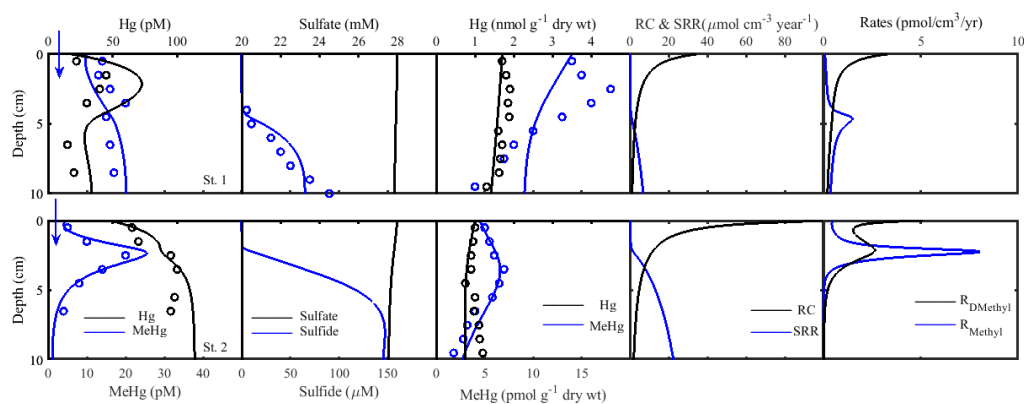
Figure 5.4 *Sediment profiles of mercury (Hg), methylmercury (MeHg), sulfate, solid phase mercury, solid phase methylmercury, and methylation (R_{Methyl}) and demethylation ($R_{DMethyl}$) rates for two stations in marine sediments (Hammerschmidt et al. 2004). Symbols correspond to measured values and lines are results from the model. Blue arrows correspond to the direction of MeHg flux at the sediment water interface, resulted from the model.*

5.5. Sensitivity Analysis of the Model

To investigate the robustness of the modeling results against parameter variations, we conducted a sensitivity analysis. Model parameters were varied within their reasonable ranges (specified in Table 5.3), and changes in the methylmercury diffusive flux were recorded. Multiple geochemical parameter sets were obtained by randomly and independently selecting model parameter values within their uncertainty ranges (Table 5.3), assuming uniform probability distributions. For parameters whose uncertainty ranges span several orders of magnitude, such as reaction rate constants, the values were selected assuming uniform probability distributions of their logarithms. The results are shown in Fig. 5.5 and 5.6. The calculated fluxes were weakly sensitive to most parameters including pH, initial age of organic matter deposited into sediment, diffusion

182

coefficients, porosity, burial velocity, rate constants for oxidation of sulfide and FeS precipitation, Monod constants for sulfate reduction (*Km*), oxic respiration, and iron reduction, adsorption/desorption coefficients for MeHg and Hg, and elemental sulfur disproportionation rate constant. The methylmercury fluxes, however, are most strongly affected by the amount of organic matter, oxygen and sulfate concentrations in bottom water, and notably, mercury and methylmercury concentrations at the SWI (Fig. 5.5 & 5.6).

5.5.1. Controls on MeHg diffusive flux

Higher sulfate concentrations enhance methylation and result in higher fluxes of MeHg from sediment. Higher sulfate concentrations result in higher depth-integrated rates of sulfate reduction, and higher SRB activities increase the methylation rate. A higher MeHg concentration, in turn, stimulates demethylation. Maximum methylation fluxes at different sites are obtained for sulfate concentrations around 200-300 µM. Above this range, the increased sulfide concentration inhibits methylation, decreasing the MeHg flux (Fig. 5.5). This decrease in the MeHg flux stops at the sulfate level around 500 µM. At this level, the sulfate reduction rate stops being limited by sulfate and instead becomes limited by the amount and reactivity of organic matter (Fakhraee et al. 2017). This trend is consistent with results from incubation experiments (Gilmour et al. 1992) where increasing sulfate at mM concentrations did not correlate with changees in the amounts of produced methylmercury, suggesting an insignificant role of sulfate in the methylmercury production at high sulfate levels (Johnson et al. 2016).

Oxygen is an important control on the methylation and demethylation rates and MeHg fluxes. Fig. 5.5 shows the effect of bottom water oxygen on the MeHg flux. Oxygen enhances aerobic oxidation of organic matter, which decreases the amount and reactivity of organic matter that reaches the anoxic zone of the sediment, lowering the sulfate reduction and methylation rates. At low oxygen, sulfate reduction and methylation have higher rates and occur closer to the sediment-water interface, resulting in an increased efflux of MeHg. There is, however, a threshold oxygen concentration, below which the rate of methylation exceeds that of demethylation (Fig. 5.5), causing an efflux of MeHg from sediment. This critical oxygen level (COL) (Fig. 5.5) depends on factors such as organic matter content, sulfate level, and concentrations of Hg and MeHg at the sediment-water interface, as illustrated in Fig. 5.5 & 5.6. Our model suggests, however, that an oxygen threshold at which the direction of MeHg flux reverses exists in all systems.

MeHg effluxes decrease with increasing organic matter content (Fig. 5.5). This is caused by: 1) attenuated methylation rate at high sulfide concentrations (Benoit et al. 1992), promoted by stronger sulfate reduction at higher organic levels, and 2) increased demethylation rate, due to higher carbon degradation rates. This is consistent with the evidence of suppressed methylation in organic- rich environments, where higher sulfide was suggested to inhibit methylation and decrease MeHg fluxes (Gilmour et al. 1992).

5.5.2. Effect of bioirrigation

While the model helps untangle the effects of individual parameters on the diffusive flux of methylmercury, the total flux is a sum of the contributions from diffusion and bioirrigation:

$$F_{\text{Total}} = -\varphi D_i \frac{\partial C_i}{\partial x} + \int_0^{x_{burr}} \varphi \alpha_{irr}\left(C_i^0 - C_i^{burr}\right) dx \qquad (5.10)$$

The first term (Eq. 5.9) corresponds to the molecular diffusion, and the second term represents the bioirrigation flux, integrated over sediment water interface to the maximum depth of bioirrigated burrows (x_{burr}), which was assumed to be 3 cm.

Calculated total fluxes in SLRE suggest that bioirrigation strongly affects the magnitude and direction of the total flux. For instance, at SB1 not only the direction of the total flux is different from the direction of the diffusive flux (negative flux), but its magnitude is about an order of magnitude higher than the diffusive flux (Fig. 5.7). This is consistent with the results in marine sediments where diffusive fluxes, calculated based on MeHg concentration gradients below the sediment-water interface, were much lower than the total fluxes, indicating a prevailing role of bioirrigation in determining the total flux values (Benoit et al. 2009).

Unlike the diffusive flux, where the flux values are mechanistically related to the geochemical parameters such as the concentration of oxygen, sulfate, and organic matter (Fig. 5.5), bioirrigation fluxes are relatively uncorrelated to geochemical parameters (Fig.

185

5.7). The total flux values, however, are strongly governed by the bioirrigation flux. This can potentially explain a lack of correlation between the total flux and the geochemical parameters in several studies (Gilmour et al. 1992; Beck and Johnson 2014). For instance, results from an incubation, carried out by Gilmour et al. (1992), not only demonstrate a lack of correlation between the sulfate levels and total fluxes, but the observed sinusoidal shape for the sulfate vs total flux profile is, interestingly, consistent with the trend suggested by our model (Fig. 5.7).

While bioirrigation generally dominates over diffusive fluxes, diffusion becomes dominant at lower oxygen levels (Fig. 5.7). While bioirrigation generally dominates over diffusive fluxes, diffusion becomes dominant at lower oxygen levels (Fig. 5.7). This effect can be explained through steepening of the MeHg concentration gradients at the sediment water interface at low oxygen levels, where high anaerobic respiration stimulates methylation. This sharper gradient in MeHg would, in turn, increase the diffusive flux, increasing its contribution relative to that of bioirrigation. Accordingly, similar to the results above for the diffusive flux, our modeling results suggest a critical oxygen threshold for the total flux, below which sediment act as a source with respect to methylmercury. The COL value, however, is lower than the COL for purely diffusive fluxes (Fig. 5.7). Our model did not account for a lower bioirrigation effect at lower oxygen level, but due to limited fauna activities under low oxygen conditions, bioirrigation effect would become even less important, resulting in greater contribution of diffusion in determining the direction and magnitude of the total flux at lower oxygen levels.

186
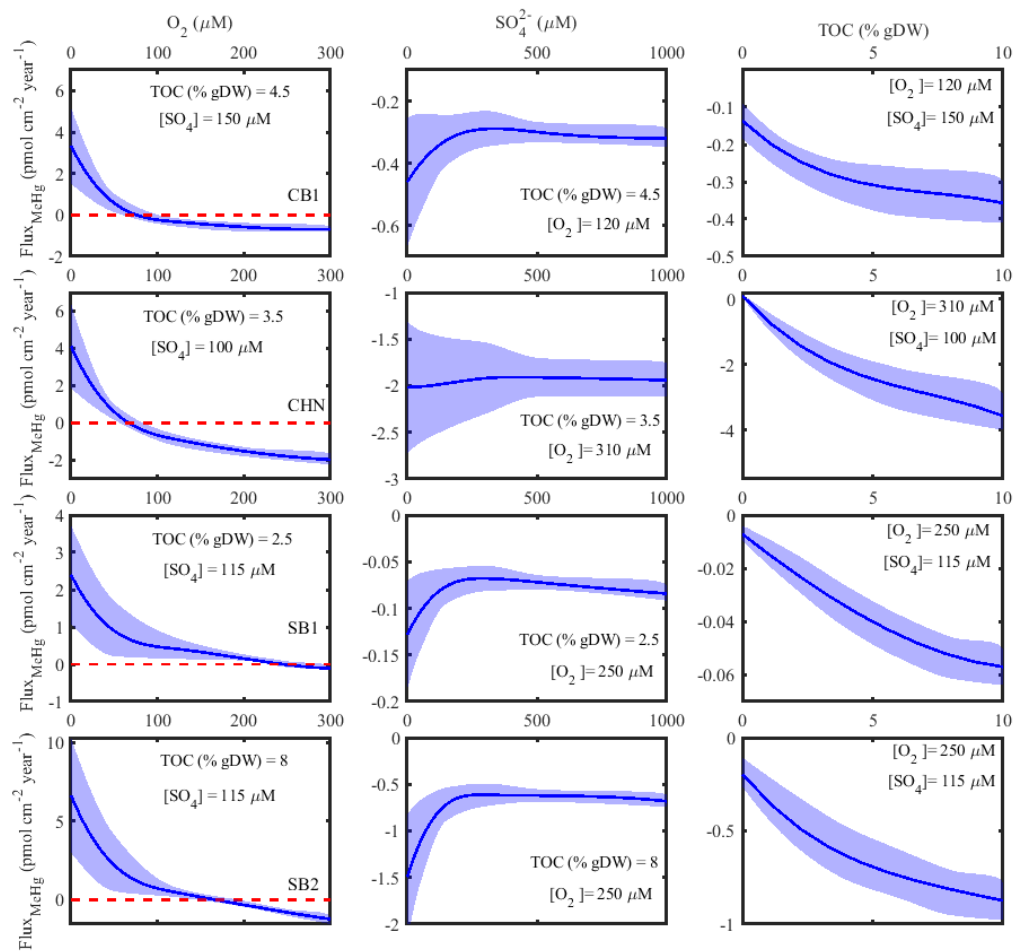
***Figure* 5.5** *Effects of sulfate, oxygen, and total organic matter (TOC) on methylmercury diffusive flux from sediment, for SLRE conditions, based on the model sensitivity analysis. Shaded bands reflect the ±1σ ranges obtained when model parameters were randomly varied within their expected ranges (Table. 5.3). Above the red dashed lines sediment serves as a source of MeHg to overlying waters.*
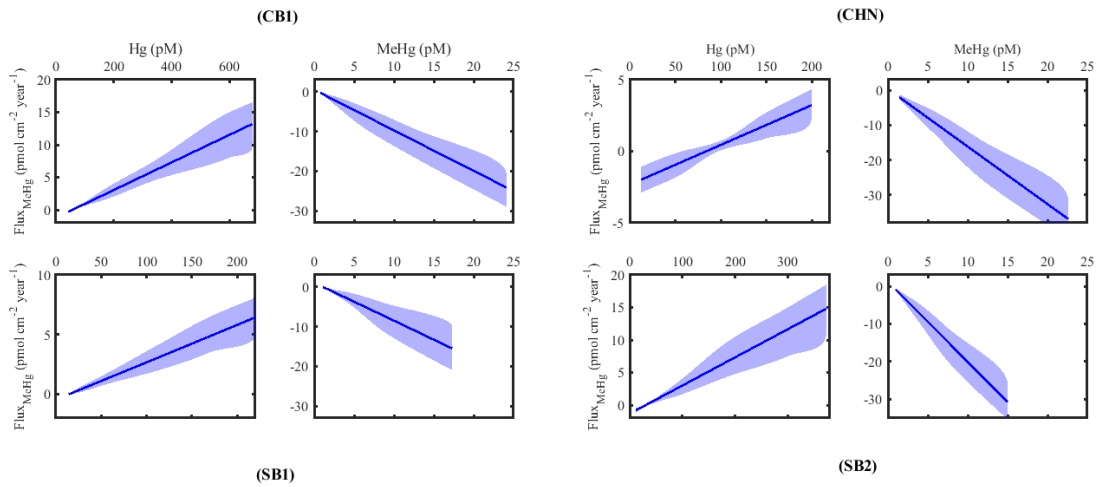
Figure 5.6 *Effect of MeHg and Hg concentrations at sediment water interface on methylmercury diffusive flux, for SLRE, based on the model sensitivity analysis. Shaded bands correspond to ±1σ range.*
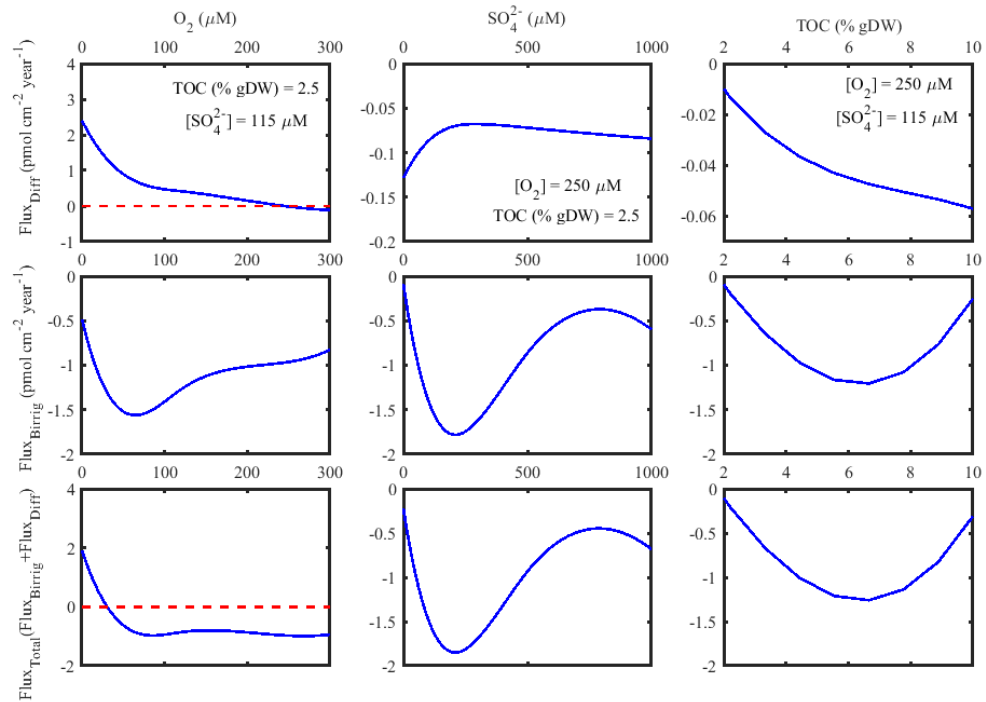
Figure 5.7 *Effect of bioirrigation on total methylmercury flux from SB1 sediment, SLRE. Flux$_{Diff}$ corresponds to the diffusion flux (Fig 5.5, and 5.6), Flux$_{Birrig}$ corresponds to the bioirrigation flux, and Flux$_{Total}$ is the total flux - sum of the fluxes from diffusion and bioirrigation (Eq. 5.10).*

188

5.6. Conclusion

Diffusive methylmercury fluxes in aquatic sediments are controlled by the supplies of oxygen, sulfate, and organic matter. Sulfate increases mercury methylation, causing higher MeHg fluxes. Above certain levels of sulfate, however, high sulfide concentrations, promoted by sulfate reduction, inhibit methylation, decreasing the MeHg flux. By regulating the balance between methylation and demethylation, oxygen controls the direction of the sediment MeHg exchanges with overlying water. In sediments where bioirrigating macro fauna are active, the total fluxes across the sediment-water interface are mostly controlled by bioirrigation. At lower oxygen levels, however, the total flux is largely governed by molecular diffusion. Weakly oxygenated systems ($O_2 < 50 \mu M$) with relatively low sulfate levels (200-300 µM) and organic matter content (TOC < 4 % g DW) are predicted to have high methylmercury fluxes from sediments. This conclusion is, however, strongly dependent on the concentrations of MeHg and Hg at the sediment water interface (Fig. 5.6). Sediments in systems with relatively high Hg concentration, and yet low MeHg concentration in the overlying water, are expected to act as a source of MeHg to the water. These trends, identified through exploratory modeling, should be verified in the future by measurements of the MeHg fluxes under the conditions where the identified control parameters -- oxygen, sulfate and organic matter content – are all adequately constrained. While no such comprehensive dataset is currently available, our modeling indicates that constraining a relatively small number of parameters may be

sufficient to allow predictions of MeHg fluxes, with obvious benefits to environmental management.

Thesis conclusion

In this thesis, efforts were made to put a spotlight on low sulfate environments, and yet challenge the traditionally accepted paradigm of sulfur cycling which was built upon the studies from modern marine systems with high sulfate concentration. Taking advantage of theoretical and modeling approaches, some of the most major insights into low sulfate environments can be listed as:

1) In low-sulfate environments, mineralization of organic sulfur compounds can be an important source of sulfate and sedimentary sulfide

2) Primordial low sulfate oceans had oxygen 250 million years before the atmosphere

3) Seawater sulfate through most of the earth history – first 3.5 billion years - remained below mM range, less than 1.5% of modern values.

While the present work opens a new window into sulfur cycling in low sulfate environments, future steps can be taken to study organic sulfur (S_{org}) speciation in low sulfate environments, role of S_{org} in supporting sulfide oxidation by Large Sulfur Bacteria, sulfur isotope fractionation during S_{org} hydrolysis/minerlization, and the effect of Precambrian (>0.5 billion yrs) sub-mM seawater sulfate on methane cycling and climate perturbations.

Summary of contributions

Below is the summary of research contributions resulting from the present thesis, as well

as from related collaborative efforts:

Publications

1. **M. Fakhraee**, S. A. Crowe, S. Katsev (2017) "Sedimentary sulfur isotopes and Neoarchean ocean oxygenation", *Science Advances, 4(1), e1701835.*

2. **M. Fakhraee**, J. Li, S. Katsev. (2017) "Significant role of organic sulfur in supporting sedimentary sulfate reduction in low-sulfate environments", *Geochimica et Cosmochimica Acta. 213, 502-516.*

3. **M. Fakhraee**, S. Katsev (2018) "The organic component of the earliest sulfur cycling", submitted to *Nature Communications.*

4. **M. Fakhraee,** O. Hancisse, D. E. Canfield, S. A. Crowe, S. Katsev (2018) "Seawater sulfate scarcity, ferruginous oceans, and a methane-rich Proterozoic atmosphere", in review, *Nature Geoscience*

5. **M. Fakhraee**, A. White, N. W. Johnson, S. Katsev "Geochemical constraints on methylmercury flux from sediments", in prep to be submitted to *Environmental Science and Technology.*

6. N. Lambrecht, C. Wittkop, S. Katsev, **M. Fakhraee**, E. D. Swanner, "Geochemical characterization of two ferruginous meromictic lakes in the Upper Midwest, U.S.A.", in revision, *JGR-Biogeosciences*

7. C. Wittkop, E. D. Swanner, N. Lambrecht, **M. Fakhraee**, A. Myrbo, A. Grengs, J. Torgeson, S. Katsev (2018) "Manganese carbonates signal suboxic methanotrophy in ferruginous waters", in prep to be submitted to *Earth and Planetary Science Letters*

8. N. Lambrecht, C. Wittkop, S. Katsev, C. Sheik, **M. Fakhraee**, S. J. Hall, E. D. Swanner (2018) "Controls on methane release in Midwestern ferruginous meromictic lakes: Impacts on modern climate and early Earth", in prep to be submitted to *Geobiology*

Conferences Abstracts

1. **M. Fakhraee,** O. Hancisse, D. E. Canfield, S. A. Crowe, S. Katsev (2018) "Sub-mM Levels of Sulfate and Inefficient AOM in Proterozoic Oceans" *Goldschmidt Conference*, Aug 12 – 17, Boston, USA

2. **M. Fakhraee**, S. A. Crowe, B. M. Toner, S. Katsev (2018) "Low Sulfate Systems: Does Organic Sulfur Affect Isotopic Fractionations?" *Goldschmidt Conference*, Aug 12 – 17,

Boston, USA

3. E. D. Swanner, N. Lambrecht, **M. Fakhraee**, C. Sheik, S. Katsev, C. Wittkop, "Microbes and Minerals from Two Ferruginous Lakes on a Spectrum of Physical and Chemical Characteristics. (2018), *Goldschmidt Conference*, Aug 12 – 17, Boston, USA

4. **M. Fakhraee**, S. Katsev, S. A. Crowe. (2017) " Sediment Sulfur Isotopes Reflect Seawater Oxygen Rise in Neoarchean", *AGU Fall Meeting*", 11-15 Dec 2017, New Orleans, Louisiana.

5. S. Katsev, **M. Fakhraee**, J. Li, K. Schreiner, C. Sheik. (2016) "Significant role of organic and mineral sulfur in supporting sedimentary sulfate reduction in low-sulfate environments", *The 26th Goldschmidt Conference*", 26 June – 1 July 2016, Yokohama, Japan.

Research Expeditions

Brownie Lake, MN – May 2017, and Jul 2017
Obtaining profiles for light, oxygen using flow-through unisense oxygen sensor, chlorophyll using fluoroprobe. Sediment sampling with gravity corer followed by slicing the sediments.

Brownie Lake, MN – Sep 2017, and Jun 2018
Obtaining profiles for light, oxygen using flow-through unisense oxygen sensor, chlorophyll using fluoroprobe. We also sampled waters for sulfur isotope analysis. We filtered (0.45-micron filter) about 400ml water samples into a PVC bottles covered with a dark plastic bag (To inhibit sulfur phototrophy) containing 25ml Zn acetate solution – Filtering water samples using 0.2-micron filter and using filters for sulfide isotope analysis - Adding 10ml $BaCl_2$, and 10ml 1N HCl to the filtered waters in order to precipitate $BaSO_4$ and re-filter the waters and storing filters for isotopic analysis.

Canyon Lake, MI – June 2017, Sep 2017, and May 2018
Obtaining profiles for light, oxygen using flow-through unisense oxygen sensor, chlorophyll using fluoroprobe. Sediment sampling with gravity corer followed by slicing the sediments. Deploying thermometers to obtain temperature variation across the water column throughout the summer and fall. Sampling water for sulfur isotope analysis (same method discussed above).

Lake Superior, MN – June 2017
Surface sediment sampling using ponar grab sampler. Sediment core sampling using multicorer. Obtaining oxygen profile on-board using unisense oxygen sensor.

Pike Lake, MN – Mar 2016
Sediment sampling with gravity corer under the ice.

Lake Superior, MN – Sep 2014

Water column sampling using CTD mounted with Niskin bottles, sediment sampling with the multi-corer, piston corer and grab sampler, zooplankton sampling with vertical net tow, R/V Blue Heron.

References

Amrani, A. (2014). Organosulfur compounds: molecular and isotopic evolution from biota to oil and gas. Annual Review of Earth and Planetary Sciences, 42, 733-768.

Andersson, J. H., Wijsman, J. W., Herman, P. M., Middelburg, J. J., Soetaert, K., & Heip, C. (2004). Respiration patterns in the deep ocean. Geophysical Research Letters, 31(3).

Aoyama, S., & Ueno, Y. (2018). Multiple sulfur isotope constraints on microbial sulfate reduction below an Archean seafloor hydrothermal system. Geobiology, 16(2), 107-120.

Bailey, L. T., Mitchell, C. P., Engstrom, D. R., Berndt, M. E., Wasik, J. K. C., & Johnson, N. W. (2017). Influence of porewater sulfide on methylmercury production and partitioning in sulfate-impacted lake sediments. Science of the Total Environment, 580, 1197-1204.

Beck, B. F., & Johnson, N. W. (2014). Geochemical factors influencing the production and transport of methylmercury in St. Louis River Estuary sediment. Applied geochemistry, 51, 44-54.

Bekker, A., Holland, H. D., Wang, P. L., Rumble Iii, D., Stein, H. J., Hannah, J. L., ... & Beukes, N. J. (2004). Dating the rise of atmospheric oxygen. Nature, 427(6970), 117.

Bellinger, B. J., Van Mooy, B. A., Cotner, J. B., Fredricks, H. F., Benitez-Nelson, C. R., Thompson, J., ... & Godwin, C. M. (2014). Physiological modifications of seston

in response to physicochemical gradients within Lake Superior. Limnology and Oceanography, 59(3), 1011-1026.

Benoit, J. M., Gilmour, C. C., Mason, R. P., & Heyes, A. (1999). Sulfide controls on mercury speciation and bioavailability to methylating bacteria in sediment pore waters. Environmental Science & Technology, 33(6), 951-957.

Benoit, J. M., Shull, D. H., Harvey, R. M., & Beal, S. A. (2009). Effect of bioirrigation on sediment− water exchange of methylmercury in Boston Harbor, Massachusetts. *Environmental science & technology*, *43*(10), 3669-3674.

Berner, R. A. (1980). Early diagenesis: a theoretical approach (No. 1). Princeton University Press.

Black, T. J. (1997). Evaporite karst of northern Lower Michigan. Carbonates and Evaporites, 12(1), 81.

Bottrell, S. H., & Newton, R. J. (2006). Reconstruction of changes in global sulfur cycling from marine sulfate isotopes. Earth-Science Reviews, 75(1-4), 59-83.

Boudreau, B. P. (1997). Diagenetic models and their implementation (Vol. 606). Berlin: Springer.

Bradley, A. S., Leavitt, W. D., Schmidt, M., Knoll, A. H., Girguis, P. R., & Johnston, D. T. (2016). Patterns of sulfur isotope fractionation during microbial sulfate reduction. Geobiology, 14(1), 91-101.

Bridou, R., Monperrus, M., Gonzalez, P. R., Guyoneaud, R., & Amouroux, D. (2011). Simultaneous determination of mercury methylation and demethylation capacities

of various sulfate-reducing bacteria using species-specific isotopic tracers. Environmental Toxicology and Chemistry, 30(2), 337-344.

Burdige, D. J. (2006). Geochemistry of marine sediments. Princeton University Press.

Burdige, D. J. (2007). Preservation of organic matter in marine sediments: controls, mechanisms, and an imbalance in sediment organic carbon budgets?. Chemical reviews, 107(2), 467-485.

Cameron, E. M. (1982). Sulphate and sulphate reduction in early Precambrian oceans. Nature, 296(5853), 145.

Canfield, D. E. (1989). Sulfate reduction and oxic respiration in marine sediments: implications for organic carbon preservation in euxinic environments. Deep Sea Research Part A. Oceanographic Research Papers, 36(1), 121-138.

Canfield, D. E. (1994). Factors influencing organic carbon preservation in marine sediments. Chemical Geology, 114(3-4), 315-329.

Canfield, D. E. (1998). A new model for Proterozoic ocean chemistry. Nature, 396(6710), 450.

Canfield, D. E. (2001). Isotope fractionation by natural populations of sulfate-reducing bacteria. Geochimica et Cosmochimica Acta, 65(7), 1117-1124.

Canfield, D. E. (2006). Models of oxic respiration, denitrification and sulfate reduction in zones of coastal upwelling. Geochimica et Cosmochimica Acta, 70(23), 5753-5765.

Canfield, D. E., & Farquhar, J. (2009). Animal evolution, bioturbation, and the sulfate concentration of the oceans. Proceedings of the National Academy of Sciences, 106(20), 8123-8127.

Canfield, D. E., & Teske, A. (1996). Late Proterozoic rise in atmospheric oxygen concentration inferred from phylogenetic and sulphur-isotope studies. Nature, 382(6587), 127.

Canfield, D. E., & Thamdrup, B. (1994). The production of 34S-depleted sulfide during bacterial disproportionation of elemental sulfur. Science, 266(5193), 1973-1975.

Canfield, D. E., Boudreau, B. P., Mucci, A., & Gundersen, J. K. (1998). The early diagenetic formation of organic sulfur in the sediments of Mangrove Lake, Bermuda. Geochimica et Cosmochimica Acta, 62(5), 767-781.

Canfield, D. E., Farquhar, J., & Zerkle, A. L. (2010). High isotope fractionations during sulfate reduction in a low-sulfate euxinic ocean analog. Geology, 38(5), 415-418.

Canfield, D. E., Habicht, K. S., & Thamdrup, B. O. (2000). The Archean sulfur cycle and the early history of atmospheric oxygen. Science, 288(5466), 658-661.

Canfield, D. E., Jørgensen, B. B., Fossing, H., Glud, R., Gundersen, J., Ramsing, N. B., ... & Hall, P. O. (1993). Pathways of organic carbon oxidation in three continental margin sediments. Marine Geology, 113(1-2), 27-40.

Canfield, D. E., Kristensen, E., & Thamdrup, B. (2005). The sulfur cycle. In Advances in Marine Biology (Vol. 48, pp. 313-381). Academic Press.

Canfield, D. E., Kristensen, E., & Thamdrup, B. (2005). Aquatic geomicrobiology. Gulf Professional Publishing.

Canfield, D. E., Poulton, S. W., Knoll, A. H., Narbonne, G. M., Ross, G., Goldberg, T., & Strauss, H. (2008). Ferruginous conditions dominated later Neoproterozoic deep-water chemistry. Science, 321(5891), 949-952.

Canfield, D. E., & Thamdrup, B. (2009). Towards a consistent classification scheme for geochemical environments, or, why we wish the term 'suboxic'would go away. *Geobiology*, *7*(4), 385-392.

Canfield, D. E., Rosing, M. T., & Bjerrum, C. (2006). Early anaerobic metabolisms. Philosophical Transactions of the Royal Society of London B: Biological Sciences, 361(1474), 1819-1836.

Canfield, D. E., Stewart, F. J., Thamdrup, B., De Brabandere, L., Dalsgaard, T., Delong, E. F., ... & Ulloa, O. (2010). A cryptic sulfur cycle in oxygen-minimum–zone waters off the Chilean coast. Science, 1196889.

Caraco, N. F., Cole, J. J., & Likens, G. E. (1989). Evidence for sulphate-controlled phosphorus release from sediments of aquatic systems. Nature, 341(6240), 316.

Chapra, S. C., Dove, A., & Warren, G. J. (2012). Long-term trends of Great Lakes major ion chemistry. Journal of Great Lakes Research, 38(3), 550-560.

Christensen, J. P., Devol, A. H., & Smethie Jr, W. M. (1984). Biological enhancement of solute exchange between sediments and bottom water on the Washington continental shelf. Continental Shelf Research, 3(1), 9-23.

Cleckner, L. B., Gilmour, C. C., Hurley, J. P., & Krabbenhoft, D. P. (1999). Mercury methylation in periphyton of the Florida Everglades. Limnology and Oceanography, 44(7), 1815-1825.

Cody, G. D., Boctor, N. Z., Filley, T. R., Hazen, R. M., Scott, J. H., Sharma, A., & Yoder, H. S. (2000). Primordial carbonylated iron-sulfur compounds and the synthesis of pyruvate. Science, 289(5483), 1337-1340.

Coelho, J. P., Pereira, M. E., Duarte, A., & Pardal, M. A. (2005). Macroalgae response to a mercury contamination gradient in a temperate coastal lagoon (Ria de Aveiro, Portugal). Estuarine, Coastal and Shelf Science, 65(3), 492-500.

Compeau, G. C., & Bartha, R. (1985). Sulfate-reducing bacteria: principal methylators of mercury in anoxic estuarine sediment. Applied and environmental microbiology, 50(2), 498-502.

Compeau, G., & Bartha, R. (1984). Methylation and demethylation of mercury under controlled redox, pH and salinity conditions. Applied and Environmental Microbiology, 48(6), 1203-1207.

Cook, R. B., & Schindler, D. W. (1983). The biogeochemistry of sulfur in an experimentally acidified lake. Ecological Bulletins, 115-127.

Couture, R. M., Fischer, R., Van Cappellen, P., & Gobeil, C. (2016). Non-steady state diagenesis of organic and inorganic sulfur in lake sediments. Geochimica et Cosmochimica Acta, 194, 15-33.

Craig, P. J., & Bartlett, P. D. (1978). The role of hydrogen sulphide in environmental transport of mercury. Nature, 275(5681), 635-637.

Craig, P. J., & Moreton, P. A. (1983). Total mercury, methyl mercury and sulphide in River Carron sediments. Marine pollution bulletin, 14(11), 408-411.

Crowe, S. A., Døssing, L. N., Beukes, N. J., Bau, M., Kruger, S. J., Frei, R., & Canfield, D. E. (2013). Atmospheric oxygenation three billion years ago. Nature, 501(7468), 535.

Crowe, S. A., Paris, G., Katsev, S., Jones, C., Kim, S. T., Zerkle, A. L., ... & Farquhar, J. (2014). Sulfate was a trace constituent of Archean seawater. Science, 346(6210), 735-739.

Czaja, A. D., Johnson, C. M., Roden, E. E., Beard, B. L., Voegelin, A. R., Nägler, T. F., ... & Wille, M. (2012). Evidence for free oxygen in the Neoarchean ocean based on coupled iron–molybdenum isotope fractionation. Geochimica et Cosmochimica Acta, 86, 118-137.

David, L. A., & Alm, E. J. (2011). Rapid evolutionary innovation during an Archaean genetic expansion. Nature, 469(7328), 93.

David, M. B., & Mitchell, M. J. (1985). Sulfur constituents and cycling in waters, seston, and sediments of an oligotrophic lake. Limnology and Oceanography, 30(6), 1196-1207.

Del Giorgio, P. A., & Duarte, C. M. (2002). Respiration in the open ocean. Nature, 420(6914), 379.

Dell, C. I. G. (1971). Late quaternary sedimentation in Lake Superior (Doctoral dissertation, University of Michigan.).

Dermott, R., & Legner, M. (2002). Dense mat-forming bacterium Thioploca ingrica (Beggiatoaceae) in eastern Lake Ontario: implications to the benthic food web. Journal of Great Lakes Research, 28(4), 688-697.

Devol, A. H., & Hartnett, H. E. (2001). Role of the oxygen-deficient zone in transfer of organic carbon to the deep ocean. Limnology and Oceanography, 46(7), 1684-1690.

D'hondt, S., Jørgensen, B. B., Miller, D. J., Batzke, A., Blake, R., Cragg, B. A., ... & Holm, N. G. (2004). Distributions of microbial activities in deep subseafloor sediments. Science, 306(5705), 2216-2221.

D'hondt, S., Rutherford, S., & Spivack, A. J. (2002). Metabolic activity of subsurface life in deep-sea sediments. Science, 295(5562), 2067-2070.

Dickens, G. R., Koelling, M., Smith, D. C., & Schnieders, L. (2007). Rhizon sampling of pore waters on scientific drilling expeditions: an example from the IODP Expedition 302, Arctic Coring Expedition (ACEX).

Domagal-Goldman, S. D., Kasting, J. F., Johnston, D. T., & Farquhar, J. (2008). Organic haze, glaciations and multiple sulfur isotopes in the Mid-Archean Era. Earth and Planetary Science Letters, 269(1-2), 29-40.

Dornblaser, M., Giblin, A. E., Fry, B., & Peterson, B. J. (1994). Effects of sulfate concentration in the overlying water on sulfate reduction and sulfur storage in lake sediments. Biogeochemistry, 24(3), 129-144.

Dyrssen, D., & Kremling, K. (1990). Increasing hydrogen sulfide concentration and trace metal behavior in the anoxic Baltic waters. Marine Chemistry, 30, 193-204.

Eaton, A. E., Clesceri, L. S., & Rice, E. W. (2005). Standard Methods for the Examination of Water & Wastewater: Centennial Edition. American Public

Health Association, American Water Works Association, Water Environment Federation.

Eckley, C. S., & Hintelmann, H. (2006). Determination of mercury methylation potentials in the water column of lakes across Canada. Science of the Total Environment, 368(1), 111-125.

Eickmann, B., Hofmann, A., Wille, M., Bui, T. H., Wing, B. A., & Schoenberg, R. (2018). Isotopic evidence for oxygenated Mesoarchaean shallow oceans. Nature Geoscience, 11(2), 133.

Eigenbrode, J. L., Summons, R. E., Steele, A., Freissinet, C., Millan, M., Navarro-González, R., ... & Archer, P. D. (2018). Organic matter preserved in 3-billion-year-old mudstones at Gale crater, Mars. Science, 360(6393), 1096-1101.

Fagerbakke, K. M., Heldal, M., & Norland, S. (1996). Content of carbon, nitrogen, oxygen, sulfur and phosphorus in native aquatic and cultured bacteria. Aquatic Microbial Ecology, 10(1), 15-27.

Fakhraee, M., Crowe, S. A., & Katsev, S. (2018). Sedimentary sulfur isotopes and Neoarchean ocean oxygenation. Science advances, 4(1), e1701835.

Fakhraee, M., Li, J., & Katsev, S. (2017). Significant role of organic sulfur in supporting sedimentary sulfate reduction in low-sulfate environments. Geochimica et Cosmochimica Acta, 213, 502-516.

Farquhar, J., & Wing, B. A. (2003). Multiple sulfur isotopes and the evolution of the atmosphere. Earth and Planetary Science Letters, 213(1-2), 1-13.

Farquhar, J., Bao, H., & Thiemens, M. (2000). Atmospheric influence of Earth's earliest sulfur cycle. Science, 289(5480), 756-758.

Farquhar, J., Savarino, J., Airieau, S., & Thiemens, M. H. (2001). Observation of wavelength-sensitive mass-independent sulfur isotope effects during SO2 photolysis: Implications for the early atmosphere. Journal of Geophysical Research: Planets, 106(E12), 32829-32839.

Ferdelman, T. G., Church, T. M., & Luther III, G. W. (1991). Sulfur enrichment of humic substances in a Delaware salt marsh sediment core. Geochimica et Cosmochimica Acta, 55(4), 979-988.

Ferdelman, T. G., Lee, C., Pantoja, S., Harder, J., Bebout, B. M., & Fossing, H. (1997). Sulfate reduction and methanogenesis in a Thioploca-dominated sediment off the coast of Chile. *Geochimica et Cosmochimica Acta*, *61*(15), 3065-3079.

Ferdelman, T. G., Fossing, H., Neumann, K., & Schulz, H. D. (1999). Sulfate reduction in surface sediments of the southeast Atlantic continental margin between 15 38'S and 27 57'S (Angola and Namibia). Limnology and Oceanography, 44(3), 650-661.

Ferdelman, T. G., Lee, C., Pantoja, S., Harder, J., Bebout, B. M., & Fossing, H. (1997). Sulfate reduction and methanogenesis in a Thioploca-dominated sediment off the coast of Chile. Geochimica et Cosmochimica Acta, 61(15), 3065-3079.

Fitzgerald, J. W. (1976). Sulfate ester formation and hydrolysis: a potentially important yet often ignored aspect of the sulfur cycle of aerobic soils. Bacteriological Reviews, 40(3), 698.

Fossing, H., Gallardo, V. A., Jørgensen, B. B., Hüttel, M., Nielsen, L. P., Schulz, H., ... & Küver, J. (1995). Concentration and transport of nitrate by the mat-forming sulphur bacterium Thioploca. *Nature*, *374*(6524), 713.

Fossing, H. (2004). Distribution and fate of sulfur intermediates—sulfite, tetrathionate, thiosulfate, and elemental sulfur—in marine sediments. Sulfur Biogeochemistry: Past and Present, 379, 97.

Friend, J. P. (1973). The global sulfur cycle. In *Chemistry of the lower atmosphere* (pp. 177-201). Springer, Boston, MA.

Furutani, A., & Rudd, J. W. (1980). Measurement of mercury methylation in lake water and sediment samples. Applied and environmental microbiology, 40(4), 770-776.

Gaines, R. R., Hammarlund, E. U., Hou, X., Qi, C., Gabbott, S. E., Zhao, Y., ... & Canfield, D. E. (2012). Mechanism for Burgess Shale-type preservation. Proceedings of the National Academy of Sciences, 109(14), 5180-5184.

Galić, A., Mason, P. R., Mogollón, J. M., Wolthers, M., Vroon, P. Z., & Whitehouse, M. J. (2017). Pyrite in a sulfate-poor Paleoarchean basin was derived predominantly from elemental sulfur: Evidence from 3.2 Ga sediments in the Barberton Greenstone Belt, Kaapvaal Craton. Chemical Geology, 449, 135-146.

Gilmour, C. C., & Henry, E. A. (1991). Mercury methylation in aquatic systems affected by acid deposition. Environmental pollution, 71(2-4), 131-169.

Gilmour, C. C., Henry, E. A., & Mitchell, R. (1992). Sulfate stimulation of mercury methylation in freshwater sediments. Environmental Science & Technology, 26(11), 2281-2287.

Goldhaber, M. B. (2003). Sulfur-rich sediments. Treatise on Geochemistry, 7, 407.

Goldhaber, M. B., & Kaplan, I. R. (1980). Mechanisms of sulfur incorporation and isotope fractionation during early diagenesis in sediments of the Gulf of California. Marine Chemistry, 9(2), 95-143.

Gorham, E., Lund, J. W., Sanger, J. E., & Dean Jr, W. E. (1974). Some relationships between algal standing crop, water chemistry, and sediment chemistry in the English Lakes 1. Limnology and oceanography, 19(4), 601-617.

Grannemann, N. G., Hunt, R. J., Nicholas, J. R., Reilly, T. E., & Winter, T. C. (2000). The importance of ground water in the Great Lakes region (No. 2000-4008). US Geological Survey.

Guo, Q., Strauss, H., Kaufman, A. J., Schröder, S., Gutzmer, J., Wing, B., ... & Farquhar, J. (2009). Reconstructing Earth's surface oxidation across the Archean-Proterozoic transition. Geology, 37(5), 399-402.

Habicht, K. S., & Canfield, D. E. (1996). Sulphur isotope fractionation in modern microbial mats and the evolution of the sulphur cycle. Nature, 382(6589), 342.

Habicht, K. S., Canfield, D. E., & Rethmeier, J. (1998). Sulfur isotope fractionation during bacterial reduction and disproportionation of thiosulfate and sulfite. Geochimica et Cosmochimica Acta, 62(15), 2585-2595.

Habicht, K. S., Gade, M., Thamdrup, B., Berg, P., & Canfield, D. E. (2002). Calibration of sulfate levels in the Archean ocean. Science, 298(5602), 2372-2374.

Halevy, I., Johnston, D. T., & Schrag, D. P. (2010). Explaining the structure of the Archean mass-independent sulfur isotope record. Science, 329(5988), 204-207.

Hammerschmidt, C. R., & Fitzgerald, W. F. (2008). Sediment–water exchange of methylmercury determined from shipboard benthic flux chambers. Marine Chemistry, 109(1-2), 86-97.

Hammerschmidt, C. R., Fitzgerald, W. F., Lamborg, C. H., Balcom, P. H., & Visscher, P. T. (2004). Biogeochemistry of methylmercury in sediments of Long Island Sound. Marine Chemistry, 90(1-4), 31-52.

Han, S., Obraztsova, A., Pretto, P., Deheyn, D. D., Gieskes, J., & Tebo, B. M. (2008). Sulfide and iron control on mercury speciation in anoxic estuarine sediment slurries. Marine Chemistry, 111(3-4), 214-220.

Havig, J. R., Hamilton, T. L., Bachan, A., & Kump, L. R. (2017). Sulfur and carbon isotopic evidence for metabolic pathway evolution and a four-stepped Earth system progression across the Archean and Paleoproterozoic. Earth-Science Reviews, 174, 1-21.

Hayes, J. M., Strauss, H., & Kaufman, A. J. (1999). The abundance of 13C in marine organic matter and isotopic fractionation in the global biogeochemical cycle of carbon during the past 800 Ma. Chemical Geology, 161(1-3), 103-125.

He, T., Feng, X., Guo, Y., Qiu, G., Li, Z., Liang, L., & Lu, J. (2008). The impact of eutrophication on the biogeochemical cycling of mercury species in a reservoir: a case study from Hongfeng Reservoir, Guizhou, China. Environmental Pollution, 154(1), 56-67.

Heinen, W., & Lauwers, A. M. (1996). Organic sulfur compounds resulting from the interaction of iron sulfide, hydrogen sulfide and carbon dioxide in an anaerobic

aqueous environment. Origins of Life and Evolution of the Biosphere, 26(2), 131-150.

Ho, T. Y., Quigg, A., Finkel, Z. V., Milligan, A. J., Wyman, K., Falkowski, P. G., & Morel, F. M. (2003). THE ELEMENTAL COMPOSITION OF SOME MARINE PHYTOPLANKTON 1. Journal of Phycology, 39(6), 1145-1159.

Hoffman, J. C., Peterson, G. S., Cotter, A. M., & Kelly, J. R. (2010). Using stable isotope mixing in a Great Lakes coastal tributary to determine food web linkages in young fishes. Estuaries and Coasts, 33(6), 1391-1405.

Hoffman, P. F., Kaufman, A. J., Halverson, G. P., & Schrag, D. P. (1998). A Neoproterozoic snowball earth. science, 281(5381), 1342-1346.

Hoggarth, C. G., Hall, B. D., & Mitchell, C. P. (2015). Mercury methylation in high and low-sulphate impacted wetland ponds within the prairie pothole region of North America. Environmental pollution, 205, 269-277.

Hohmann-Marriott, M. F., & Blankenship, R. E. (2011). Evolution of photosynthesis. Annual review of plant biology, 62, 515-548.

Holland, H. D. (1994). Early Proterozoic atmospheric change. Early Life in Earth.

Holland, H. D. (2002). Volcanic gases, black smokers, and the Great Oxidation Event. Geochimica et Cosmochimica Acta, 66(21), 3811-3826.

Holmer, M., & Storkholm, P. (2001). Sulphate reduction and sulphur cycling in lake sediments: a review. Freshwater Biology, 46(4), 431-451.

Holmer, M., Jensen, H. S., Christensen, K. K., Wigand, C., & Andersen, F. Ø. (1998). Sulfate reduction in lake sediments inhabited by the isoetid macrophytes Littorella uniflora and Isoetes lacustris. Aquatic Botany, 60(4), 307-324.

Holmkvist, L., Ferdelman, T. G., & Jørgensen, B. B. (2011). A cryptic sulfur cycle driven by iron in the methane zone of marine sediment (Aarhus Bay, Denmark). Geochimica et Cosmochimica Acta, 75(12), 3581-3599.

Hurtgen, M. T., Arthur, M. A., & Halverson, G. P. (2005). Neoproterozoic sulfur isotopes, the evolution of microbial sulfur species, and the burial efficiency of sulfide as sedimentary pyrite. Geology, 33(1), 41-44.

Ingvorsen, K., & Jørgensen, B. B. (1984). Kinetics of sulfate uptake by freshwater and marine species ofDesulfovibrio. Archives of Microbiology, 139(1), 61-66.

J. Li, thesis, University of Minnesota, (2014).

J⊘ rgensen, B. B. (1978). A comparison of methods for the quantification of bacterial sulfate reduction in coastal marine sediments: II. Calculation from mathematical models. Geomicrobiology Journal, 1(1), 29-47.

Jeremiason, J. D., Engstrom, D. R., Swain, E. B., Nater, E. A., Johnson, B. M., Almendinger, J. E., ... & Kolka, R. K. (2006). Sulfate addition increases methylmercury production in an experimental wetland. Environmental science & technology, 40(12), 3800-3806.

Johnson, T. C., Evans, J. E., & Eisenreich, S. J. (1982). Total organic carbon in Lake Superior sediments: Comparisons with hemipelagic and pelagic marine environments1. Limnology and Oceanography, 27(3), 481-491.

Johnson, T. C., Van Alstine, J. D., Rolfhus, K. R., Colman, S. M., & Wattrus, N. J. (2012). A high resolution study of spatial and temporal variability of natural and anthropogenic compounds in offshore Lake Superior sediments. Journal of Great Lakes Research, 38(4), 673-685.

Johnston, D. T. (2011). Multiple sulfur isotopes and the evolution of Earth's surface sulfur cycle. Earth-Science Reviews, 106(1-2), 161-183.

Johnston, D. T., Wing, B. A., Farquhar, J., Kaufman, A. J., Strauss, H., Lyons, T. W., ... & Canfield, D. E. (2005). Active microbial sulfur disproportionation in the Mesoproterozoic. science, 310(5753), 1477-1479.

Johnston, S. G., Burton, E. D., Aaso, T., & Tuckerman, G. (2014). Sulfur, iron and carbon cycling following hydrological restoration of acidic freshwater wetlands. Chemical geology, 371, 9-26.

Jorgensen, B. B. (1979). A theoretical model of the stable sulfur isotope distribution in marine sediments. Geochimica et Cosmochimica Acta, 43(3), 363-374.

Jørgensen, B. B. (1982). Mineralization of organic matter in the sea bed—the role of sulphate reduction. Nature, 296(5858), 643-645.

Jørgensen, B. B. (1988). Ecology of the sulphur cycle: oxidative pathways in sediments. The nitrogen and sulphur Cycles, 42, 31-63.

Jørgensen, B. B. (1989). Sulfate reduction in marine sediments from the Baltic Sea-North Sea transition. Ophelia, 31(1), 1-15.

Jørgensen, B. B. (1990). The sulfur cycle of freshwater sediments: role of thiosulfate. Limnology and Oceanography, 35(6), 1329-1342.

Jourabchi, P. (2007). New developments in early diagenetic modeling: pH distributions, calcite dissolution and compaction(Doctoral dissertation, Utrecht University).

Jourabchi, P., Van Cappellen, P., & Regnier, P. (2005). Quantitative interpretation of pH distributions in aquatic sediments: A reaction-transport modeling approach. American Journal of Science, 305(9), 919-956.

Kah, L. C., Lyons, T. W., & Chesley, J. T. (2001). Geochemistry of a 1.2 Ga carbonate-evaporite succession, northern Baffin and Bylot Islands: implications for Mesoproterozoic marine evolution. Precambrian Research, 111(1-4), 203-234.

Karhu, J. A., & Holland, H. D. (1996). Carbon isotopes and the rise of atmospheric oxygen. Geology, 24(10), 867-870.

Kasting, J. F. (2001). The rise of atmospheric oxygen. Science, 293(5531), 819-820.

Katsev, S. (2016). Phosphorus effluxes from lake sediments. Soil Phosphorus, Taylor and Francis.

Katsev, S., & Crowe, S. A. (2015). Organic carbon burial efficiencies in sediments: The power law of mineralization revisited. Geology, 43(7), 607-610.

Katsev, S., & Dittrich, M. (2013). Modeling of decadal scale phosphorus retention in lake sediment under varying redox conditions. Ecological modelling, 251, 246-259.

Katsev, S., Chaillou, G., Sundby, B., & Mucci, A. (2007). Effects of progressive oxygen depletion on sediment diagenesis and fluxes: A model for the lower St. Lawrence River Estuary. Limnology and Oceanography, 52(6), 2555-2568.

Katsev, S., Rancourt, D. G., & L'Heureux, I. (2004). dSED: A database tool for modeling sediment early diagenesis. Computers & geosciences, 30(9-10), 959-967.

Katsev, S., Sundby, B., & Mucci, A. (2006). Modeling vertical excursions of the redox boundary in sediments: Application to deep basins of the Arctic Ocean. Limnology and Oceanography, 51(4), 1581-1593.

Katsev, S., Tsandev, I., L'Heureux, I., & Rancourt, D. G. (2006). Factors controlling long-term phosphorus efflux from lake sediments: Exploratory reactive-transport modeling. Chemical Geology, 234(1-2), 127-147.

Kempe, S., & Degens, E. T. (1985). An early soda ocean?. Chemical Geology, 53(1-2), 95-108.

Kharasch, N. (Ed.). (2013). Organic sulfur compounds. Elsevier.

King, G. M., & Klug, M. J. (1980). Sulfhydrolase activity in sediments of wintergreen lake, kalamazoo county, michigan. Applied and Environmental Microbiology, 39(5), 950-956.

King, G. M., & Klug, M. J. (1982). Comparative aspects of sulfur mineralization in sediments of a eutrophic lake basin. Applied and environmental microbiology, 43(6), 1406-1412.

King, J. K., Kostka, J. E., Frischer, M. E., & Saunders, F. M. (2000). Sulfate-reducing bacteria methylate mercury at variable rates in pure culture and in marine sediments. Applied and Environmental Microbiology, 66(6), 2430-2437.

King, J. K., Kostka, J. E., Frischer, M. E., Saunders, F. M., & Jahnke, R. A. (2001). A quantitative relationship that demonstrates mercury methylation rates in marine sediments are based on the community composition and activity of sulfate-reducing bacteria. Environmental Science & Technology, 35(12), 2491-2496.

212

Kitajima, K., Maruyama, S., Utsunomiya, S., & Liou, J. G. (2001). Seafloor hydrothermal alteration at an Archaean mid-ocean ridge. Journal of Metamorphic Geology, 19(5), 583-599.

Knittel, K., & Boetius, A. (2009). Anaerobic oxidation of methane: progress with an unknown process. Annual review of microbiology, 63, 311-334.

Knoll, A. H., Bergmann, K. D., & Strauss, J. V. (2016). Life: the first two billion years. Phil. Trans. R. Soc. B, 371(1707), 20150493.

Kokkonen, P., & Tolonen, K. (1987). Analysis of organic and inorganic sulfur constituents and 34 S-isotopes in dated sediments of forest lakes in southern Finland. Water, Air, and Soil Pollution, 35(1-2), 157-170.

Korthals, E. T., & Winfrey, M. R. (1987). Seasonal and spatial variations in mercury methylation and demethylation in an oligotrophic lake. Applied and Environmental Microbiology, 53(10), 2397-2404.

Ksionzek, K. B., Lechtenfeld, O. J., McCallister, S. L., Schmitt-Kopplin, P., Geuer, J. K., Geibert, W., & Koch, B. P. (2016). Dissolved organic sulfur in the ocean: Biogeochemistry of a petagram inventory. Science, 354(6311), 456-459.

Kuivila, K. M., Murray, J. W., Devol, A. H., & Novelli, P. C. (1989). Methane production, sulfate reduction and competition for substrates in the sediments of Lake Washington. Geochimica et Cosmochimica Acta, 53(2), 409-416.

Kuivila, K. M., Murray, J. W., Devol, A. H., Lidstrom, M. E., & Reimers, C. E. (1988). Methane cycling in the sediments of Lake Washington. Limnology and Oceanography, 33(4), 571-581.

Kump, L. R., & Seyfried Jr, W. E. (2005). Hydrothermal Fe fluxes during the Precambrian: Effect of low oceanic sulfate concentrations and low hydrostatic pressure on the composition of black smokers. Earth and Planetary Science Letters, 235(3-4), 654-662.

Lavik, G., Stührmann, T., Brüchert, V., Van der Plas, A., Mohrholz, V., Lam, P., ... & Kuypers, M. M. (2009). Detoxification of sulphidic African shelf waters by blooming chemolithotrophs. Nature, 457(7229), 581.

Lenton, T. M., Boyle, R. A., Poulton, S. W., Shields-Zhou, G. A., & Butterfield, N. J. (2014). Co-evolution of eukaryotes and ocean oxygenation in the Neoproterozoic era. Nature Geoscience, 7(4), 257.

Levine, N. M. (2016). Putting the spotlight on organic sulfur. Science, 354(6311), 418-419.

Li, J. (2014). Sediment diagenesis in large lakes Superior and Malawi, geochemical cycles and budgets and comparisons to marine sediments.

Li, J., & Katsev, S. (2014). Nitrogen cycling in deeply oxygenated sediments: Results in Lake Superior and implications for marine sediments. Limnology and Oceanography, 59(2), 465-481.

Li, J., Crowe, S. A., Miklesh, D., & Katsev, S. (2009, December). Nutrient fluxes and temporal and spatial variability in organic poor sediments in Lake Superior. In AGU Fall Meeting Abstracts.

Li, J., Crowe, S. A., Miklesh, D., Kistner, M., Canfield, D. E., & Katsev, S. (2012). Carbon mineralization and oxygen dynamics in sediments with deep oxygen penetration, Lake Superior. Limnology and Oceanography, 57(6), 1634-1650.

Liu, X. M., Kah, L. C., Knoll, A. H., Cui, H., Kaufman, A. J., Shahar, A., & Hazen, R. M. (2015). Tracing Earth's O2 evolution using Zn/Fe ratios in marine carbonates.

Lockhart, W. L., Wilkinson, P., Billeck, B. N., Danell, R. A., Hunt, R. V., Brunskill, G. J., ... & Louis, V. S. (1998). Fluxes of mercury to lake sediments in central and northern Canada inferred from dated sediment cores. Biogeochemistry, 40(2-3), 163-173.

LoVLEY, D. R., & Klug, M. J. (1986). Model for the distribution of sulfate reduction and methanogenesis in freshwater sediments. Geochimica et Cosmochimica Acta, 50(1), 11-18.

Luo, G., Ono, S., Huang, J., Algeo, T. J., Li, C., Zhou, L., ... & Xie, S. (2015). Decline in oceanic sulfate levels during the early Mesoproterozoic. Precambrian Research, 258, 36-47.

Lyons, T. W., Reinhard, C. T., & Planavsky, N. J. (2014). The rise of oxygen in Earth's early ocean and atmosphere. Nature, 506(7488), 307.

Mackenzie, F. T., & Garrels, R. M. (1971). Evolution of sedimentary rocks. New York: Norton.

Marin-Carbonne, J., Remusat, L., Sforna, M. C., Thomazo, C., Cartigny, P., & Philippot, P. (2018). Sulfur isotope's signal of nanopyrites enclosed in 2.7 Ga stromatolitic organic remains reveal microbial sulfate reduction. Geobiology, 16(2), 121-138.

Marnette, E. C., Horditk, C. A., & Van Breemen, N. (1992). Sulfate reduction and S-oxidation in a moorland pool sediment. Biogeochemistry, 17(2), 123-143.

Martin, W., Baross, J., Kelley, D., & Russell, M. J. (2008). Hydrothermal vents and the origin of life. Nature Reviews Microbiology, 6(11), 805.

Marvin-DiPasquale, M., Agee, J., Bouse, R., & Jaffe, B. (2003). Microbial cycling of mercury in contaminated pelagic and wetland sediments of San Pablo Bay, California. Environmental Geology, 43(3), 260-267.

Marzocchi, U., Trojan, D., Larsen, S., Meyer, R. L., Revsbech, N. P., Schramm, A., ... & Risgaard-Petersen, N. (2014). Electric coupling between distant nitrate reduction and sulfide oxidation in marine sediment. *The ISME journal*, *8*(8), 1682.

Merritt, K. A., & Amirbahman, A. (2009). Mercury methylation dynamics in estuarine and coastal marine environments—a critical review. *Earth-Science Reviews*, *96*(1-2), 54-66.

Michel, R. L., Turk, J. T., Campbell, D. H., & Mast, M. A. (2002). Use of natural 35 S to trace sulphate cycling in small lakes, Flattops Wilderness Area, Colorado, USA. Water, Air and Soil Pollution: Focus, 2(2), 5-18.

Michiels, C. C., Darchambeau, F., Roland, F. A., Morana, C., Llirós, M., García-Armisen, T., ... & Descy, J. P. (2017). Iron-dependent nitrogen cycling in a ferruginous lake and the nutrient status of Proterozoic oceans. Nature Geoscience, 10(3), 217-221.

Middelburg, J. J. (1989). A simple rate model for organic matter decomposition in marine sediments. Geochimica et Cosmochimica Acta, 53(7), 1577-1581.

Milliman, J. D., & Meade, R. H. (1983). World-wide delivery of river sediment to the oceans. The Journal of Geology, 91(1), 1-21.

Minnesota Pollution Control Agency (2002). Annual Pollution Report.

Miskimmin, B. M., Rudd, J. W., & Kelly, C. A. (1992). Influence of dissolved organic carbon, pH, and microbial respiration rates on mercury methylation and demethylation in lake water. Canadian Journal of Fisheries and Aquatic Sciences, 49(1), 17-22.

Ndu, U., Barkay, T., Schartup, A. T., Mason, R. P., & Reinfelder, J. R. (2016). The effect of aqueous speciation and cellular ligand binding on the biotransformation and bioavailability of methylmercury in mercury-resistant bacteria. Biodegradation, 27(1), 29-36.

Neff, B. P., & Nicholas, J. R. (2005). Uncertainty in the Great Lakes Water Balance, Date Posted: November 23, 2005: US Geological Survey Scientific Investigations Report 2004-5100, 42 p.

Newton, R. J., Reeves, E. P., Kafousia, N., Wignall, P. B., Bottrell, S. H., & Sha, J. G. (2011). Low marine sulfate concentrations and the isolation of the European epicontinental sea during the Early Jurassic. Geology, 39(1), 7-10.

Nielsen, L. P., Risgaard-Petersen, N., Fossing, H., Christensen, P. B., & Sayama, M. (2010). Electric currents couple spatially separated biogeochemical processes in marine sediment. *Nature*, *463*(7284), 1071.

Nriagu, J. O. (1968). Sulfur metabolism and sedimentary environment: Lake Mendota, Wisconsin. Limnology and Oceanography, 13(3), 430-439.

Nriagu, J. O. (1984). Role of inland water sediments as sinks for anthropogenic sulfur. Science of the total environment, 38, 7-13.

Nriagu, J. O., & Soon, Y. K. (1985). Distribution and isotopic composition of sulfur in lake sediments of northern Ontario. Geochimica et Cosmochimica Acta, 49(3), 823-834.

O'Beirne, M. D., Werne, J. P., Hecky, R. E., Johnson, T. C., Katsev, S., & Reavie, E. D. (2017). Anthropogenic climate change has altered primary productivity in Lake Superior. Nature communications, 8, 15713.

Och, L. M., Müller, B., März, C., Wichser, A., Vologina, E. G., & Sturm, M. (2016). Elevated uranium concentrations in Lake Baikal sediments: Burial and early diagenesis. Chemical Geology, 441, 92-105.

Och, L. M., Müller, B., Voegelin, A., Ulrich, A., Göttlicher, J., Steiniger, R., ... & Sturm, M. (2012). New insights into the formation and burial of Fe/Mn accumulations in Lake Baikal sediments. Chemical Geology, 330, 244-259.

Ohmoto, H., Watanabe, Y., Ikemi, H., Poulson, S. R., & Taylor, B. E. (2006). Sulphur isotope evidence for an oxic Archaean atmosphere. Nature, 442(7105), 908.

Olson, S. L., Kump, L. R., & Kasting, J. F. (2013). Quantifying the areal extent and dissolved oxygen concentrations of Archean oxygen oases. Chemical Geology, 362, 35-43.

Olson, S. L., Reinhard, C. T., & Lyons, T. W. (2016). Limited role for methane in the mid-Proterozoic greenhouse. Proceedings of the National Academy of Sciences, 113(41), 11447-11452.

Ono, S., Eigenbrode, J. L., Pavlov, A. A., Kharecha, P., Rumble III, D., Kasting, J. F., & Freeman, K. H. (2003). New insights into Archean sulfur cycle from mass-independent sulfur isotope records from the Hamersley Basin, Australia. Earth and Planetary Science Letters, 213(1-2), 15-30.

Prokopenko, M. G., Hirst, M. B., De Brabandere, L., Lawrence, D. J. P., Berelson, W. M., Granger, J., ... & Thamdrup, B. (2013). Nitrogen losses in anoxic marine sediments driven by Thioploca–anammox bacterial consortia. *Nature*, *500*(7461), 194.

Pak, K. R., & Bartha, R. (1998). Mercury methylation by interspecies hydrogen and acetate transfer between sulfidogens and methanogens. Applied and environmental microbiology, 64(6), 1987-1990.

Parsons, B., & Sclater, J. G. (1977). An analysis of the variation of ocean floor bathymetry and heat flow with age. Journal of geophysical research, 82(5), 803-827.

Pavlov, A. A., & Kasting, J. F. (2002). Mass-independent fractionation of sulfur isotopes in Archean sediments: strong evidence for an anoxic Archean atmosphere. Astrobiology, 2(1), 27-41.

Petsch, S. T., & Berner, R. A. (1998). Coupling the geochemical cycles of C, P, Fe, and S; the effect on atmospheric O 2 and the isotopic records of carbon and sulfur. American Journal of Science, 298(3), 246-262.

Pfeifenschneider, J., Brautaset, T., & Wendisch, V. F. (2017). Methanol as carbon substrate in the bio-economy: Metabolic engineering of aerobic methylotrophic

bacteria for production of value-added chemicals. Biofuels, Bioproducts and Biorefining, 11(4), 719-731.

Pfennig, N. (1975). The phototrophic bacteria and their role in the sulfur cycle. Plant and Soil, 43(1-3), 1-16.

Philippot, P., Van Zuilen, M., Lepot, K., Thomazo, C., Farquhar, J., & Van Kranendonk, M. J. (2007). Early Archaean microorganisms preferred elemental sulfur, not sulfate. Science, 317(5844), 1534-1537.

Planavsky, N. J., Asael, D., Hofmann, A., Reinhard, C. T., Lalonde, S. V., Knudsen, A., ... & Beukes, N. J. (2014). Evidence for oxygenic photosynthesis half a billion years before the Great Oxidation Event. Nature Geoscience, 7(4), 283.

Planavsky, N. J., Bekker, A., Hofmann, A., Owens, J. D., & Lyons, T. W. (2012). Sulfur record of rising and falling marine oxygen and sulfate levels during the Lomagundi event. Proceedings of the National Academy of Sciences, 109(45), 18300-18305.

Planavsky, N. J., McGoldrick, P., Scott, C. T., Li, C., Reinhard, C. T., Kelly, A. E., ... & Lyons, T. W. (2011). Widespread iron-rich conditions in the mid-Proterozoic ocean. Nature, 477(7365), 448.

Planavsky, N. J., Reinhard, C. T., Wang, X., Thomson, D., McGoldrick, P., Rainbird, R. H., ... & Lyons, T. W. (2014). Low Mid-Proterozoic atmospheric oxygen levels and the delayed rise of animals. Science, 346(6209), 635-638.

Planavsky, N. J., Rouxel, O. J., Bekker, A., Lalonde, S. V., Konhauser, K. O., Reinhard, C. T., & Lyons, T. W. (2010). The evolution of the marine phosphate reservoir. Nature, 467(7319), 1088.

Planavsky, N., Bekker, A., Rouxel, O. J., Kamber, B., Hofmann, A., Knudsen, A., & Lyons, T. W. (2010). Rare earth element and yttrium compositions of Archean and Paleoproterozoic Fe formations revisited: new perspectives on the significance and mechanisms of deposition. Geochimica et Cosmochimica Acta, 74(22), 6387-6405.

Poulton, S. W., & Canfield, D. E. (2011). Ferruginous conditions: a dominant feature of the ocean through Earth's history. Elements, 7(2), 107-112.

Prietzel, J., Botzaki, A., Tyufekchieva, N., Brettholle, M., Thieme, J., & Klysubun, W. (2011). Sulfur speciation in soil by SK-edge XANES spectroscopy: comparison of spectral deconvolution and linear combination fitting. Environmental science & technology, 45(7), 2878-2886.

Rabus, R., Hansen, T. A., & Widdel, F. (2006). Dissimilatory sulfate-and sulfur-reducing prokaryotes. In The prokaryotes(pp. 659-768). Springer, New York, NY.

Raven, M. R., Sessions, A. L., Fischer, W. W., & Adkins, J. F. (2016). Sedimentary pyrite δ34S differs from porewater sulfide in Santa Barbara Basin: Proposed role of organic sulfur. Geochimica et Cosmochimica Acta, 186, 120-134.

Reeburgh, W. S. (1983). Rates of biogeochemical processes in anoxic sediments. Annual Review of Earth and Planetary Sciences, 11(1), 269-298.

Reinhard, C. T., Planavsky, N. J., Gill, B. C., Ozaki, K., Robbins, L. J., Lyons, T. W., ... & Konhauser, K. O. (2017). Evolution of the global phosphorus cycle. Nature, 541(7637), 386.

Reinhard, C. T., Raiswell, R., Scott, C., Anbar, A. D., & Lyons, T. W. (2009). A late Archean sulfidic sea stimulated by early oxidative weathering of the continents. Science, 326(5953), 713-716.

Revsbech, N. P. (1989). An oxygen microsensor with a guard cathode. Limnology and Oceanography, 34(2), 474-478.

Roden, E. E., & Wetzel, R. G. (2002). Kinetics of microbial Fe (III) oxide reduction in freshwater wetland sediments. Limnology and Oceanography, 47(1), 198-211.

Sagemann, J., Jørgensen, B. B., & Greeff, O. (1998). Temperature dependence and rates of sulfate reduction in cold sediments of Svalbard, Arctic Ocean. Geomicrobiology Journal, 15(2), 85-100.

Sahoo, S. K., Planavsky, N. J., Kendall, B., Wang, X., Shi, X., Scott, C., ... & Jiang, G. (2012). Ocean oxygenation in the wake of the Marinoan glaciation. Nature, 489(7417), 546.

Sass, H., Cypionka, H., & Babenzien, H. D. (1997). Vertical distribution of sulfate-reducing bacteria at the oxic-anoxic interface in sediments of the oligotrophic Lake Stechlin. FEMS Microbiology Ecology, 22(3), 245-255.

SAUNDERS, W. (1961). Some applications of isotopic sulfur. In Organic Sulfur Compounds (pp. 41-46).

Schippers, A., Neretin, L. N., Kallmeyer, J., Ferdelman, T. G., Cragg, B. A., Parkes, R. J., & Jørgensen, B. B. (2005). Prokaryotic cells of the deep sub-seafloor biosphere identified as living bacteria. Nature, 433(7028), 861.

Schopf, J. W., & Klein, C. (Eds.). (1992). The Proterozoic biosphere: a multidisciplinary study. Cambridge University Press.

Schopf, J. W., & Klein, C. (Eds.). (1992). The Proterozoic biosphere: a multidisciplinary study. Cambridge University Press.

Schulz, H. D., & Zabel, M. (2006). Marine geochemistry (Vol. 2). Berlin: Springer.

Selin, N. E. (2009). Global biogeochemical cycling of mercury: a review. Annual Review of Environment and Resources, 34, 43-63.

Shen, Y., & Buick, R. (2004). The antiquity of microbial sulfate reduction. Earth-Science Reviews, 64(3-4), 243-272.

Sievert, S. M., Kiene, R. P., & Schulz-Vogt, H. N. (2007). The sulfur cycle. Oceanography, 20(2), 117-123.

Sim, M. S., Bosak, T., & Ono, S. (2011). Large sulfur isotope fractionation does not require disproportionation. Science, 333(6038), 74-77.

Sinke, A. J., Cornelese, A. A., Cappenberg, T. E., & Zehnder, A. J. (1992). Seasonal variation in sulfate reduction and methanogenesis in peaty sediments of eutrophic Lake Loosdrecht, The Netherlands. Biogeochemistry, 16(1), 43-61..

Smith, V. H., Tilman, G. D., & Nekola, J. C. (1999). Eutrophication: impacts of excess nutrient inputs on freshwater, marine, and terrestrial ecosystems. Environmental pollution, 100(1-3), 179-196.

Spangler, W. J., Spigarelli, J. L., Rose, J. M., Flippin, R. S., & Miller, H. H. (1973). Degradation of methylmercury by bacteria isolated from environmental samples. Applied microbiology, 25(4), 488-493.

Sperling, E. A., Wolock, C. J., Morgan, A. S., Gill, B. C., Kunzmann, M., Halverson, G. P., ... & Johnston, D. T. (2015). Statistical analysis of iron geochemical data suggests limited late Proterozoic oxygenation. Nature, 523(7561), 451.

Steenbergen, C. L. M., Sweerts, J. P. R. A., Cappenberg, T. E., & Ford, T. E. (1993). Microbial biogeochemical activities in lakes: stratification and eutrophication. Aquatic microbiology: An ecological approach, 66-99.

Stolper, D. A., & Keller, C. B. (2018). A record of deep-ocean dissolved O 2 from the oxidation state of iron in submarine basalts. Nature, 553(7688), 323.

Sunderland, E. M., Gobas, F. A., Branfireun, B. A., & Heyes, A. (2006). Environmental controls on the speciation and distribution of mercury in coastal sediments. Marine chemistry, 102(1-2), 111-123.

Taylor, B. F., & Gilchrist, D. C. (1991). New routes for aerobic biodegradation of dimethylsulfoniopropionate. Applied and environmental microbiology, 57(12), 3581-3584.

Teske, A., & Salman, V. (2014). The family beggiatoaceae. In *The Prokaryotes* (pp. 93-134). Springer, Berlin, Heidelberg.

Thomsen, U., Thamdrup, B., Stahl, D. A., & Canfield, D. E. (2004). Pathways of organic carbon oxidation in a deep lacustrine sediment, Lake Michigan. Limnology and Oceanography, 49(6), 2046-2057.

Tostevin, R., Wood, R. A., Shields, G. A., Poulton, S. W., Guilbaud, R., Bowyer, F., ... & Clarkson, M. O. (2016). Low-oxygen waters limited habitable space for early animals. Nature communications, 7, 12818.

Ueno, Y., Ono, S., Rumble, D., & Maruyama, S. (2008). Quadruple sulfur isotope analysis of ca. 3.5 Ga Dresser Formation: New evidence for microbial sulfate reduction in the early Archean. Geochimica et Cosmochimica Acta, 72(23), 5675-5691.

Urban, N. R. (1994). Retention of sulfur in lake sediments.

Urban, N. R., Brezonik, P. L., Baker, L. A., & Sherman, L. A. (1994). Sulfate reduction and diffusion in sediments of Little Rock Lake, Wisconsin. Limnology and Oceanography, 39(4), 797-815.

Urban, N. R., Ernst, K., & Bernasconi, S. (1999). Addition of sulfur to organic matter during early diagenesis of lake sediments. Geochimica et cosmochimica acta, 63(6), 837-853.

Vairavamurthy, A., Zhou, W., Eglinton, T., & Manowitz, B. (1994). Sulfonates: a novel class of organic sulfur compounds in marine sediments. Geochimica et Cosmochimica Acta, 58(21), 4681-4687.

Van Cappellen, P., & Wang, Y. (1996). Cycling of iron and manganese in surface sediments; a general theory for the coupled transport and reaction of carbon, oxygen, nitrogen, sulfur, iron, and manganese. American Journal of Science, 296(3), 197-243.

Van Mooy, B. A., Rocap, G., Fredricks, H. F., Evans, C. T., & Devol, A. H. (2006). Sulfolipids dramatically decrease phosphorus demand by picocyanobacteria in oligotrophic marine environments. Proceedings of the National Academy of Sciences, 103(23), 8607-8612.

Vaynshteyn, M. B., Tokarev, V. G., Shakola, V. A., Lein, A., & Ivanov, M. V. (1986). The geochemical activity of sulfate-reducing bacteria in sediments in the western part of the Black Sea. Geochemistry International, 23(1), 110-122.

Visscher, P. T., & Taylor, B. F. (1994). Demethylation of dimethylsulfoniopropionate to 3-mercaptopropionate by an aerobic marine bacterium. Applied and environmental microbiology, 60(12), 4617-4619.

Waldbauer, J. R., Newman, D. K., & Summons, R. E. (2011). Microaerobic steroid biosynthesis and the molecular fossil record of Archean life. Proceedings of the National Academy of Sciences, 108(33), 13409-13414.

Warner, K. A., Roden, E. E., & Bonzongo, J. C. (2003). Microbial mercury transformation in anoxic freshwater sediments under iron-reducing and other electron-accepting conditions. Environmental science & technology, 37(10), 2159-2165.

Watras, C. J., Bloom, N. S., Claas, S. A., Morrison, K. A., Gilmour, C. C., & Craig, S. R. (1995). Methylmercury production in the anoxic hypolimnion of a dimictic seepage lake. Water, Air, and Soil Pollution, 80(1-4), 735-745.

Watras, C. J., Morrison, K. A., Host, J. S., & Bloom, N. S. (1995). Concentration of mercury species in relationship to other site-specific factors in the surface waters of northern Wisconsin lakes. Limnology and Oceanography, 40(3), 556-565.

Werne, J. P., Lyons, T. W., Hollander, D. J., Schouten, S., Hopmans, E. C., & Damsté, J. S. S. (2008). Investigating pathways of diagenetic organic matter sulfurization using compound-specific sulfur isotope analysis. Geochimica et Cosmochimica Acta, 72(14), 3489-3502.

Wiatrowski, H. A., Ward, P. M., & Barkay, T. (2006). Novel reduction of mercury (II) by mercury-sensitive dissimilatory metal reducing bacteria. Environmental science & technology, 40(21), 6690-6696.

Wille, M., Kramers, J. D., Nägler, T. F., Beukes, N. J., Schröder, S., Meisel, T., ... & Voegelin, A. R. (2007). Evidence for a gradual rise of oxygen between 2.6 and 2.5 Ga from Mo isotopes and Re-PGE signatures in shales. Geochimica et Cosmochimica Acta, 71(10), 2417-2435.

Zahnle, K., Claire, M., & Catling, D. (2006). The loss of mass-independent fractionation in sulfur due to a Palaeoproterozoic collapse of atmospheric methane. Geobiology, 4(4), 271-283.

Zhang, S., Wang, X., Wang, H., Bjerrum, C. J., Hammarlund, E. U., Costa, M. M., ... & Canfield, D. E. (2016). Sufficient oxygen for animal respiration 1,400 million years ago. Proceedings of the National Academy of Sciences, 113(7), 1731-1736.

Zhao, F. J., Lehmann, J., Solomon, D., Fox, M. A., & McGrath, S. P. (2006). Sulphur speciation and turnover in soils: evidence from sulphur K-edge XANES

spectroscopy and isotope dilution studies. Soil Biology and Biochemistry, 38(5), 1000-1007.

Zhelezinskaia, I., Kaufman, A. J., Farquhar, J., & Cliff, J. (2014). Large sulfur isotope fractionations associated with Neoarchean microbial sulfate reduction. Science, 346(6210), 742-744.

Zigah, P. K., Minor, E. C., Werne, J. P., & Leigh McCallister, S. (2012). An isotopic (Δ 14 C, δ 13 C, and δ 15 N) investigation of the composition of particulate organic matter and zooplankton food sources in Lake Superior and across a size-gradient of aquatic systems. Biogeosciences, 9(9), 3663-3678.

Zillioux, E. J., Porcella, D. B., & Benoit, J. M. (1993). Mercury cycling and effects in freshwater wetland ecosystems. Environmental Toxicology and Chemistry, 12(12), 2245-2264.